1506
UNIVERSITÀ
DEGLI STUDI
DI URBINO
CARLO BO

DIPARTIMENTO DI SCIENZE DI BASE
CORSO DI DOTTORATO DI RICERCA IN SCIENZE DI BASE E APPLICAZIONI
Curriculum Scienze della Terra
XXX CICLO

Oceanic Anoxic Event (OAE) 1b (late Aptian – early Albian): evolutionary, palaeoecological, palaeoceanographic and palaeoclimatic implications

SSD Geo/01

TUTOR
Chiar.mo Prof. Rodolfo Coccioni

DOTTORANDO
Dott. Serena Ferraro

CO-TUTOR
Dott. Mario Sprovieri

ANNO ACCADEMICO 2016 - 2017

Abstract

The late Aptian – early Albian interval (110 – 118 Ma) represents a crucial period of pronounced biotic and climate/ocean changes. It was characterized by enhanced volcanic activity linked to the progressive opening of the Indian Ocean, increased levels of atmospheric greenhouse gases, and high climate instability. The widespread deposition of multiple prominent black shale horizons in the Northern Tethyan and North Atlantic realms is the sedimentary expression of Oceanic Anoxic Event (OAE) 1b, a major perturbation of global carbon cycle. The late Aptian – early Albian OAE 1b is also the scenario of the first major turnover in the planktonic foraminifera evolutionary history, with an event of dramatic extinction of large-sized, heavy ornamented planktonic species, and subsequent diversification of small and thin-walled taxa. Investigation of the complex nature and dynamics of oceanographic changes in response to the OAE 1b are the goals of this thesis, along with a deep analysis of the ecological stressors affecting the evolutionary behaviour of the planktonic foraminiferal community. A high-resolution study of multiple paleontological, organic and inorganic geochemical proxies (microfaunal assemblage composition, morphometry of *Pa. rohri*, $\delta^{13}C_{carb}$, TOC, $CaCO_3$, trace elements, organic biomarkers) has been performed on the nearly continuous and undisturbed pelagic sedimentary succession of Poggio le Guaine (Umbria-Marche Basin, central Italy). The results clearly suggest the emplacement of the Southern Kerguelen Plateau as the external driver triggering global climatic/oceanographic changes. The consequent complex feedback mechanisms among ocean, land and atmosphere, strictly controlled by the regional features, led to intermittent episodes of water column anoxia/dysoxia, inducing enhanced burial and preservation of marine organic carbon. The high environmental variability destabilized the marine ecosystems, triggering ecological stress and forcing biotic crises. The planktonic foraminifera turnover has been therefore the result of an irreversible and drastic regime shift toward more mesotrophic – eutrophic ecosystem that promoted the blooming of opportunistic/disaster species and siliceous organism as Radiolaria, which dominated the microfaunal assemblages. The comparison of the planktonic foraminifera records from the Poggio le Guaine succession and the DSDP Site 511 section chosen as “control

ocean section", provided the evidence that widely separated marine ecosystems had similar response to global drivers, both experiencing relevant ecological system shift. The dwarfism of planktonic foraminifera prior the extinction turned out to be an ecological response to increasing environmental stresses rather an evolutive behaviour preceding the extinction.

Acknowledgments

Firstly, I would like to thank my supervisors, Prof. Rodolfo Coccioni of the University of Study of Urbino – Carlo Bo, and Dr Mario Sprovieri of the IAMC-CNR UOS of Capo Granitola, for their advice, support and encouragement throughout my PhD. In particular, thanks to Prof. Coccioni for sharing some of his vast knowledge of micropaleontology and for introducing me into the Cretaceous Planktonic Foraminifera world. Without his encouragement and help with forams identification much of this work could not have been accomplished. I would especially like to thank Mario for supporting my metamorphosis from mere micropaleontologist to fully-fledged palaeoceanographer. His unfailing enthusiasm for research and learning has been extremely inspiring. To the both of you thank you for helping me make what has sometimes seemed like an eclectic and abstract mix of subjects and techniques into a somewhat more orderly body of work.

I am particularly indebted to Dr. Nadia Sabatino for freely giving her time and advice in relation to this research. During my PhD Nadia was extremely patient with me, offering her help, her constant enthusiasm, guidance, support, also listening and pushing me to do things better. My sincere thank also goes to Dr. Angela Cuttitta of the IAMC-CNR UOS of Capo Granitola, who gave access to the microscopy laboratory, crucial to conduct my research.

Big thanks also go to Prof. R. Pancost and Dr. David Naafs of the OGU in the School of Chemistry, University of Bristol, for giving me the great opportunity to use of their laboratory facilities for three months. In particular, thank you to David, for showing me the ropes of Organic Geochemistry at the beginning and for being so patient with me. I would also like to thank all members of the OGU for making it such a fun and interesting place to work and for always being so willing to help. Above all, thanks to Georgia, Alexandra, Leila, Emmanuelle, Gordon, John and Cathrine for keeping me cheerful and making the lab such a pleasure to work in.

Sampling and the field observations were conducted on Poggio le Guaine (Umbria-Marche, Italy) and I am very grateful to Dr. F. Frontalini, Dr. Marianna Sideri and Dr. Carla Bucci for allowing this. They are thanked for their assistance and availability.

I am grateful to the Integrated Ocean Drilling Program for all the samples they provided for this work and to IAMC- CNR of Capo Granitola for funding this project, giving me the opportunity to carry out this multidisciplinary research. The team at IAMC-CNR of Capo Granitola have absolutely been the best collaborators I could have asked for. Always interested and willing to support my ideas and provide assistance whenever requested. I am so grateful.

A very special thank you goes to my fellow adventurers: Dr. Gemma Biondo and my “Asso” Dr. Linda Monastero. They represent the best gift my PhD gave me, wholeheartedly supporting and encouraging me every time I plunged into distress.

They have made the PhD experience all the more enjoyable! I am also very grateful to my colleague and friend Luigi Giaramita for our lifelong friendship and for allaying all my anxieties.

Finally, my family is thanked for his continual support over the years, for having more faith in me than I do myself. Thank you to my life-partner Pietro for putting up with me for the last year or so, for keeping me smiling and for dragging me through the last 3 months of writing.

Specially to my wonderful mother, for always pushing me to be the best I can be, and for being behind me every single step of the way, no matter what I have chosen to do. This is for you.

Table of contents

List of figures

List of Abbreviations

µA	Microampere
µg	Microgram
µl	Microliter
µm	Micrometre
$^{40}Ar/^{30}Ar$	Ratio of Argon-40 to Argon-30
Å	Ångströms
AABI	Aptian Albian Boundary Interval
AS	Average Shale
$BaSO_4$	Barite
BF	Benthic Foraminifera
$CaCO_3$	Calcium carbonate
CH_4	Methane
CIE	Carbon Isotopic Excursion
CKP	Central Kerguelen Plateau
cm	Centimetres
CNR	Council of National Research
CO_2	Carbon dioxide
CPI	Carbon Preference Index
$\delta^{13}C$	Ratio of carbon-13 to carbon-12 relative to VPDB
DCM	Dichloromethane
DSDP	Deep Sea Drilling Program
E	East
eV	Elettronvolt
g	Gram
GC	Gorgo a Cerbara
GC-MS	Gas chromatography – mass spectrometry
h	Hour
H_2O	Water
H_2O_2	Hydrogen peroxide
H_2S	Hydrogen sulfide
H_3BO_3	Boric acid
HCl	Hydrochloridric acid
Hd.	*Hedbergella*
HF	Hydrofluoric acid
HgS	Mercuric sulphide
HNO_3	Nitric acid
HO	Highest Occurrence
IAMC	Institute for marine and coastal environment
ICP-OES	Inductively coupled plasma optical emission spectrometer
km	Kilometres
kyr	Thousand years
Lat.	Latitude
LIP	Large Igneous Plateau
LO	Lowest Occurrence
Long.	Longitude
m	Meter
M	Molar

m/z	Mass-to-charge ratio
M^+	Molecular ion
Ma	Mega annum
MAC	Most Abundant Compound
mbsf	Meters Below Sea Floor
mbsl	Meters Below Sea Level
MeHg	Methylmercury
MeOH	Methanol
Mi.	*Microhedbergella*
min	Minute
minigl.	*miniglobularis*
ml	Millilitre
mm	Millimetre
MS	Mass Spectrometry
Myr	Million years
N	North
N_2	Nitrogen gas
n-C_x	Normal alkane with x atoms of carbon
ng	Nanogram
NKP	Northern Kerguelen Plateau
OAE	Oceanic Anoxic Event
ODP	Ocean Drilling Program
OGU	Organic Geochemistry Unit
OM	Organic Matter
OMZ	Oxygen minimum layer
Pa.	*Paraticinella*
pCO_2	Partial pressure of atmospheric carbon dioxide
PF	Planktonic Foraminifera
Ph	Phytane
PLG	Poggio le Guaine
PLG-GC	Poggio le Guaine – Gorgo a Cerbara composite section
PMI	2,6,10,15,19-pentamethylicosane
ppb	Parts per billion
ppm	Parts per million
Pr	Pristane
RDS	Relative standard deviation
S	South
Sect.	Section
SiO_2	Silica
STO	Ocean stagnation model
TAR	Terrigenous / aquatic *n*-alkanes ratio
TE	Trace Element
TEX_{86}	Tetraether index of tetraethers containing 86 carbon atoms
TIC	Total Ion Current
TLE	Total Lipid Extract
TM	Trace Metal
TMI	2,6,15,19-tetramethylicosane
TOC	Total Organic Carbon
v/v	Volume (of solute) per volume (of solvent)
VPDB	Vienna Pee Dee Belemnite

Chapter 1
Introduction

1.1 The late early-Cretaceous time

The late early-Cretaceous (~120-90 Ma) is generally considered as the period of most extreme greenhouse conditions in the Earth's history. It was characterized by sea surface temperatures 5°C warmer than the present time, absence of polar ice-caps, low thermal latitudinal gradients and the sea level 50-170 m higher than today (Barron, 1983; Sellwood et al., 1994; Huber et al., 1995; Price et al., 1998; Fassel and Bralower, 1999; Hay, 2008). It was a time of considerable changes in plate tectonics, continental rifting, and volcanism associated with the rapid breakup of Gondwana into African and South American plates (Larson, 1991, Tarduno et al., 1991; Arthur et al., 1991; Erba and Larson, 1991; Bralower et al., 1994). Large volcanic episodes led to the formations of seamount chains, continental flood basalts and production of the so-called Large Igneous Plateau (LIP), as Ontong Java, Kerguelen, and Caribbean Plateau (Hays and Pitman, 1973; Schlanger et al., 1981), which affected ecological, climatic, and oceanic conditions across the planet (Föllmi, 2012). The late early-Cretaceous greenhouse climate was probably caused by increased levels of atmospheric greenhouse gasses as mantle CO_2, methane (CH_4) and water vapor (H_2O) due to extensive submarine volcanic degassing (Arthur et a., 1985; Weissert and Lini, 1991; Huber, et al., 1995; Price, et al., 1998; Hay, 2008; Madhavaraju, et al., 2013; Millán, et al., 2014). Several events of volcanic CO_2 release into the atmosphere linked to the emplacement of LIP have been inferred from pronounced negative shifts of both carbon and strontium isotope compositions of marine carbonates associated with the main Cretaceous OAEs (Jenkyns, 2010; Erba, 2004; Wagner et al., 2007; Erba et al., 2010; Barral et al., 2017). The largest event of CO_2 release events in terms of magnitude of carbon isotope excursions was related to OAE 1b and lasted ca. 25 kyr (Erba, 2004; Wagner et al., 2007; Barral et al., 2017).

Several studies suggest that the late early-Cretaceous climate was far from stability, and the upper Aptian and the Aptian–Albian transition interval was

characterized by global cooling and possible formation of ice-caps (Weissert and Lini, 1991; Pirrie et al., 1995; Mütterlose et al., 2009; McAnena et al., 2013). Evidence of cool climate comes from i) information of stable isotopes and detection of poleward expansion of vegetational provinces and thermophilic organisms (e.g., Kauffman, 1973; Vakhrameev, 1991; Tarduno et al., 1998; Bice and Norris, 2002; Huber et al., 2002; Wilson et al., 2002; Norris et al., 2002; Barral et al., 2017), ii) evidence of dropstones and glendonites deposition occurred at high latitudes (Kemper and Schmitz, 1981; Price and Nunn, 2010), iii) proof of extreme glacio-eustatic sea level drop based on subsurface seismic and core data (Maurer et al., 2013), iv) signal of relevant variations in calcareous nannofossil assemblages (Mütterlose et al., 2005).

1.2 The Oceanic Anoxic Events (OAEs)

The late early-Cretaceous climate and ocean dynamics promoted episodic deposition of anoxic sediments by effect of intense oceanic periods of dysoxia-anoxia, referred as Oceanic Anoxic Events (OAEs; Schlanger and Jenkyns, 1976). These were generally short-lived (<1 Myr) intervals of increased organic carbon burial in marine sediments, marked by the widespread deposition of dark-coloured, laminated, organic-carbon-rich shales (the so-called “black shales”), and the preferential removal of ^{12}C from the ocean and atmosphere compartments, inducing relative positive carbon isotopic excursion (tipically 1.0-2.5‰) in biogenic carbonate (Schlanger and Jenkyns, 1976; Ryan and Cita, 1977; Arthur and Premoli Silva, 1982; Arthur et al., 1990; Erbacher and Thurow, 1997; Wilson et al., 1998; Erbacher et al., 2001; Leckie et al., 2002; Erba 2004; Pacton et al., 2007; Jenkyns, 2010; Trabucho Alexandre et al., 2010; Huber and Leckie, 2011; Millán et al., 2014). Some of these black shales horizons are synchronous and have a supra-regional or even global distribution, as the early Aptian Selli Event (OAE 1a), and the Cenomanian/Turonian Bonarelli level (OAE 2) (e.g., Arthur et al., 1990; Bralower et al., 1994; Leckie et al., 2002). Others regionally and locally distributed black shales are common in the Aptian to Albian sedimentary successions of the Northern Tethys and the Northern and Central Atlantic Oceans, as the late Aptian – early Albian OAE 1b and the upper Albian OAE 1c and 1d (e.g. Tornaghi et al., 1989; Bréhéret, 1994, 1997; Leckie et al., 2002; Herrle et al., 2004; Tiraboschi et

al., 2009). These latter horizons are partly characterized by a cyclic pattern organization and have been interpreted as a result of changes in seasonality and monsoonal activity confined to certain regions (e.g. de Boer, 1982; Herbert and Fischer, 1986; Erba, 1992; Bellanca et al., 1996; Herrle, 2002; Friedrich et al., 2003; Galeotti et al., 2003; Herrle et al., 2003a,b; Tiraboschi et al., 2009).

Although the mechanisms responsible for OAEs has been strongly debated and are not yet definitely understood, there is no doubt that they significantly contributed to changes and evolution of the biological marine community, especially particularly in the planktonic assemblages (Fig. 1.1). Microfossil and organic geochemical records suggest drastic change in assemblages of marine organisms during OAEs, associated to dramatic biotic turnovers on planktic protists (Erbacher et al., 1998; 1999; Kuypers et al., 2002; Leckie et al., 2002; Dumitrescu and Brassell., 2005; Okano et al., 2008).

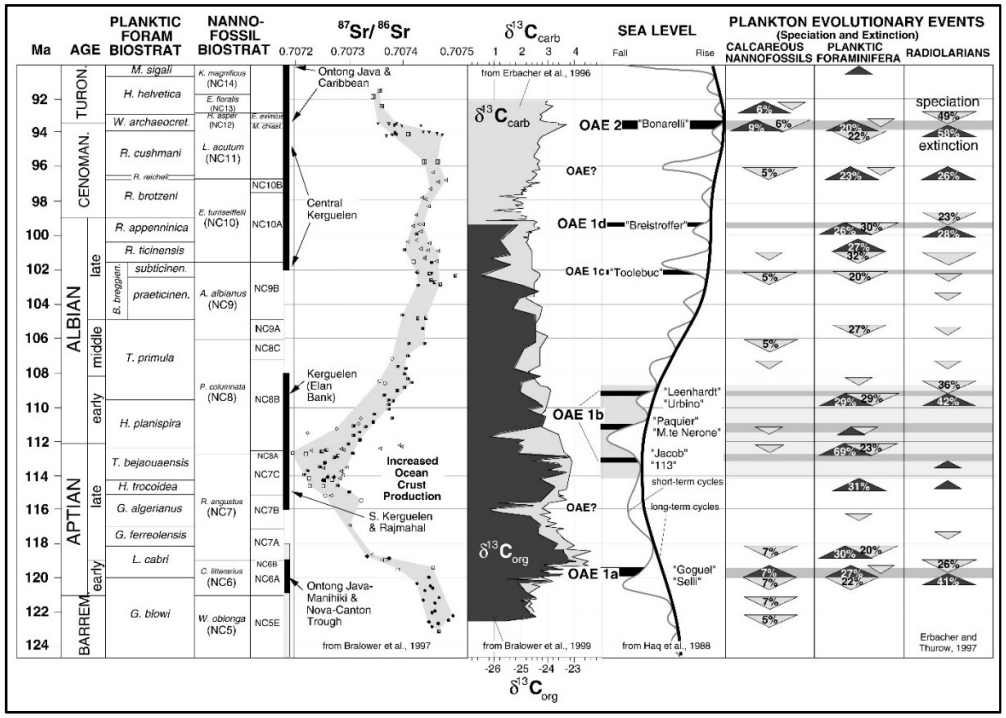

Fig. 1.1. The late early-Cretaceous record of major black shales and oceanic anoxic events (OAEs) in the context of the carbon isotopic record (Erbacher et al., 1996; Bralower et al., 1999), changing global sea level (Haq et al., 1988), seawater chemistry (Bralower et al., 1997), and plankton evolutionary events. (From Leckie et al., 2002).

1.3 The OAE 1b

The Oceanic Anoxic Event 1b replicates many features of the late early-Cretaceous in terms of dynamics of climate, tectonics, sea level, lithofacies and marine plankton. It is shaped by 4 black shale horizons that straddle the Aptian/Albian boundary (named Jacob, Kilian, Paquier and Leenhardt), probably linked to shorter-term perturbations of the carbon cycle (Arthur and Premoli Silva, 1982; Bréhéret et al., 1986; Bréhéret and Delamette, 1987; 1989; Bréhéret, 1988; 1994; 1997 Premoli Silva e Sliter, 1999; Leckie et al., 2002; Huber and Leckie, 2011; Sabatino et al., 2015). The overall duration of the OAE 1b has been estimated 3.8 Myr by Coccioni et al. (2014) based on Grippo et al. (2004) and Huang et al. (2010) studies. This multiple event is associated with cooling interval and sea level fall in the latest Aptian and later, sea level rise and global warming during the early Albian (Leckie et al., 2002; McAnena 2013), documented as the break point between the end of a positive $\delta^{13}C$ excursion in the latest Aptian and the beginning of a pronounced negative shift of $\delta^{13}C$ in the early Albian (Weissert and Lini, 1991; Herrle et al., 2004).

The black shale horizons of the OAE 1b are enriched in organic matter deposited under dysoxic-anoxic conditions and correlate with negative excursions in the $\delta^{13}C_{carb}$ record, interrupted by brief periods of oxygenation and pelagic carbonate deposition (Moullade et al. 2011; Coccioni et al., 2014; Kennedy et al., 2014; Sabatino et al., 2015). The black shales of the OAE 1b do not have global distribution, being documented only in Northern Tethys and North-Central Atlantic palaeo-domains; this is also due to unavailable samples from Tethyan and Pacific crust, that was significantly subducted (Li et al., 2016). The lithological and geochemical signatures, as well as the number of black shale levels, vary geographically and can be clearly attributed to different palaeoceanographical settings, variations in the source of OM or diagenetic effects (e.g., Bralower et al. 1999; Erbacher et al. 2001; Kuypers et al. 2002; Herrle et al. 2004; Tsikos et al. 2004). Multiple proxies have been used to investigate OAE 1b intervals: C-O and Sr isotopes, microfossil assemblages, Tex_{86}, TOC, $CaCO_3$, trace metals on sediment and foraminiferal test, molecular biomarker (e.g. Bralower et al., 1999; Erbaker et al., 1999, 2001; Kuypers et al., 2002; Ludvigson et al., 2010; Huber and Leckie,

2011; Trabucho Alexandre et al., 2011; Coccioni et al., 2014; Herrle et al., 2004; McAnena et al., 2013; Hu et al., 2014; Millán et al., 2014; Sabatino et al., 2015). To date, the Jacob, Kilian, Paquier and Leenhardt anoxic sub-events are considered the record of the regional short-term carbon isotope responses to the global OAE 1b, superimposed on a long-term disturbance of carbon isotope signature of the carbon reservoirs in the global ocean-atmosphere system.

The uppermost Aptian black shale horizon of the OAE 1b is known as the Jacob sub-event and its duration has been estimated 40 ky by Huang et al. (2010). It was interpreted as a "detrital OAE", induced by land-derived organic matter (Erbacher et al., 1996; Bralower et al., 1993; Leckie et al., 2002). It has been documented only in the Vocontian basin and in Central Italy, where it is referred as 113 level (Herrle, 2002; Friedrich et al., 2005; Coccioni et al., 2012; 2014). However, Coccioni et al. (2014) suggest a possible expression of the Jacob sub-event in the North Atlantic (DSDP Site 545), on the basis of the negative CIEs reported by McAnena et al. (2013). The Jacob sub-event falls in the *Paraticinella rohri* Zone of Coccioni et al. (2014), corresponding to the *Ticinella bejaouensis* Zone of Herrle (2002) and Herrle et al. (2004), and to the *Paraticinella rohri* Zone of Petrizzo et al. (2012).

The Kilian level is the second sub-event of the OAE 1b, and it falls within the Aptian/Albian boundary. It records a 120 kyr-long perturbation documented in the Vocontian Basin, Central Italy, and North and Central Atlantic Ocean (Huang et al., 2010; Trabucho-Alexandre et al., 2011; Petrizzo et al., 2012; Coccioni et al., 2014; Kennedy et al., 2014; Sabatino et al., 2015). According to Herrle (2002) and Herrle et al. (2004), the Kilian level falls in the *Hedbergella planispira* Zone, whereas Petrizzo et al. (2012), Coccioni et al. (2014) and Kennedy et al. (2014) consider the Kilian level as spanning from the top of the *Mi. miniglobularis* Zone to the lower part of the *Mi. renilaevis* Zone.

The lower Albian black shales of the Paquier sub-event is documented in Vocontian basin, Central Italy, North and Central Atlantic Ocean, Pacific Ocean and Mexico (Bréhéret 1983; 1994; Tribovillard and Gorin 1991; Bralower et al. 1999; Erbacher et al. 1999; 2001; Herrle et al. 2003b; 2004; Tsikos et al. 2004; Wagner et al. 2008; Trabucho Alexandre et al. 2011; Coccioni et al., 2014; Sabatino et al., 2015). It has been interpreted as formed by deposition of marine organic

matter and controlled by rising sea level (Herrle et al. 2004; Friedrich et al. 2005; Browning and Watkins 2008; Wagner et al. 2008; Huber and Leckie 2011; Huber et al. 2011; Trabucho Alexandre et al. 2011). Its thickness varies in different sedimentary sequences (e.g. 1.63 m in the Vocontian Basin, 46 cm at ODP Hole1049C) and it lies in the middle part of the *Hedbergella planispira* Planktonic Foraminiferal Zone (currently the *Microhedbergella rischi* planktonic foraminiferal Zone of Huber and Leckie 2011).

Finally, the Leenhardt sub-event has been documented only in the Vocontian basin and in Central Italy (Bréhéret, 1994; Herrle, 2002; Coccioni et al., 2014; Sabatino et al., 2015). According to Herrle (2002) and Herrle et al. (2004), the Leenhardt level occurs in the upper part of the *Hedbergella planispira* Planktonic Foraminiferal Zone (currently the *Microhedbergella rischi* planktonic foraminiferal Zone of Huber and Leckie, 2011). In analogy with the Paquier level, also the Leenhardt sub-event is considered as "productivity-induced OAE" (Leckie et al., 2002).

Confined only to the Poggio le Guaine section in Central Italy, the Monte Nerone interval comprises several thin levels of dark to black shales, whose equivalents have not been correlated in other sections.

1.4 The late Aptian – early Albian planktonic foraminifera turnover

The late Aptian – early Albian OAE 1b represents a hinge period of biological events on marine biota, recording a major turnover in marine flora and fauna, mainly reflected in changes in the belemnite, radiolarian, and benthic foraminifera taxa, radiation and diversification of planktonic foraminifera (PF) and silicoflagellates, and diversification and crisis within the calcareous nannofossils (Fig. 1.1) (Bralower et al., 1999; Aguado et a., 1999; Leckie et al., 2002). Several studies documented this crucial evolutionary period, even if the continuous sedimentation across the Aptian – Albian Boundary Interval (AABI) is rare, as it is often marked by unconformity (e.g., Amedro, 1992) or dissolution (e.g., Leckie, 1984; Tornaghi et al., 1989) in deeper water sections, or ecological collapse in shallow carbonate-platform sections, providing further evidence of a global environmental perturbation at the boundary level (e.g., Föllmi et al., 2006, Iba and

Sano, 2007). Papers by Huber and Leckie (2011), Petrizzo et al. (2012), and Coccioni et al. (2014) represents reference works for the late Aptian – early Albian planktonic foraminiferal turnover and provide a robust biostratigraphic framework.

Planktonic foraminifera evolved since the Middle Jurassic and their evolution in the late early-Cretaceous period records short episodes of elevated rates of turnover alternating with longer times of relatively diminished rates or stasis. According to Premoli Silva and Silter (1999), the early Cretaceous evolutionary history of PF could be divided into three phases: a first diversification phase in the early Valanginian to the latest Aptian, with continuous diversification pattern temporally interrupted by a single moderate turnover near the Selli Event (OAE 1a). A second evolutionary interval that encompasses the late Aptian - early Albian boundary and records higher diversification rates, and the third phase from the middle Albian to the end of the Cretaceous. Therefore, the AABI records the first and most significant species turnover in the evolutionary history of PF, with the 69% of the late Aptian species becoming extinct and a speciation rate of 23%, for a total of 92% species turnover (Fig. 1.1; Leckie et al., 2002). This turnover resulted in the net change from latest Aptian assemblages dominated by large-sized (mean diameters >250 μm), robust, and coarsely ornamented species, to early Albian assemblages comprised only of minute (mean diameters <100 μm), weakly calcified forms that lack ornamentation (Leckie, 1989; Tornaghi and others, 1989; Erbacher et al., 1999; Premoli Silva and Sliter, 1999; Leckie et al., 2002; Herrle and Mutterlose, 2003; Huber and Leckie, 2011; Petrizzo et al., 2012; Coccioni et al., 2014).

Notably, Radiolaria show strikingly similar patterns of evolutionary turnover to the planktic foraminifera (Erbacher et al., 1996; Aguado et al., 1999; Leckie et al., 2002), and the highest rates of turnover in both organisms occur at or near the major OAEs (Fig. 1.1). Instead, calcareous nannofossils undergone to rapid turnover only at OAE 1a in the early Aptian and OAE 2 at the Cenomanian/Turonian boundary (Fig. 1.1; Leckie et al., 2002).

1.5 Aims and structure of this thesis

The late Aptian / early Albian OAE 1b represents a crucial period of pronounced biotic and climatic/ocean changes. It is indisputable that this OAE induced major perturbations in the oceanic environment and severe disturbance of the biosphere which, in turn, triggered the ecological stress forcing biotic crises. Despite the number of studies reported from literature, the nature and dynamics of oceanographic changes in response to the OAE 1b are still poorly detailed and understood, as well as the role and modes of ecological stressors on the evolutionary behaviour of planktonic foraminiferal community.

Thus, the main aim of this research is to provide additional information and knowledge about the potential relationship between the Oceanic Anoxic Event 1b (OEA 1b) and the first major planktonic foraminiferal turnover occurring at the late Aptian – early Albian interval. This objective will be accomplished using an innovative and multiproxy approach based on high resolution inorganic and organic geochemical analyses, together with micropaleontological and morphometrical investigations of the Poggio le Guaine section, an expanded and well stratigraphically constrained sedimentary succession from the Umbria-Marche Basin (Western Tethys paleo-domain). The late Aptian – early Albian sedimentary sequence from DSDP Site 511 will be used as "control section" to compare the microfaunal signals.

To achieve the overall aim of this thesis, the following specific objectives have been addressed:

i) Investigate the environmental perturbations linked to the OAE 1b, by reconstructing the evolution of oceanic anoxic conditions leading to the Jacob and Kilian black shales deposition, as well as the subsequent gradual restoring of normal oceanic oxic conditions.

ii) Investigate "if" and "how" the regional palaeoceanographic setting amplifies or mitigated the effects of global environmental changes.

iii) Assess the key features of the planktonic foraminifera evolutive turnover and discriminate which signals could represent biotic responses due to basin-scale factors.

iv) Provide new insights into the process which control the intermittent black shale deposition during the OAE 1b.

In a nutshell, Chapter 1 presents a general introduction on late early-Cretaceous climate and a brief review of the state of the art of knowledge on OAEs and in particular on OAE 1b.

Chapter 2 outlines the geological setting of the three sedimentary successions selected for this study, also providing the lithostratigraphic description and the biostratigraphic frameworks for each of them.

Chapter 3 describes the sampling strategies adopted in this study and provides a scheme of the micropaleontological and geochemical dataset produced. The detailed description of the used analytical techniques is also reported.

Chapter 4 offers details about the results of investigations conducted on PLG and GC sections, whereas the results of DSDP Site 511 are described in Chapter 5.

Chapter 6 provides the overall discussion that tie together the main results of this study, attempting to draw conclusions about the climate and ocean evolution and triggers of the OAE 1b, the major environmental changes linked to this multi-event, and the response of the planktonic foraminifera *Pa. rohri*, (considered as representative of Aptian taxa) to the environmental changes.

Chapter 2
Geological setting, litho- and biostratigraphy

2.1 Poggio le Guaine and Gorgo a Cerbara sections

The Umbria-Marche Basin is a Triassic to Messinian extensional basin developed in the northern offshore of the continental margin of the Apulia block, in the southwestern part of Tethys ocean. This basin experienced the pre-orogenic deformation linked to the northward movement of the Adria continental microplate from Africa relative to northern Europe, such as extensional normal faulting (Marchegiani et al., 1999) that resulted in the deposition of upper Jurassic – lower Miocene pelagic strata above the Triassic to lower Jurassic carbonate platforms. During the Neogene, the succession underwent tectonic inversion linked to the Alpine-Himalayan orogeny, and became part of the foreland fold-and-thrust belt of the Umbria Marche Apennines of central Italy. The Cretaceous sedimentary sequence of the Umbria-Marche Basin is now exposed in the outer part of the arcuate NE-verging northern Apennine fold and thrust belt, and it has been subdivided into four discrete formations: the Maiolica (upper Tithonian – lower Aptian), Marne a Fucoidi (lower Aptian – upper Albian), Scaglia Bianca (upper Albian – lowest Turonian) and Scaglia Rossa (lowest Turonian to middle Eocene) Formations.

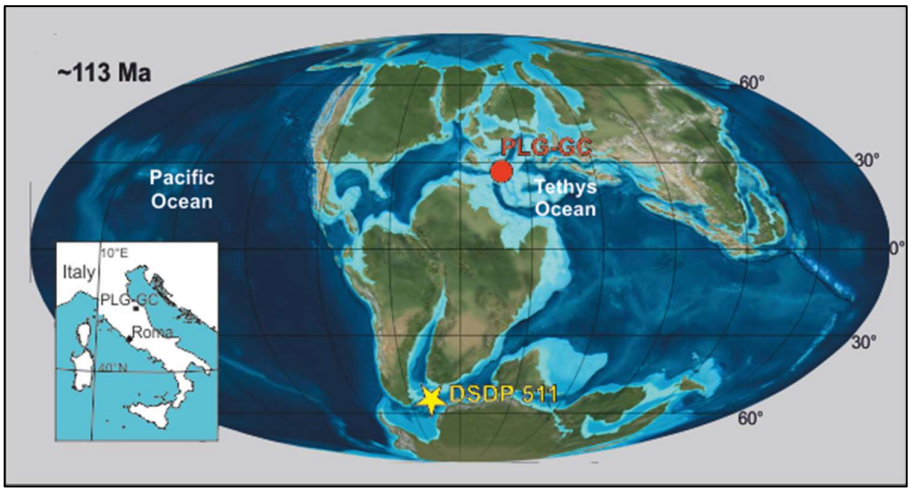

Fig. 2.1. Palaeogeographic map at ~113 Ma modified after Huber and Leckie (2011) showing the location of the Poggio le Guaine (PLG) and Gorgo a Cerbara section (red dots), and of DSDP Site 511 (yellow star).

The Poggio le Guaine (PLG) section (lat. 43°32'29.06" N, long. 12°34'51.09" E; Fig 2.1) is situated on the eastern limb of the Monte Nerone anticline, 500 m southwest of the PLG relief, 6 km west of the town of Cagli (Marche Region) (Fig 2.2).

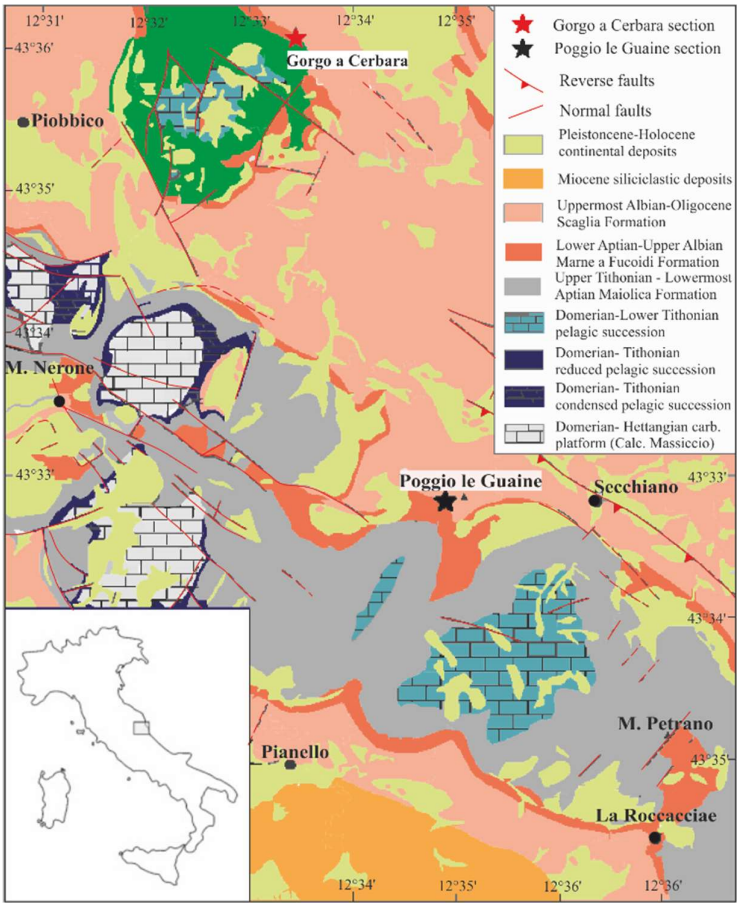

Fig. 2.2 Schematic geological map (modified from Satolli et al., 2008) of the study area and location of the studied section.

The Aptian – Albian succession of PLG belongs to the Marne a Fucoidi Formation and it deposited at well above the calcite compensation depth, at middle to lower bathyal depths (1000-1500 mbsl) (Coccioni, 1990), in a relatively isolated pelagic basin at ~20°N paleolatitude over the southern margin of the western Tethys Ocean (Coccioni et al., 2012, 2014). It consists primarily of pale reddish to dark reddish, and pale olive to greyish olive argillaceous limestones and calcareous marlstones, marlstones, slightly calcareous mudstones to argillaceous mudstones intercalated with several organic–rich black shales, some of which have been identified as the regional to global sedimentary expression of the anoxic sub-events of the OAE1b (Coccioni et al. 1987a,b; 1989a,b; 1990ab; 2006; 2012; 2014; Coccioni and

Battistini 1989; Erba et al. 1989; Coccioni 1996; Leckie et al. 2002; Trabucho Alexandre et al. 2011; Petrizzo et al. 2012; 2013; Kennedy et al. 2014; Sabatino et al., 2015).

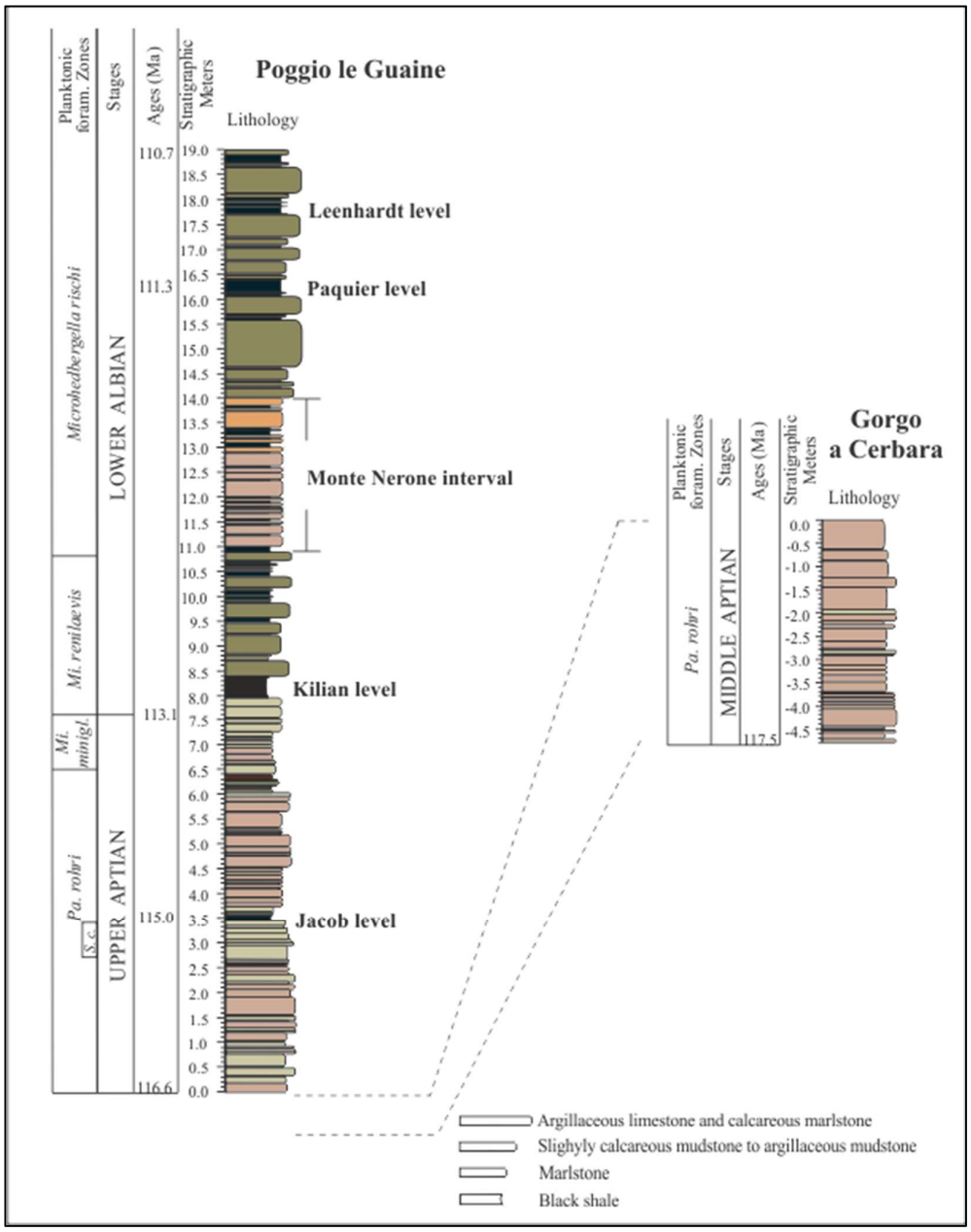

Fig. 2.3. Stratigraphy of the studied interval at Poggio le Guaine and Gorgo a Cerbara sections. Biostratigraphic and age data are from Coccioni et al. (2014) and Coccioni personal communications. Colours were estimated by visual comparison of samples with the Munsell color chart (Munsell, 1907). Dashed line indicates the stratigraphic relationship between the PLG and GC sections.

The Gorgo a Cerbara section (lat. 43°36'01" N, long. 12°33'16" E, Fig. 2.1) is located in the northeastern part of the umbro-marchean Ridge, 4 km east of the town

of Piobbico (Marche Region), along the Candigliano River (Fig. 2.2). The section crops out in the bed of the Candigliano River east of Monte Nerone, by the km 41.800 of the "Apecchiese" State Road N. 257 and belongs to the Maiolica, the Marne a Fucoidi, the Scaglia Bianca and the Scaglia Rossa Formations (Fig. 2.3). The Gorgo a Cerbara section has been proposed for the GSSP stratotype of the Barremian – Aptian boundary (Erba et al., 1996; Channell et al., 2000; Gradstein et al., 2012) and detailed magnetostratigraphy, chemostratigraphy, cyclostratigraphy, and biostratigraphy has been established by several authors (e.g. Herbert et al., 1995; Channell et al., 1995, 2000; Speranza et al., 2005; Tejada et al., 2009; Stein et al., 2011 Bralower et al., 1989, Coccioni et al., 1992, 2006, 2012; Erba, 1994, 1996; Patruno et al., 2015; Unida and Patruno, 2015; Li et al., 2016).

2.1.1 Lithostratigraphy of Poggio le Guaine section

The studied outcrop covers a 19 m thick succession of late Aptian – early Albian marine sediments with no physical evidence of unconformable surfaces, thus basically confirming the stratigraphic continuity of the section. Contacts between different lithotypes are sharp and planar, calcite veins are extremely rare, and no macroscopic diagenetic minerals were observed. Stratigraphic positions of samples are expressed in terms of distance from the base level (Figs. 2.3, 2.4).

The lower part of the section, from 0.00 to 3.40 m, is mainly composed by reddish argillaceous limestone and calcareous marlstone levels with thickness ranging from few centimetres up to 30 cm. The stiffer intercalated greenish-white limestone strata create prominent morphological break in the outcrop. Few thin layers of dark and soft marlstones occur at 0.5 m, 1.0 m, 1.4 m, 1.55 m, and 2.55 m (Fig. 2.4a).

At 3.46 m an abrupt contact marks the deposition of the organic rich black-shale level of the Jacob sub-event. This blackish interval is 10 cm-thick and does not show evidence of inner lamination. The Jacob level passes upward to soft dark greenish argillaceous marlstones, strongly laminated, with total thickness of 8 cm.

A monotonous series of pale reddish argillaceous and marly limestones starts at 3.65 m, without main sedimentary change for about 2.36 m. The only interruption are the sporadic beds of greyish marly limestones whose thickness do not exceed 10 centimetres.

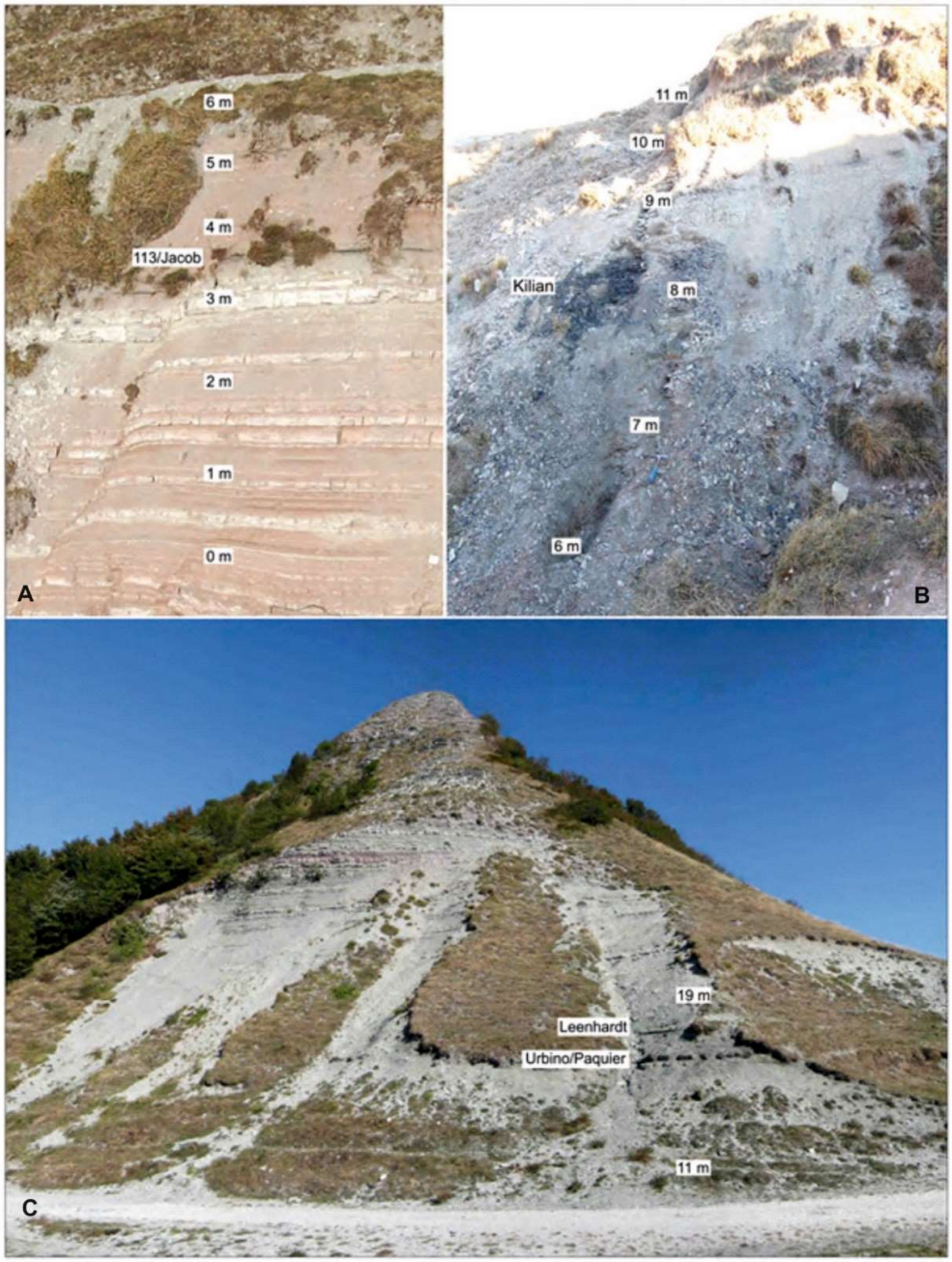

Fig 2.4. The Poggio le Guaine outcrop. A: lower part of the section from 0 to 6 m; B: section from 6 to 11 m; C: section from 11 to 19 m. Stratigraphical meters and the location of black-shale horizons are shown. (from Coccioni et al., 2014).

At about 6.00 m the lithology becomes gradually more clay-rich, and thin bedded, dark green and brown coloured argillaceous marlstones span over 40 centimetres (Fig. 2.4b). From ~6.50 m, the succession is characterised by argillaceous limestones with upward chromatic change from pale reddish to mainly pale olive levels. Also the thickness of the single strata changes in parallel with colour, increasing from initial 2-5 cm up to 20 cm at the quote of 7.30 m. Above this

interval, the 40 cm-thick (from 7.97 m to 8.37 m) black shales of the Kilian sub-event are characterized by very fine laminations (Fig. 2.5a), without evidence of bioturbation. Interesting, strata from 10 cm below and above the Kilian level contain small smudges and inclusions of black muds without isorientation (see Fig. 2.5b). Above the sharp boundary with the Kilian level, a rhythmic alternation of dark olive-greyish calcareous mudstone strata and blackish mud and shale horizons occurs, and the frequency of the muddy and shale layers increase upward.

Fig. 2.5. a: Detail of the Kilian black shale level showing the characteristic very fine laminations. b: small smudges and inclusions of black mud in strata below and above the Kilian black shale level.

The "Monte Nerone" interval (10.99 - 13.93 m) consists of about 3 m-thick alternation of pale reddish slightly calcareous mudstones, argillaceous mudstones and black shales. From 14.00 m upward, argillaceous limestones show again the grey-greenish coloration, and show decimetric thicknesses (Fig. 2.4c). The lithological expression of the Paquier sub-event is a 25cm-thick interval of organic-rich black shales (from 16.12 m to 16.37 m), distinctly laminated and with bituminous appearance. Between *ca* 16.38 m to 17.70 m grey-greenish argillaceous limestones are interrupted by sporadic beds of black clays thinner than 4.5 centimetres. From 17.71 m to 18.00 m, the 29cm-thick black shale of the Leenhardt sub-event is found. The lower part of the level (*ca* 10 cm) does not show any lamination despite the upper portion that shows an overall waxy and fissile appearance. Finally, from 18.00 m to the top of the studied section, the succession continues with grey-greenish argillaceous limestone strata interbedded with few levels of dark muds and shales.

2.1.2 Lithostratigraphy of Gorgo a Cerbara section

The studied interval of the Gorgo a Cerbara section (4.80 meters) belong to the Marne a Fucoidi formation and it is dominated by bioturbated dark-red marlstones and thick beds of red marly limestones (Figs. 2.3 and 2.6). Red-brownish calcareous shales occur in thin layers which are more common from -4.80 m to -3.70 m. Two centimetric layers of green-grey-coloured marly limestones interrupt the monotonous series of reddish lithologies at -2.00 and -2.80 meters. The correlation with the PLG section is based on the biostratigraphic observations on planktonic foraminifera assemblages carried out by Prof. Coccioni (personal communications).

Fig. 2.6. Alternation of marls, calcareous marls and argillaceous limestones of the *Paraticinella rohri* Zone at Gorgo a Cerbara section. Scale bars is 50 cm.

2.1.3 Biostratigraphy of the PLG-GC composite section

The plankton foraminifera biostratigraphy of the uppermost Aptian–lower Albian sedimentary sequence exposed at the Poggio le Guaine was reported in detail by Coccioni et al., (2014). Based on the biozonal schemes of Huber and Leckie (2011) and of Petrizzo et al. (2012), the authors identified different major events that, along

with minor bioevents, allowed the subdivision in 4 biozones. The terminology of lowest occurrence (LO) and highest occurrence (HO) is here used to delineate the appearance and disappearance of taxa. The major bioevents identified at the PLG section are:

1) HO of *Paraticinella rohri* at 6.50 m (= *Ticinella bejaouaensis* in Herrle et al. 2004, and *Paraticinella eubejaouensis* in Huber and Leckie 2011, and McAnena et al. 2013);

2) LO of the planktonic foraminifera *Microhedbergella renilaevis* at 7.6 m;

3) LO of the planktonic foraminifera *Microhedbergella rischi* at 10.8 m.

The minor bioevents identified are:

1) HO of the planktonic foraminifera *Pseudoplanomalina cheniourensis* at 1.9 m;

2) LO of the benthic foraminifera *Pleurostomella subnodosa* at 2.3 m;

3) acme of the planktonic foraminifera *Schackoina cepedai* from 2.7 m to 3.4 m;

4) LO of the planktonic foraminifera *Microhedbergella miniglobularis* at 6.42 m;

5) LO of the planktonic foraminifera *Microhedbergella praeplanispira* at 11.53 m;

6) the LO of the planktonic foraminifera *Microhedbergella pseudoplanispira* at 12.1 m.

The horizons corresponding to the 3 main bioevents have been used as horizons boundary of the following planktonic foraminiferal biozones:

1) the *Paraticinella rohri* Total Range Zone (that is the *Ticinella bejaouaensis* Zone of Robaszynski and Caron 1995, and the *Paraticinella eubejaouensis* Zone of Huber and Leckie 2011), from the base of the section to the HO of *Pa. rohri* at 6.50 m (see Appendix 1);

2) the *Microhedbergella miniglobularis* Interval Zone spans from the HO of *Pa. rohri* to the LO of *Mi. renilaevis* recorded at 7.60 m (see Appendix 1);

3) the *Microhedbergella renilaevis* Partial–range Zone corresponding to the stratigraphic interval from the LO of *Mi. renilaevis* to the LO of *Mi. rischi* (see Appendix 1), and lastly

4) the *Microhedbergella rischi* Total–range Zone, comprising the stratigraphical interval from the LO of *Mi. rischi* to the top of the section (see Appendix 1).

The lowest occurrence of *Pa. rohri* at -4.8 m in the Gorgo a Cerbara section was identified by Coccioni (unpublished biostratigraphic data).

Estimated ages for the studied section are inferred after Grippo et al. (2004), Huang et al. (2010), Ogg and Hinnov (2012) (GTS 2012), and Ogg et al. (2016) (GTS 2016).

2.2 DSDP Site 511

Cretaceous cores from DSDP Leg 71 Site 511 (51°00.28′S, 46°58.30′W; Fig. 2.1) were drilled on the back slope of a cuesta-type ridge in the basin province of Falkland Plateau (southwest Atlantic Ocean), about 10 km south of Maurice Ewing Bank (Ludwig et al., 1983; Plancq et al., 2014; Fig. 2.7, Tab 2.1).

Fig. 2.7 Actual ubication of the DSDP Site 511 (red dot) and main physiographic features of the area.

The Falkland Plateau extends eastwards off southernmost South America, and is bounded by the Falkland Island Platform to the west, the narrow ridge of Falkland Escarpment to the north and by the Falkland Trough and North Scotia Ridge to the south. The occidental portion of the plateau is a segment of oceanic crust (or thinned continental crust) overlaid by a 4-6 km thick sediment wedge, gently dipping southward. During the Jurassic to middle Cretaceous this site was located at about 60°S in a relatively narrow est-west trending ocean basin that had limited or no connection with the South Atlantic (Hay et al., 1999; Huber and Leckie, 2011). Paleowater depth has been estimated to have been between 100-400 m (Basow and Krashenninikov, 1983). Open marine conditions were probably established by the early Albian, and rapid subsidence leaded to a progressive deepening of the basin resulting in the deposition of pelagic clays rich in planktonic fossils (Huber et al., 1995).

Tab. 2.1. Technical data of the DSDP Site 511 coring

DSDP Site 511	
Leg	71 (15 – 21 January 1980)
Coordinate	51° 00.28'S, 46°58.30'W
Water depth	2586 m
Penetration	632 m
Number of Core	70
Meters cored	632
Meters recovered	385.62
Percentage recovered	61

2.2.1 Lithostratigraphy of DSDP Site 511

The sediments assigned to upper Aptian – early Albian interval of the DSDP Site 511 (Core 55 Sect. 2 – 6 and Core 56 Sect. 1-3, from 482.00 to 493.20 m sub-bottom) correspond to the Unit 5 descripted by Ludwig et al. (1981). The lithology is mainly composed of light-grey to dark grey claystone and mudstone with subordinate amounts of brownish mudstone. In many cases, colours appear to grade from the lightest to the darkest (Fig 2.8), suggesting some gradational environmental change. The darker intervals that rhythmically occur in Core 56 Sect. 2 and 3, coincide with higher content of clay and in place are very fissile.

The moderate to intense bioturbation is a common feature to most samples, and mainly consist of burrows filled with matrix of lighter colour compared to that of the surrounding sediment.

Pyrite is widespread in most of the samples, in the form of macro-aggregates of prismatic crystals, scattered loose aggregate of octahedral micro-crystals, small framboidal spheres, or as long solid or hollow rods which resemble the pyritic "worm tube" described by Siesser and Rogers (1976).

Layers of skeletal carbonate macro-debris, principally pelecypods occur frequently as muddy microcoquinas. Single, thin, whole pelecypod valves (e.g. *Aucellina*) occur as well throughout the unit, and a small rytholite was also found in Core 55 Sect. 5 interval 5.0-8.0 cm (485.76 msb). Almost all the samples contain calcite in the form of mollusc shell prims which are probably from *Inoceramus*, and that are often concentrated in thin bands.

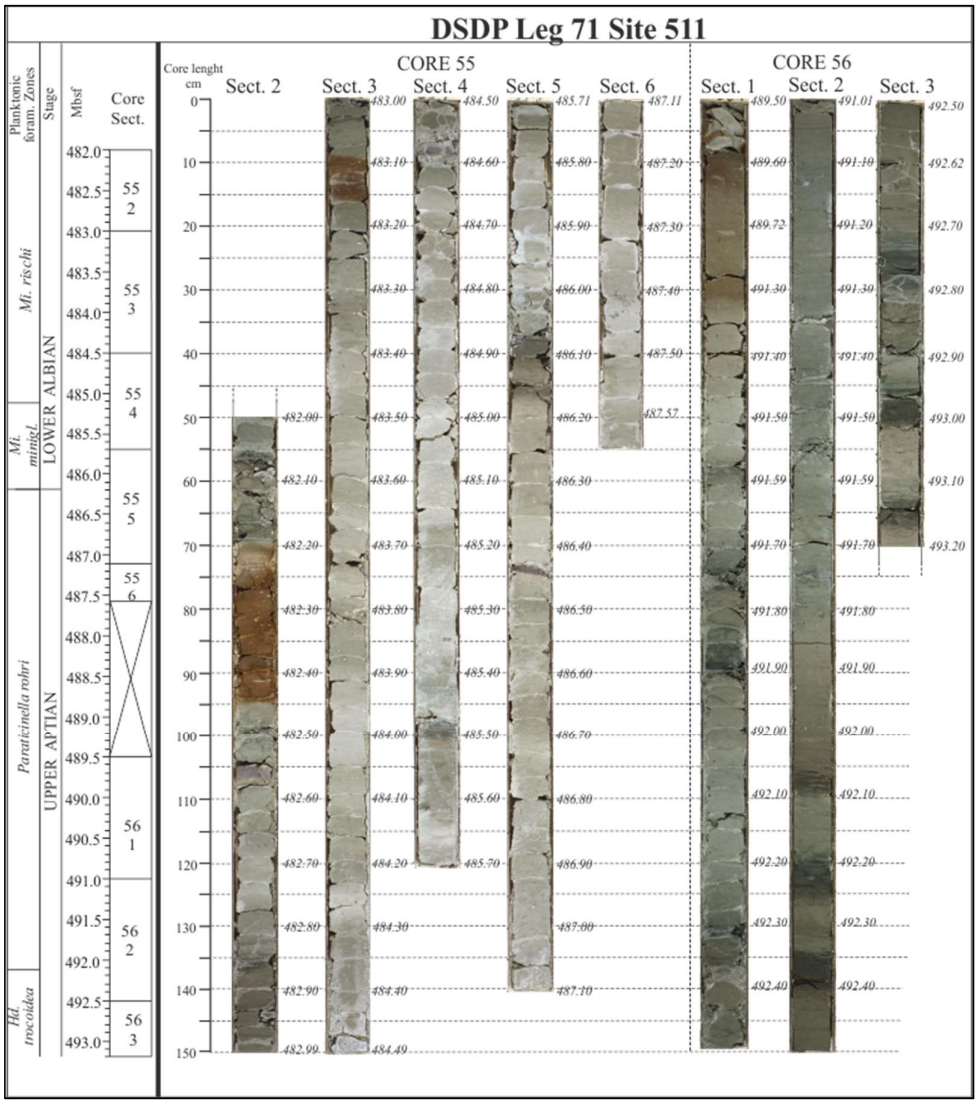

Fig. 2.8. Biostratigraphic scheme and photographs of the upper Aptian – early Albian cored interval from DSDP Site 511. The interval comprises sediments from Core 56 Section 3, 70-72 cm to Core 55 Section 2, 50-51.5 cm. (From Ludwig et al., 1983; Huber and Leckie, 2011).

2.2.2 Biostratigraphy of the DSDP Site 511

The biostratigraphic framework adopted in this study for the DSDP Site 511 is based on the reference scheme proposed by Huber e Leckie (2011). On the basis of a sampling resolution varing from 1-150 cm, the authors identified the LO of *Pa. eubejaouaensis* (= *Pa. rorhi* in this study and *Ticinella bejaouaensis* of Herrle et al., 2004; see Appendix 1) at 491.23 mbsf. This horizon marks the base of the *Pa. eubejaouaensis* Taxon Zone, characterized by the occurrence of the nominated taxon along with several specimens of *Pa. transitoria*, *Hedbergella excelsa*, *Hd. aptiana*, *Hd. praelippa* e few specimen of *Hd. infracretacea*. The LO of *Microhedbergella miniglobularis* is recorded at 486.70 mbsf (see Appendix 1), and

hence *Pa. eubejaouaensis* and *Mi. miniglobularis* co-occur in a very short stratigraphic interval, which is similar to observation made by Coccioni et al. (2014) at Poggio le Guaine (Umbria-Marche Basin). The upper boundary of the biozone is marked by the HO of *Pa. eubejaouaensis* at 486.14 mbsf, coinciding with the biotic turnover level of planktonic foraminifera and in coincidence of which Huber and Leckie (2011) place the Aptian/Albian boundary. From this horizon upward, PF assemblages decrease in maximum diameters and species diversity. The overlaying *Mi. miniglobularis* Zone spans from the HO of *Pa. eubejaouaensis* to the LO of *Mi. rischi* at 484.75 mbsf (see Appendix 1). This ~1 m -thick biozone comprises the evolutionary transition from *Mi. miniglobularis* to *Mi. renilaevis*, and the extinction of *Hd. praelippa*. The stratigraphic interval from the LO of *Mi. rischi* to the highest studied sample (482.00 mbsf) belongs to the *Mi. rischi* Partial-range Zone. In the lower part *Mi. miniglobularis* decreases in abundance and then becomes extinct, while Mi. renilaevis becomes increasingly abundant.

The high-resolution micropaleontological observations conducted in this study and the low abundances of planktonic foraminifera along the sedimentary sequence, may slightly change the exact position of some bio-events respect to those reported by Huber and Leckie (2011), as the case of the LO of *Pa. eubejaouaensis*, (at 491.23 mbsf for Huber and Leckie (2011), at 492.10 mbsf in this study).

Chapter 3
Materials and Methods

3.1 Sampling strategy and data sets

3.1.1 Poggio le Guaine and Gorgo Cerbara sections

This study stays in a framework of three decades of dedicated and detailed stratigraphic research on the Poggio le Guaine section (Arthur and Premoli Silva 1982; Coccioni and Cocon 1987; Coccioni et al. 1987a; 1987b; 1989a,b; Erba, 1988; Coccioni and Battistini 1989; Erba et al., 1989; Tornaghi et al. 1989; Coccioni, 1990; Coccioni et al. 1990a; 1990b; 1991; 1992; Coccioni and Galeotti 1993; Ingram et al. 1994; Coccioni 1996; Baudin et al. 1998; Coccioni et al., 2006; 2012; Fiet and Masure 2001; Satolli et al. 2008; Tiraboschi et al. 2009; Turchyn et al. 2009; Coccioni et al., 2014; Sabatino et al., 2015). This offered the opportunity to start with a large pre-existing dataset and i) to implement knowledge by increasing sampling resolution in specific intervals and ii) enriching the dataset with a new spectrum of chemical/micropaleontological analyses.

The scheme in Figure 3.1 offers a graphical view of the micropaleontological and geochemical dataset produced for the composite section Poggio le Guaine – Gorgo Cerbara.

The main aim of this study was to investigate the potential relationship between the environmental evolution associated to the Oceanic Anoxic Event 1b (OEA 1b) and the first major planktonic foraminiferal turnover occurring at the late Aptian – early Albian interval. To achieve that, new investigation, at high resolution, of the environmental changes potentially related to the Oceanic Anoxic Event 1b (using a multiproxy and innovative approach) provided new constrain for reconstructing the palaeoceanographic evolution of the studied geological interval in term of i) variations in deep-water oxygenation and productivity, and ii) the role of ecological stressors on the evolutionary behaviour of planktonic foraminiferal community.

The stratigraphic interval encompassing the PF turnover (from 3.00 m to 9.00 m) was chosen as primary "target interval" for all the geochemical investigation. The $\delta^{13}C$ and $\delta^{18}O$ isotope stratigraphy, and $CaCO_3$ content provided by previous works

of Coccioni et al. (2014) and Sabatino et al., (2015) cover the entire section of Poggio le Guaine at centimetric resolution (from 5 cm to 1 cm in proximity of crucial levels), and therefore they didn't require any implementation. To assess the correct correspondence between the previously logged section and the new one, all the data were re-calibrated by correlating markers beds (e.g. black shales levels).

Elemental geochemistry analyses (Al, Ba, Cd, Co, Cr, Cu, Fe, Hg, K, Mg, Mn, Ni; P, Pb, Sr, Ti, V, Zn, Zr) were carried out for the "target interval" with resolution ranging from 10 to 2 cm, in order to improve the lower sampling resolution reported by Sabatino et al. (2015) for this interval. Samples comprise black-shales of Jacob and Kilian sub-events, marly limestones and argillaceous marlstones.

The biomarkers investigation was carried out on the Poggio le Guaine section. In the absence of previous data in literature, a total of 59 samples was selected along the 19 m-thick section, in order to fully reconstruct the palaeoceanographycal changes linked to all the sub-events of the OAE 1b. Higher resolution was adopted in the "target interval", with sample spacing from 2 cm in black shales levels to 20 cm in the argillaceous limestone – marlstone intervals. An average resolution of 60 cm was adopted for the marly limestone from 0.00 to 3.00 meters. These represent "control samples" with low contents of organic matter and recording the environmental conditions predating the onset of the OAE 1b. In the upper part of the section, from 9.00 m to 19.00m, samples were taken from the organic-rich black-shale levels.

A higher resolution with respect to the previously reported TOC dataset (Coccioni et al., 2014; Sabatino et al., 2015) was achieved by analysing further 64 samples from the "target interval" and from the specific black shale level in the upper part of the section. More specifically, black-shales of the Jacob and Kilian sub-events were sampled every 2 cm and marly limestones and marls of the "target interval" were selected every 10 cm. From 9.00 and 19.00 meters, samples were selected in order to identify a good correspondence with the samples used for the organic biomarkers analysis.

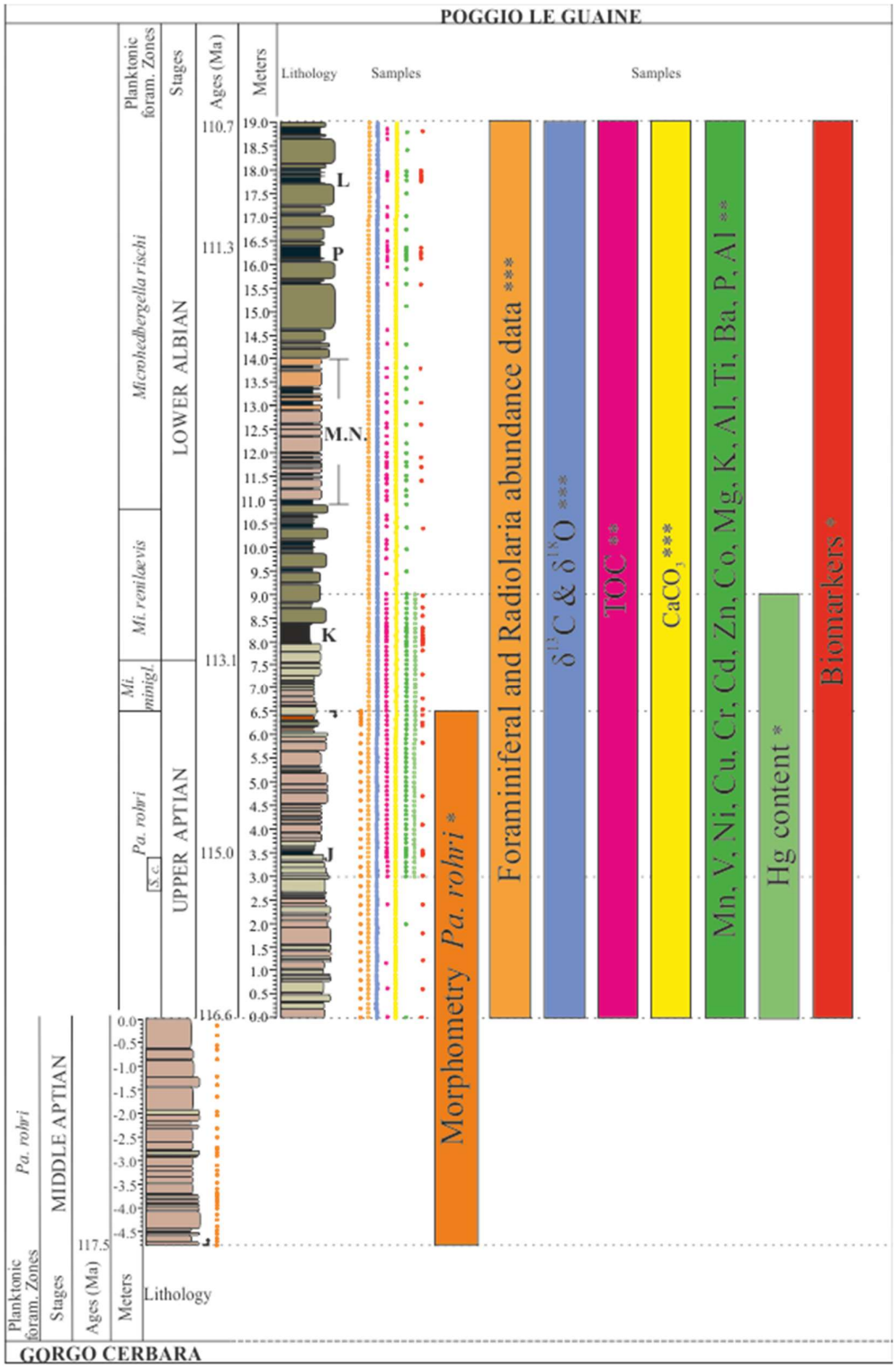

Fig. 3.1. Graphical scheme of data sets collected during the three-years doctoral research and samples positioning along the composite-log Gorgo Cerbara – Poggio le Guaine. Keys to symbols and abbreviations: J: Jacob sub-event; K: Kilian sub-event; M.N.: Monte Nerone black-shales interval; P: Paquier sub-event; L: Leenhardt sub-event; Up arrow: LO of *Pa. rohri*; Down arrow: HO of *Pa. rohri*; *: new dataset produced in this study; **: data set from Coccioni et al. (2014) and Sabatino et al. (2015) implemented in this study; ***: data set from Coccioni et al. (2014) and Sabatino et al. (2015).

Finally, the planktonic and benthic foraminiferal and radiolarian assemblages were investigated along the "target interval". This allowed the positioning along the section of the major foraminiferal bioevents previously identified by Coccioni et al. (2014). The documentation of magnitude and rate of microfaunal turnover across the AABI is based on micropaleontological observations conducted on the target interval with a resolution of 1 sample every 4 cm, and on high resolution abundance data reported in Coccioni et al. (2014).

3.1.2 The morphometrical investigation on Pa. rohri: aims and sampling strategy

After the assessment of the palaeoenvironmental framework and the definition of the turnover event in the microfaunal assemblaeges, it was necessary identify a planktonic foraminifera taxon which would best represent the effect of biotic crisis, until the final extinction, of the late Aptian, and also permitting worldwilde stratigraphic correlations. Among all the possible candidates, *Paraticinella rohri* best fitted specific requisites. In particular, *Pa. rohri* is a large-sized, heavy ornamented, and thick-walled taxon (see Appendix 1), very abundant in most of PLG samples, and its presence is reported in several coeval sections such as the Vocontian Basin (Southeastern France; Petrizzo et al., 2012), the North (ODP Sites 1049, DSDP Site 390 and 39, ODP Site 545; Huber and Leckie, 2011) and South (DSDP Sites 511; Huber and Leckie, 2011) Atlantic Ocean, and the South Indian Ocean (ODP Site 763, Huber and Leckie, 2011).

Morphometric analyses were carried out on picked specimens of *Pa. rohri* going backwards from its highest occurrence (HO) at 6.50 m in the section. The sampling strategy for picking was one sample every 20 cm, in order to ensure an average temporal resolution of ~20 ky based on the age model and sedimentation rates estimated by Coccioni et al. (2014). In proximity of significant morphological and/or abundance changes, sample frequency was enhanced until 1 cm (e.g. from 6.23 to 6.50 m). The 4.8 m belonging to the middle Aptian of Gorgo Cerbara section were also analysed for picking of *Pa. rohri* specimens, allowing to complete and fully describe the total range of this taxon, from its lowest occurrence (LO at -4.8 m at Gorgo Cerbara) to its extinction (HO at 6.5m at PLG). The sampling criteria in GC section were identical to those adopted for PLG section: minimum resolution

20 cm and higher resolution, until 1 samples/5 cm in correspondence of significant and/or *Pa. rohri*-barren intervals.

3.1.3 DSDP Site 511

As already stated, this study wants to assess "if" and "how" the oceanic anoxic event 1b (OEA 1b) influences the major planktonic foraminiferal turnover occurring at the late Aptian – early Albian interval. For this purpose, data collected from the Tethyan sedimentary successions of PLG and GC necessarily required the comparison and correlation with coeval records from different palaeo-domains, in order to discriminate signals representing biotic responses due to basin-scale factors, as basin physiography, sea-connections, proximity to continents, ecological niches, from signal that could be related to global evolutionary process. The study of the DSDP Leg 71 Site 511, appropriate for its continuous and well-preserved record for the upper Aptian – early Albian interval, offered a great chance to record the morphometric changes of *Pa. rohri* in a the South Atlantic paleodomain. Based on the planktonic foraminifera biostratigraphic ranges reported by Huber and Leckie (2011), 10 to 5 cm-spaced samples from Core 55 – Section 2 to Core 56 Section 3 (overall 11 meters) were requested to the IODP Core Repository of the University of Bremen, and, because of a gap due to the partial recovery of Core 55 – Sect. 6, only 125 samples were received.

The Figure 3.2 provide a simple scheme of the sampling strategies adopted for DSDP Site 511.

All the samples were processed for micropaleontological observations in order to identify the major planktonic foraminifera bioevents. All the samples belonging to the *Pa. rohri* Total Range Zone were analysed to pick-up the *Pa. rohri* specimens object of morphometric analysis.

The analysis of microfossils assemblages and the relative percentages of planktonic and benthic foraminifera, and radiolarian were estimated with a sampling resolution of about 20 cm, in order to ensure the regular control of biotic fluctuations through the section.

Finally, stable carbon and oxygen isotopes and the total organic carbon content were measured in all the samples.

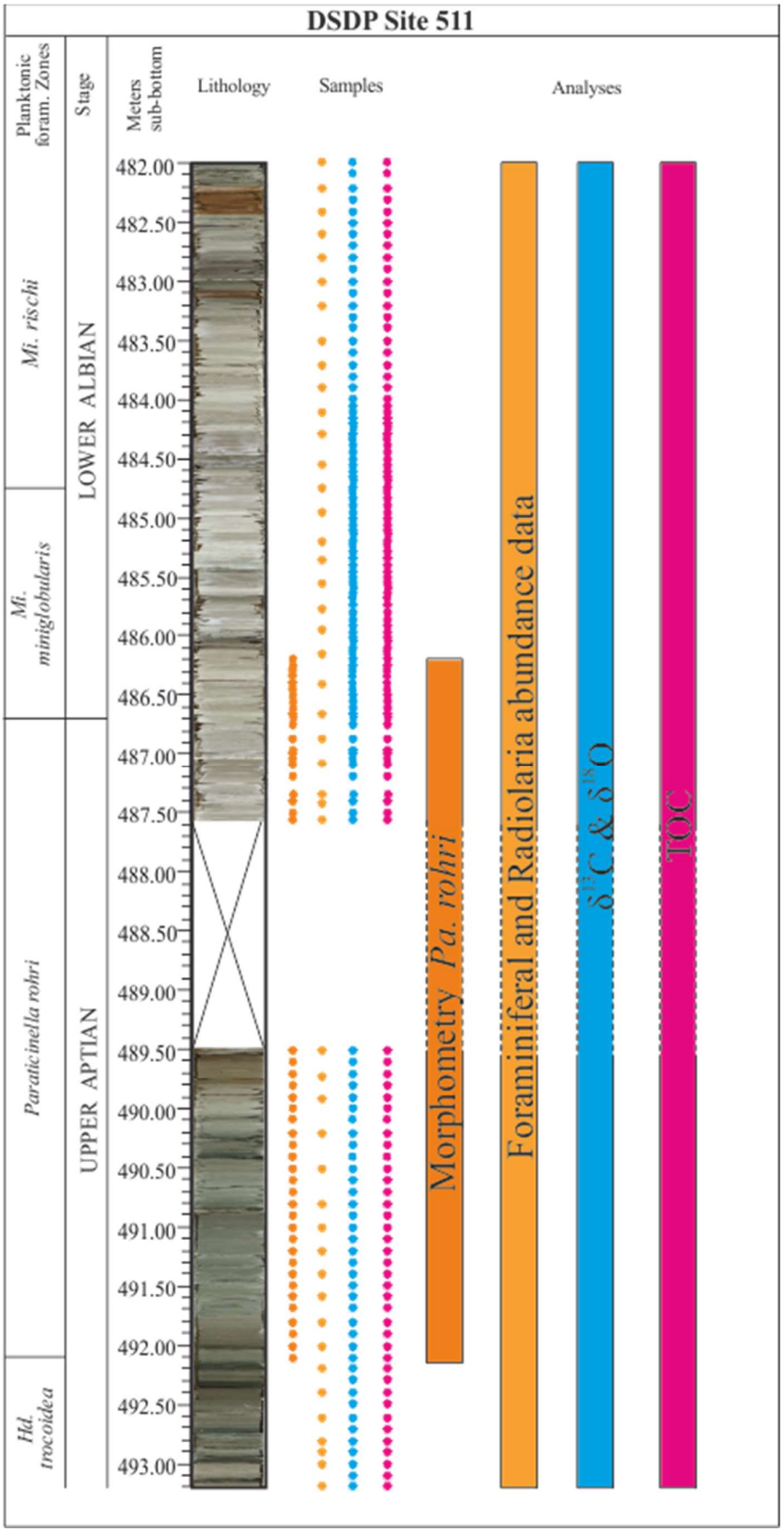

Fig. 3.2. Graphical scheme of data sets collected and sampling strategies adopted for the Core DSDP Site 511.

3.2 Methods

3.2.1 Micropaleontologycal Analysis

Samples preparation of Poggio le Guaine and Gorgo a Cerbara samples

Samples from the target interval of Poggio le Guaine section were treated following the modified cold acetolysis technique of Lirer (2000). This method consists in the mechanic disaggregation of the lithic samples in smaller fragments (~5mm), a soaking in acetic acid (80%) for 4-6 hours (according to the marly or carbonate nature of the bulk), washing under running water through a 45μm sieve, and finally drying on a hot plate. In case of residual encrustation and clay material, the residue was dipped again in a solution of Desogen and water for some hours, and then re-washed and dried on hot plate. This technique allows to extract planktonic foraminifera, as well as benthic foraminifera, Radiolaria, and other microfossils, without destroying and corroding fossil content.

Sample preparation of Core DSDP Site 511 samples

The poor lithified sediments from Core DSDP Site 511 did not require any acid or mechanic disaggregation. All 125 samples were oven-dried at 50°C for 24 hours, soaked in distilled water, and then wet sieved at 45 μm mesh.

Abundance data

Planktonic and benthic foraminiferal and radiolarian abundances were calculated in the > 63 μm fraction of PLG section by Coccioni et al. (2014).

All the samples of Core DSDP Site 511 were observed to evaluate the assemblage composition and to identify significant biostratigraphic events. Samples were also dry-sieved through 355 μm, 250 μm, 180 μm, 100 μm, and 80 μm mesh and abundance data of planktonic and benthic foraminifera and Radiolaria, were estimated in the obtained six fractions (>355 μm, 355-250 μm; 250-180 μm; 180-100 μm, 100-80 μm; 80-45 μm).

Tests showing > 50% fragmentation were excluded from the specimen counts. The planktonic foraminiferal framework used and the species concepts adopted in this study follow Coccioni et al. (2014), Huber and Leckie (2011), Petrizzo et al. (2012) and the CHRONOS online Mesozoic taxonomic dictionary located at http://portal.chronos.org with references therein. Additional reference to the

taxonomic notes of Ando et al. (2013) was also made. Herein we use the terminology of lowest occurrence (LO) and highest occurrence (HO) to delineate the appearance and disappearance of taxa.

Morphometry of Pa. rohri

About 100 samples from PLG and GC sections were analysed for the hand-picking of *Pa. rohri*, with a sample spacing varying from 20 to 1 cm (see paragraph 3.1) depending on proximity to significant levels, such as the black shale interval of the Jacob sub-event or the LO and HO of *Pa. rohri*. Samples with abundant occurrence of *Pa. rohri* were splitted to obtain aliquots with at least 100 specimens; where *Pa. rohri* was present in low percentages, the entire sample was observed and all the specimens picked up.

All the samples falling in the *Pa. rohri* Total Range Biozone of the DSDP Site 511 section were analysed for the hand-picking. Because of the low abundances of planktonic foraminifera in these sediments, residues were not splitted, and all the encountered specimens picked-up.

For both sections, test size changes across the *Pa. rohri* Total Range Biozone were obtained by manual measuring of the maximum test diameters of minimum 100 specimens (or less in case of low abundances of this species) in each sample, using a Zeiss Discovey V20 stereo-microscope and the software AxioVision SE64 Rel.4.8. For each sample, the size variability of the population was also estimated by evaluating the standard deviation (σ) from the mean diameter value. The analytical error was estimated by repeating 100 time the manual measurement of the same specimen, obtaining a value of ±2.31 μm.

3.2.2 Inorganic geochemistry

3.2.2.1 Stable Carbon and Oxygen isotopes analysis

Coccioni et al. (2014) and Sabatino et al. (2015) report the stable carbon e oxygen isotope composition of 155 bulk samples from Poggio le Guaine Section. In this study, data from 3.00 m to 9.00 m are considered.

All the 125 samples of Core DSDP Site 511 were analysed for carbon and oxygen stable isotopes using an automated continuous flow carbonate preparation GasBench II devise (Spötl and Vennemann, 2003) and a ThermoElectron Delta V Advantage mass spectrometer at the geochemistry laboratory of IAMC – CNR of

Capo Granitola. Dried samples were grounded using an agata mortar. The acidification of the samples was performed at 60 °C. Replicate measurements of NBS19 international standard ($\delta^{18}O$ = – 2.20 ‰ versus VPDB and $\delta^{13}C$ = + 1.95 ‰ vs. VPDB) yielded reproducibility better than 0.06 and 0.1 ‰ for carbon and oxygen isotope measurements, respectively.
All the isotope data are reported in δ‰ vs. VPDB

3.2.2.2 Elemental geochemistry

Major and trace elements

A total of 65 samples from Poggio le Guaine section was selected for the determination of major and trace elements by inductively coupled plasma optical emission (ICP-OES).

Sample preparation

Acid digestion procedure was employed to completely transfer the analytes of samples into solution, so they can be introduced into the determination step (ICP-OES) in liquid form. This digestion was produced by placing about 250 mg of sample (previously dried and homogenized) in Teflon closed pressure vessels with an acid mixture (2 ml H_2O_2, 8 ml HNO_3, 3 ml HCl, 1.5 ml HF) at T = 220 ± 5 °C for 90 min using a Mars 5 CEM Digestion Microwave System at the IAMC-CNR geochemistry laboratory of Naples. Subsequently, a solution of boric acid (H_3BO_3 4%) was added to buffer the hydrofluoric acid. After cooling, the resulting solution was filtered (0.45 μm) and diluted to 100 ml with ultra-pure water. A second dilution (1/20) was performed prior to analysis. Reference standard materials (PACS-2, BCR-2), reagent blanks and duplicated samples were also prepared.

Instrumental analysis: inductively coupled plasma optical emission (ICP-OES)

All the digested samples were analysed by inductively coupled plasma optical emission at the IAMC-CNR geochemistry laboratory of Capo Granitola. Reference standard materials (PACS-2, BCR-2), reagent blanks and duplicated samples allowed to assess accuracy (estimated between 90–110%), detection limits, precision (routinely better than 6%; RSD%, n = 3), and the reproducibility (better than 93% for all elements) of the analyses. Major elements are given in weight percent (wt%), minor elements in parts per million (ppm). Elemental values were

normalised to Al in order to account for dilution effects by potential biogenic components such as carbonates, silica, and phosphorites. To obtain further information, concentrations of trace metals (TM) were compared to the average shale values (AS) of Wedepohl (1971, 1991).

Total mercury content

Hg analyses were conducted in 64 samples (one for every ~10 cm) selected in the stratigraphic interval between 3.00 and 9.00 meters of Poggio le Guaine section (target interval). Hg content was determined at the IAMC-CNR geochemistry laboratory of Capo Granitola using an atomic absorption spectrophotometer specifically designed for Hg determination (Milestone_DMA-80; US-EPA 7473). Measurement are based on the direct thermal evaporation of Hg from solid matrix and do not require chemical pre-treatment of samples, thus avoiding potential contaminations during sample preparation. The accuracy of ~8% was assessed by the analysis of a Reference Standard Material (PACS-2 Marine sediment, NRCC). Excellent correspondence to the certified values was obtained with a precision routinely better than 6.5% and a standard residual deviation (RSD) of 4%. Analysis were conducted on duplicate samples (about 20% of the total number of samples) to estimate reproducibility, which was better than 7%.

3.2.3 Organic Geochemistry

3.2.3.1 Total Organic Carbon (TOC) analysis

Total organic carbon (TOC) analysis were carried out on 75 samples selected from PLG section (64 samples from the "target interval", 11 samples from the rest of the section) to integrate the dataset reported by Sabatino et al. (2015), and on 50 samples selected from Core DSDP Site 511. About 15 mg of powdered bulk sample was weighted into silver cups and then acidified using HCL 1M for 24h at ambient temperature to remove all $CaCO_3$. When reaction stopped, samples were dried in an oven at 60°C for 24 hours before loading the cups into the autosampler. TOC analysis was carried out using a Thermo Electron Flash EA 1112 at the IAMC-CNR isotope geochemistry laboratory of Capo Granitola. Analytical errors for TOC were generally better than 0.2%.

3.2.3.2 Organic biomarkers analyses

Organic biomarkers analyses were carried out during a 3 months internship at the Organic Geochemistry Unit (OGU) at the University of Bristol, thanks to a collaboration with Prof. R.D. Pancost and Dr. B.D.A. Naafs.

A total of 59 samples was selected from the entire Poggio le Guaine section, encompassing all the sub-events of OAE 1b.

Sample preparation

59 dried powdered rock samples (about 30 g) were Soxhlet extracted for 24h with 220 ml solvent mixture of dichloromethane: methanol 9:1 (v/v). Activated copper cuttings were added to the round-bottom flasks to adsorb free elemental sulphur during extraction. The Total Lipids Extract (TLE) was obtained by removing the solvent with a rotary vapor a 40°C. Subsequently, the TLE extract was taken up in a small amount of DCM:MeOH (9:1 v/v) and evaporated to dryness under N_2. As internal standard, a mixture of 5-androstane (214.9 ng/ul) and Hexadecanol (207.4 ng/ul) was added to the TLEs. The TLEs were separated in apolar and polar fractions through a column chromatography using a glass Pasteur pipette plugged with clean cotton filter and filled with SiO_2 (Sigma-Aldrich, 100-200 mesh, 75-100 mm, pore diameter 30 Å) activated for 2.5 h at 150°C. As eluents, 4ml hexane/DCM (9:1, v/v) and 4 ml methanol/DCM (2:1, v/v) were used for apolar and polar fractions, respectively. Fractions were collected in clean vials; the elution solvents were careful evaporated to dryness under a gentle stream of N_2 and the eluted fractions of each extract were dissolved in 100 µl n-hexane. A total of 8 blanks were also prepared to verify the occurrence of accidental contamination during samples preparation.

Instrumental analysis: gas chromatography – mass spectrometry (GC-MS)

GC-MS analysis was conducted with a Thermo Scientific Trace 1300 gas chromatography equipped with a Restek Rtx-1 GC non-polar column of fused silica (length 50 m, interior diameter 0.32 mm; film 0.17 µm; dimethyl polysiloxane equivalent) coupled to a Thermo Scientific ISQ LT Single Quadrupole Mass Spectrometer (electron voltage, 70 eV; emission current, 50 µA;). Helium was used as carrier gas and 1µl of each sample was introduced via an on-column injector.

The GC oven was set to 300 °C and the ion source at 200°C. The temperature was programmed as follows: initial temperature was held at 70°C for 1 min, followed by a ramp to 130°C at 20°C/min, then a second ramp to 300°C at 4°C/min, held for 24 min isothermal. The mass spectrometer continuously scanned between m/z 50 and 650 with a dwelling time of 0.2 second per scan.

Instrument control and data acquisition was carried out using Thermo Xcalibur software (v. 3.0). Apolar fraction were analysed using the MS in total ion current (TIC) scan range m/z 50-650 with a dwelling time of 0.2 second per scan.

Quality Control Procedures

Before analysing, the instrument was tuned and calibrated by injecting different concentrations of specific standard sample. Obtained result showed acceptable RSD% and mass deviation, and confirms the linearity of the method. Linearity of the method was verified by injecting different amounts of prepared sample. Obtained results showed acceptable RSD% and mass deviationof these six analyses for major and minor constituents and confirms the linearity of the method. Because response factors change with instrument conditions, and to verify optimum operating conditions blanks and FAMEs were run periodically.

Identification and quantitation of compounds

The identification of individual compounds using mass chromatograms was achieved by comparison of GC/MS retention times of identified peaks to the co-injected internal standard, mass spectra published in scientific papers and MS data base libraries.

Quantitation of compounds in samples was obtained through electronic integration of the peaks and comparison with the area of co-injected standards on specific mass chromatograms (*m*/*z*). The amount of each compound (A_{comp}) is calculated as:

$$A_{comp}\ (ppm) = \frac{(area\ peak_{Comp.}) \cdot (A_{St}) \cdot (response\ factor)}{area\ peak_{standard}}$$

where:

A_{St} is the amount of standard added to samples, and

$$response\ factor = \frac{(area\ peak_{standard}/A_{comp})}{(area\ peak_{Comp.}/A_{St})}$$

In this study, concentrations are reported as relative amount, estimated as µg compound / g TOC.

Chapter 4
Results from PLG and GC sections

4.1 Planktonic foraminiferal bioevents and remarks on microfaunal assemblages

The qualitative and quantitative micropaleontological analysis of this study allowed the detailed documentation of the microfaunal contents across the "target interval" from Poggio le Guaine section. The abundance data here used are from Coccioni et al. (2014). Planktonic foraminifera occur in almost all the samples, with relative abundance fluctuations generally accompanied by significant changes in the carbonate content.

The base of the target interval falls in the *Paraticinella rohri* Total-range Zone (Coccioni et al., 2014; corresponding to the *Ticinella bejaouaensis* Zone of Robaszynski and Caron, 1995, and the *Paraticinella eubejaouensis* Zone of Huber and Leckie, 2011). From 3.00 m to 6.2 m, planktonic foraminifera dominate the faunal assemblages, with percentages up to 97% and average value of 21%, except for few samples slightly above the black shale horizon of the Jacob sub-event in which percentages temporarily decrease to 37.3% (Fig. 4.1). Planktonic foraminiferal assemblages include *Pa. rohri* and *Pa. transitoria* in the 250 μm size fraction, and *Globigerinelloides aptiensis*, *G. duboisi, G. ferreolensis, G. maridalensis, G. paragottisi, Hedbergella aptiana, Hd. excelsa, Hd. gorbachikae, Hd. infracretacea, Hd. occulta, Hd. praelippa, Hd. praetrocoidea*,*Hd. rhinoceros, Hd. ruka, Hd. trocoidea, , Pseudoguembelitria blakenosensis, Pseudoplanomalina cheniourensis,* and *Schackoina cepedai* (more common at the base of the interval) in the smaller size fractions. The relative abundances of benthic foraminifera rise from 1% at 3.00 m up to 43.2% at 6.25 m. A progressive reduction in the number of planktonic foraminiferal species is observed from this level upward, combined with marked high-frequency fluctuations of abundances between 0.3% and 68.5%, and simultaneous and opposite shifts on the benthic foraminifera e radiolarian abundances. Moreover, the coarser fractions of washed residues contain organic particles and fish teeth, indicating enhanced superficial productivity. *Microhedbergella miniglobularis* records its lowest occurrence at 6.42 m, and therefore it co-occurs with late Aptian taxa for a short stratigraphic interval, until

the top of *Paraticinella rohri* Total-range Zone. At 6.50 m, the PF percentages definitively drop, and they are absent or occur in low to very low percentages in the overlaying stratigraphic levels. The sedimentary level at 6.50 m records the first major turnover in the evolutionary history of planktonic foraminifera, with the extinction of *Pa. rohri* and other large-size aptian species. This level marks also the deterioration of preservation, and most specimen show diagenetic alteration with different degrees of test recrystallization until the top of the target interval. The HO of *Pa. rohri* marks the lower boundary of the *Microhedbergella miniglobularis* Interval Zone, which spans from 6.50 m to the HO of *Microhedbergella renilaevis* at 7.60 m. This 1-meter-thick biozone and the following *Microhedbergella renilaeivis* Partial Range Zone are devoid of planktonic foraminifera >250 μm. Assemblages are dominated by radiolarians, followed by BF. The depauperate planktonic assemblages consist of small-sized specimens of *Mi. miniglobularis* and *Mi. renilaevis* (100 μm in average) together with rare to few specimens of Aptian taxa as *G. duboisi, G. maridalensis, G. paragottisi, Hd. excelsa, Hd. infracretacea, Hd. occulta, Hd. praelippa, Pa. transitoria e Ps. Blakenosensis.* At 7.50 m planktonic foraminifera record a temporary rapid rise in abundances up to 28.2%, but at 7.80 m percentages drop again and do not exceed 9% until the end of the target interval (9.00 m). The Kilian sub-event records the overwhelming abundance of benthic foraminifera compared to planktonic foraminifera and radiolarians, but immediately above radiolarians turn dominant again.

4.2 Test size variations in *Pa. rohri*

Pa. rohri has its lowest occurrence (LO) at the stratigraphic level -4.80 m and, for about 1.90 meters above, it shows a narrow and quite stable dimensional range, with mean values of ~380.31 μm and population variability of ± 31.94 μm (Fig. 4.1; Tab. 1 – Supplementary materials). A short increasing trend starts at meter -2.80 and culminates in correspondence of meter -2.30, reaching a maximum value of 485.11 ± 44.15 μm. After this level, *Pa. rohri* specimens show a short and rapid reduction of the test size until the value of 308.82 μm at -1.20 meters, reducing the mean diameters of about 176.29 μm in just 1.10 meters. Moreover, also the population size variability decreases its wideness from ± 56.58 to ± 21.77 μm. From this level to 3.01 m., the mean diameters show a long and gradual increasing trend

concomitant with the progressive increase of the dimensional variability in each population.

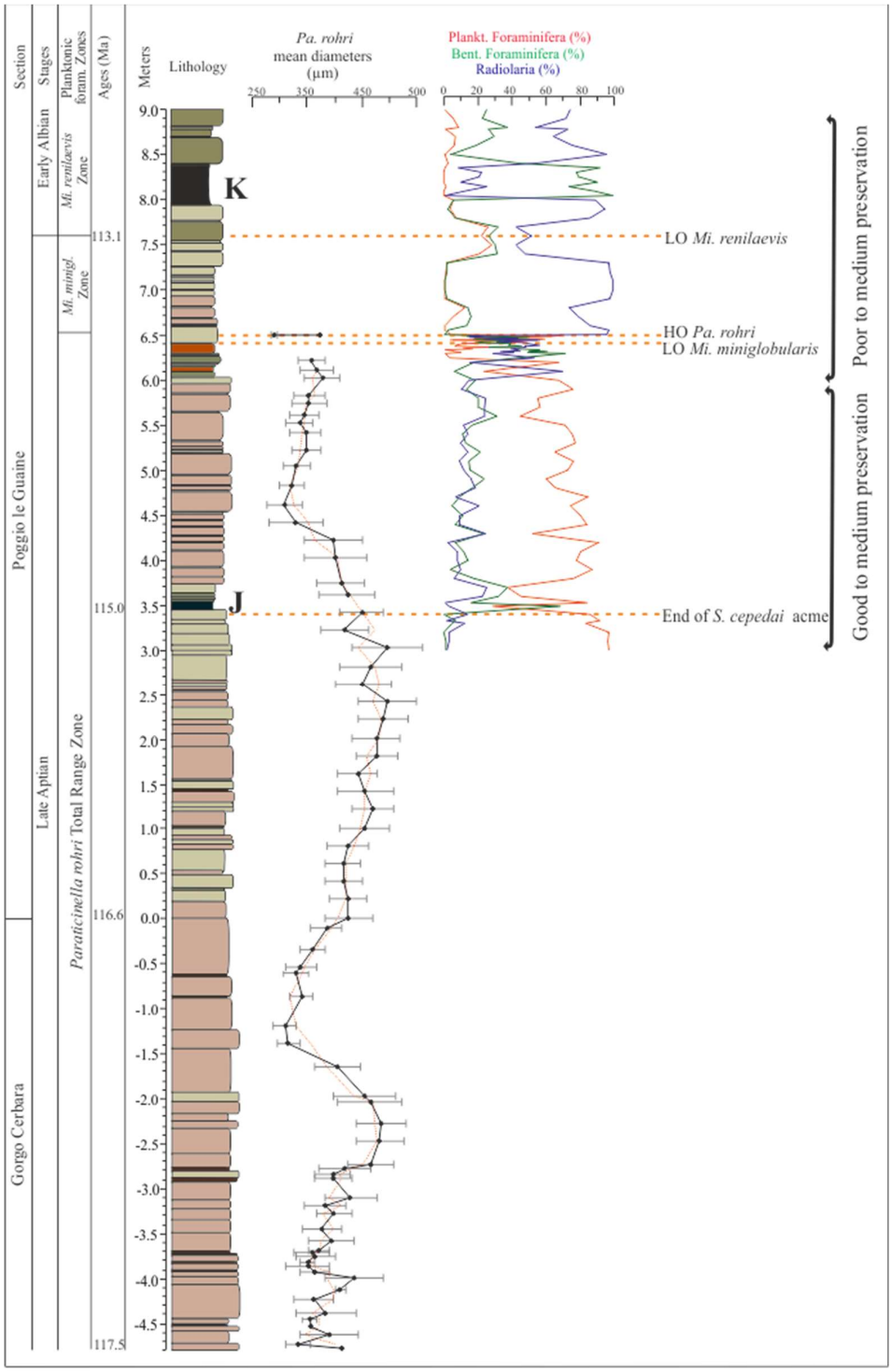

Fig. 4.1. Mean diameters of *Pa. rohri* along the composite section of PLG-GC and relative foraminiferal and radiolarian abundances through the target interval. Orange dashed lines marks major bioevents in the target interval. Estimated ages for the studied section are inferred after Grippo et al. (2004), Huang et al. (2010), Ogg and Hinnov (2012), and Coccioni et al. (2014).

Key to abbreviations: Pa. = Paraticinella, Mi. = Microhedbergella, minigl. = miniglobularis, S. = Schackoina, J = Jacob sub-event; K = Kilian sub-event.

A moderate diminution occurs between 3.00 m and the 3.45 m, which is the last carbonate level before the black shale level of the Jacob sub-event. From this horizon to the sample at 3.59 m, no specimens of *Pa. rorhi* occurred in the highly impoverished assemblages typical of the black-shales horizons. As normal marly-carbonate deposition restored, *Pa. rohri* experiences a short decline of its mean test size, but it shows a wide dimensional variability of populations (51.04 μm on average). From 4.61 to 6.21 m, mean diameters record a slightly increasing trend until the value of 357.61 ± 23.37 μm, then *Pa. rohri* temporarily disappears from 6.30 to 6.48 m, and two specimens are found at 6.49 m, with mean diameter of 289.27 μm. Finally, last occurrence of *Pa. rohri* in the PLG section is recorded at 6.50 m, where only one specimen is found with mean diameter of 372.93 μm.

4.3 Carbon Isotope Stratigraphy

The $\delta^{13}C$ data for the "target interval" of Poggio le Guaine section presented in Fig. 4.2, where magnifications of the 3.00 – 7.80 m and 7.90 – 9.00 m intervals are also reported (data from Coccioni et al., 2014; Sabatino et al., 2015).

From 3.00 to 3.46 m, $\delta^{13}C_{carb}$ values fluctuate between 2.95 and 4.16‰, defining a slight negative trend. The Jacob level is marked by a negative peak at 3.51 m followed by wide fluctuations. Values ranging around the mean value of 3.56‰ characterize the interval between 4.00 and 6.20 m, followed by a decreasing trend up to 6.70 m with $\delta^{13}C$ value of 2.70‰. From 6.70 to 7.90 m the $\delta^{13}C$ values oscillate between 2.55 and 3.88‰. Then a weak increase of the $\delta^{13}C$ occurs, followed by an abrupt drop of the values from 3.52‰ to -0.38‰ at the base of the Kilian level (7.95 - 8.13 m). This negative shift in the $\delta^{13}C$ curve is followed by an increase in values up to 2.60‰ at 8.21 m. Stratigraphically higher, a slight increasing trend characterize the $\delta^{13}C$ curve up to the top of the section.

4.4 $CaCO_3$ content

The figure 4.2 shows the curve of $CaCO_3$ content along the target interval of PLG section (data are from Coccioni et al., 2014). The moving average (5 points) curve

is also shown, as it smooths out short-term fluctuations and highlight longer-term trends.

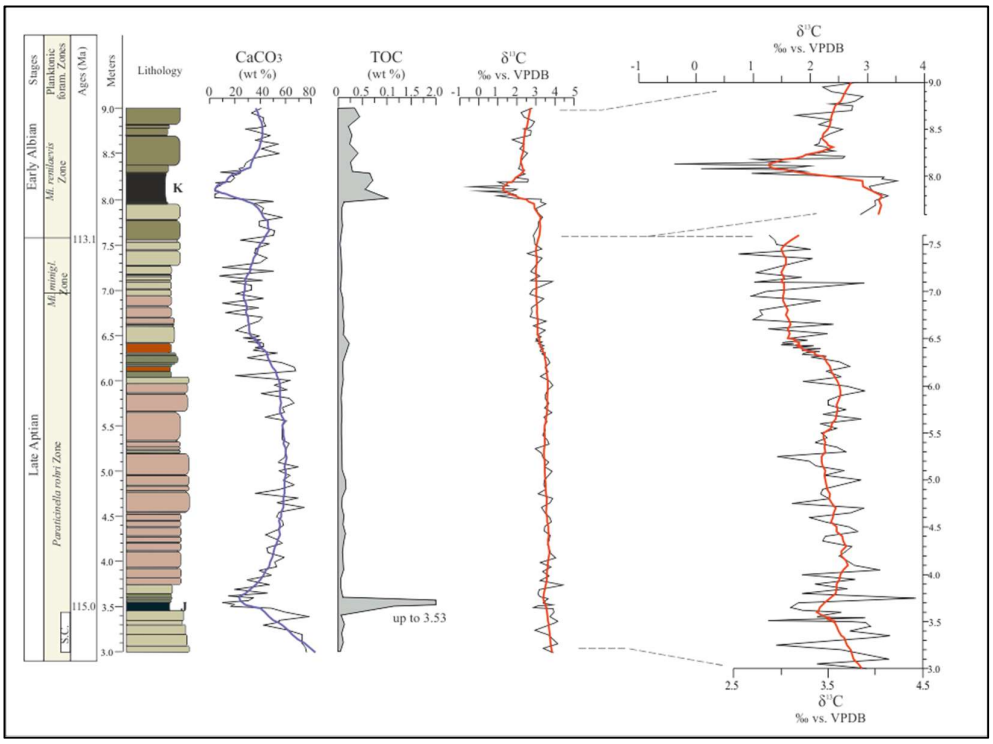

Fig. 4.2. $CaCO_3$ (%), TOC (%), and $\delta^{13}C$ depth profiles from the "target interval" of Poggio le Guaine Section. $CaCO_3$ and $\delta^{13}C$ are from Coccioni et al., (2014), TOC data from this study. Blue and red lines represent the moving average curve for $CaCO_3$ (period 5 points) and $\delta^{13}C$ (period 10 point), respectively. J = Jacob sub-event; K = Kilian sub-event.

The lower part of the target interval from 3.00 m to 3.40 m, shows $CaCO_3$ concentrations ranging from ~43 to ~78% (Fig. 4.2). The Jacob level marks an abrupt fall in the $CaCO_3$ content up to ~10%, followed by a gradual increasing trend. Between 4.60 and 5.8 m the $CaCO_3$ values are rather stable (~60%), then gradually decrease, showing several short-term drops and rises. This pattern mainly characterizes the interval between 6.00 and 7.30 m. A brief increase of the values up to 50% at 7.60 m anticipates the drastic fall linked to the onset of Kilian level. This black-shale interval shows very low $CaCO_3$ content (~4%) in the first 20 cm (8.00 - 8.19 m) in particular. From 8.50 m upward, the $CaCO_3$ content increases showing values ranging from ~29 to ~55%, with an average value of 41%.

4.5 Total Organic Carbon content

The total organic-carbon (TOC) contents of Poggio le Guaine section are reported in Table 2 (Supplementary materials).

The TOC curve from the target interval of Poggio le Guaine section shows a flat profile through the entire interval analysed, apart the peaks in correspondence of the black shales levels (Fig. 4.2). Particularly, limestones and carbonate marls show mean TOC values of ca. 0.10% with slightly increase up to 0.23% in proximity of the *Pa. rohri* Zone upper boundary (6.41 m). Black shales level of the Jacob sub-event shows the most significant enrichment in organic matter for the target interval, with values of 3.5%. The 38cm-thick black shale level of the Kilian sub-event, shows a lower enrichment in organic content, with higher TOC value at the base (up to 1%). Increases in the TOC contents occur in coincidence of the several thin black shale horizons below and within the Monte Nerone interval, with a major peak of 1.14% at 11.99 m (Tab. 2 - Supplementary materials). The organic-rich episode corresponding to the Paquier level is characterized by a TOC content up to 9.8%, slightly preceded by a TOC enrichment at ~16.1 m, where the values reach 3.2%. From 17.04 m upward, the TOC content increases up to 0.95% in coincidence with Leenhardt level, and a second rise to 0.92% at 18.82 m.

4.6 Major and trace elements

Major and trace elements concentrations (vs. Al) detected along the PLG section are reported in Table 3 (Supplementary materials) and plotted in figures from 4.3 to 4.6. Aluminium can be considered as an indicator of the aluminosilicate fraction of the sediments, with very little ability to move during diagenesis (Brumsack, 1989; Calvert and Pedersen, 1993; Morford and Emerson, 1999; Piper and Perkins, 2004; Tribovillard et al., 2006). Therefore, TM values were normalised to Al in order to account for dilution effects by potential biogenic components such as carbonates, silica, and phosphorites.

Contents of Mn in ancient sediments can be used to reconstruct temporal variation in the oxygenation of bottom water (Arthur et al., 1987; Dickens and Owen, 1994; Davis et al., 1999). The high sedimentary concentrations of manganese from 3.00 to 3.40 m, revealed by Mn/Al ratios up to $3048.33 \cdot 10^4$, suggest that these sediments originally accumulated under oxic bottom water conditions (Fig. 4.3). A drastic drop of Mn/Al ratios is recorded in coincidence of the Jacob level, where it reaches a value of $\sim 38 \cdot 10^4$, close to those of AS, followed by a rapid increase up to $1610 \cdot 10^4$ at 3.91. From this point to 4.71 m the values oscillate around the mean values of $1211.244 \cdot 10^4$, followed by a decreasing trend

up to 6.31 m. Then, the values show wide fluctuations around a mean value of $974.69 \cdot 10^4$. The Kilian level is characterized by a Mn/Al ratio of $24.73 \cdot 10^4$ at its base, after which values gradually rise up to $1377.87 \cdot 10^4$ at the top of the section (9.00 m). The Mn concentrations close to those of average shales in Jacob and Kilian levels, could indicate oxygen-depleted bottom water in which Mn cannot precipitate as oxyhydroxide, and thus it is maintained as dissolved species. Vanadium is removed from the ocean into anoxic sediments because of the propensity to precipitate as soluble oxides/hydroxides or to be strongly adsorbed on particle surface. Relative increase in the sedimentary concentration of V may, therefore, be indicative of a proportional increase of the oxygen-depletion in bottom waters (Tribovillard et al., 2006). The V/Al curve records background values close to those of AV (Fig. 4.3). An increasing trend start at the base of the target interval, with the strongest enrichment in correspondence of the Jacob level ($92.65 \cdot 10^4$). Then values slightly oscillate around the mean value of $15.77 \cdot 10^4$ up to 6.30 m (Fig. 4.3; Tab. 3 - Supplementary materials). From 6.30 m to 7.60 m, the V/Al ratios record pronounced increases in values, with major peaks at 6.40 m, 7.10 m and 7.40 m (values of $34.25 \cdot 10^4$, $54.80 \cdot 10^4$, and $32.78 \cdot 10^4$, respectively). The black shales of the Kilian level do not show any significant enrichment, but from its top the V/Al curve records an increasing trend that persists up to 9.00 m, reaching the value of $44.44 \cdot 10^4$.

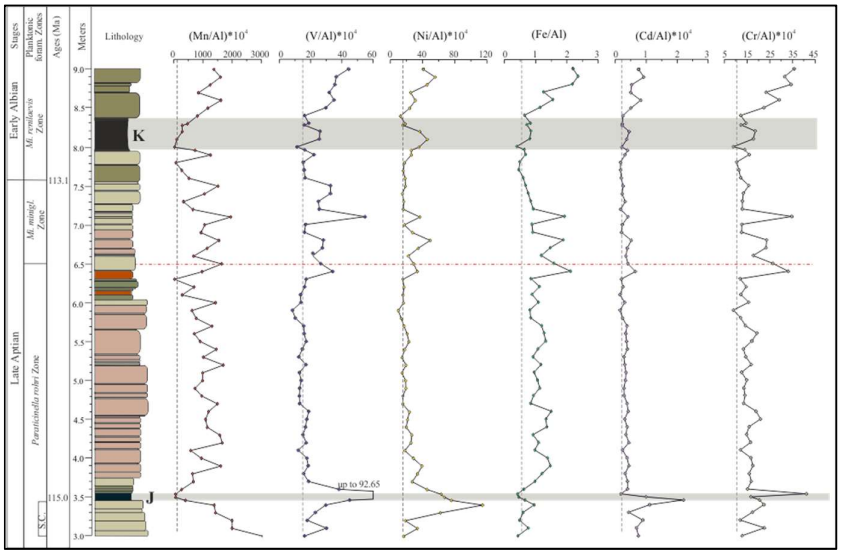

Fig. 4.3. Depth profile of Mn, V, Ni, Fe, Cd and Cr /Al ratios from Poggio le Guaine section. The grey bands highlight the black shales levels of the Jacob (J) and Kilian (K) sub-events. Dashed red line marks the extinction level of *Pa. rohri*. Dashed grey lines marks the AS values (Wedepohl, 1971, 1991).

The Fe/Al curve does not show significant enrichment in coincidence of the Jacob and Kilian black shale levels, and major increases of Fe/Al ratios are recorded at the interval from 6.40 to 7.10 m, and from 8.50 to the top of the section (Fig. 4.3; Tab. 3 - Supplementary materials). The Fe enrichment in sediments is commonly considered one of the most faithful recorders of ancient euxinia. However, the higher Fe/Al values recorded along PLG section in apparently oxic facies could be interpreted to reflect iron enrichment in the terrigenous source material rather than authigenic enhancement. The similarity of Fe/Al profile with those of the so-called "detrital proxies" (Mg, K, Ti, and Zr) seems to support this hypothesis (Fig.4.5).

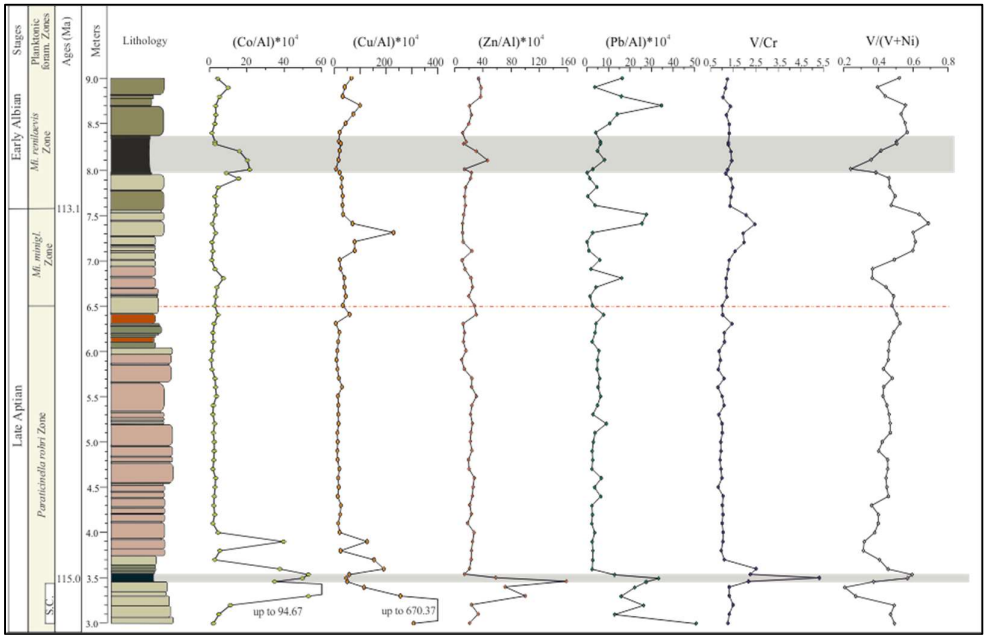

Fig. 4.4. Depth profile of Co, Cu, Zn, Pb /Al ratios and of V/Cr and V/(V+Ni) ratios from Poggio le Guaine section. The grey bands highlight the black shales levels of the Jacob (J) and Kilian (K) sub-events. Dashed red line marks the extinction level of *Pa. rohri*. Dashed grey lines marks the AS values (Wedepohl, 1971, 1991).

Other "redox-sensitive elements", as Ni, Cd, Co, Cu and Zn show significative enrichment compared to the AS concentrations just in correspondence of the Jacob level, and only a minor perturbation within the Kilian level (Figs. 4.3 - 4.4), suggesting more pronounced redox conditions during the first sub-event of the OAE 1b. However, the interval between 6.30 m and 7.10 m shows variable rises in these TM/Al ratios, suggesting the occurrence of some perturbation of the water-column chemical structure.

Pb/Al curve shows mean values of $25.20 \cdot 10^4$ from 3.00 through the Jacob black shale level, over which they drastically drop (Fig. 4.4, Tab. 3 Supplementary

materials). Only three prominent peaks are recorded at 6.80 m, 7.40 m, and 8.70 m (Pb/Al of $16.12 \cdot 10^4$, $27.55 \cdot 10^4$, $34.72 \cdot 10^4$, respectively), and the Kilian level does not record any significant enrichment.

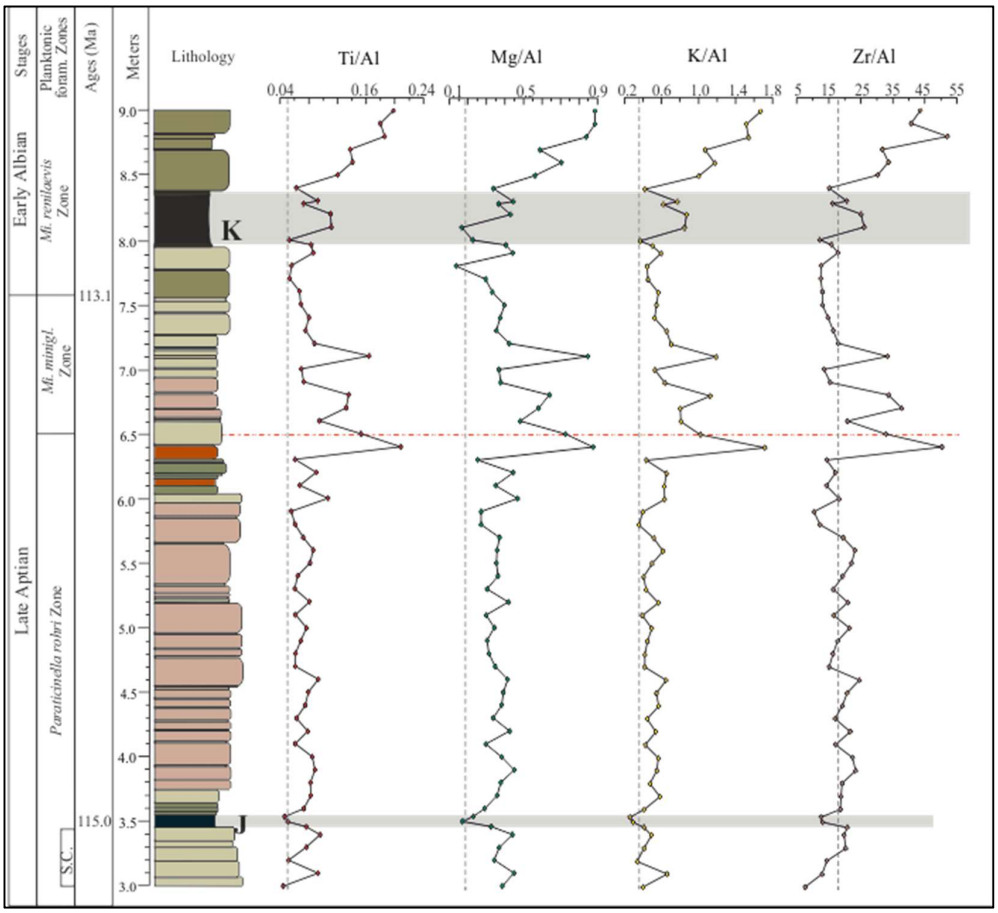

Fig. 4.5. Depth profile of Ti, Mg, K, Zr /Al ratios from Poggio le Guaine section. The grey bands highlight the black shales levels of the Jacob (J) and Kilian (K) sub-events. Dashed red line marks the extinction level of *Pa. rohri*. Dashed grey lines marks the AS values (Wedepohl, 1971, 1991).

Magnesium, K, Ti, and Zr are often used as proxy for detrital component source (Fig. 4.5). These element/Al ratios represent the proportion of heavy minerals, quartz and detrital dolomite (proxies for aeolian transport) relative to the clay fraction. Mg/Al, K/Al, Ti/Al, Zr/Al ratios show similar patterns and they have mean values relatively close to that of average shale (AS, Wedepohl, 1971, 1991) (0.34, 0.50, 0.09, and 15.77, respectively) along the lower part of the section (Fig. 4.5; Tab. 3 - Supplementary materials). More specifically, the graphical plots of Mg/Al, K/Al, Ti/Al, and Zr/Al ratios highlight rather stable values from 3.00 to the meter 6.30, with mean values of 0.35, 0.48, 0.07 and 17.79, respectively, and just a slight decrease coinciding with the deposition of the Jacob level.

Significative increase of the ratios occurs between 6.30 and 7.10 m, with three prominent peaks at 6.40 m, 6.80 m and 7.10 m, probably recording major pulse of the detrital supply. From 7.10 m upward, the metal/Al ratios gradually decrease and restore to the background values. At the Kilian level, Mg/Al ratios decrease whereas K/Al, Ti/Al and Zr/Al show a slight increase. After the Kilian interval, all the ratios rapidly rise and reach their highest values at the top of the section (0.89, 1.67, and 0.20, 52.06, respectively), suggesting another contribution from terrigenous sources.

Chromium is a "redox-sensitive" element with strong affinity for the detrital fraction (Tribovillard et al., 2006). In the PLG section, the Cr/Al profile has similar trend to Mg/Al, K/Al, Ti/Al, an Zr/Al, except for the strong peak coinciding with the black shales of the Jacob Level (up to $41.14 \cdot 10^4$). Along the section, values are comparable to AS values ($(Cr/Al)_{AS} = 10.2 \cdot 10^4$) and they cluster around $17.69 \cdot 10^4$. As in Mg/Al, K/Al, Ti/Al, and Zr/Al profiles, Cr/Al ratio records a three-peaks increase up to values of $\sim 20 \cdot 10^4$ from 6.30 to 7.10 meters, and a rapid increase from 8.50 to the top of the section (Fig. 4.3, Tab. 3 - Supplementary materials).

Barium is largely used as paleoproxy for productivity since it is incorporated into bioaggregates in the water columns or released during phytoplanktonic necromass decay (Dymond et al., 1992; Francois et al., 1995; Dymond and Collier, 1996; Kasten et al., 2001; Tribovillard et al., 2006; Paytan and Griffith, 2007; Sabatino et al., 2015). In micro-environments where Ba-sulphate reaches supersaturation, the Ba precipitate as barite by live phytoplankton marine organisms forming barite ($BaSO_4$). Hence, variations in the Ba/Al profile can be used to infer the temporal dynamics of organic matter degradation causing various shifts in the $BaSO_4$ precipitation zone (Sabatino et al., 2015). Along the PLG section, Ba/Al ratios record rather smooth pattern from 3.00 m to 6.30 m, with weak peaks below and above the Jacob level (at 3.40 m and 3.80 m), and at 5.70 m (Fig. 4.6). From 6.40 m Ba/Al curve shows an increasing trend with three prominent peaks at 6.50 m, 7.00-7.10 m and 7.40-7.50 m with values of $1679.05 \cdot 10^4$, $1527.95 \cdot 10^4$, and $1381.54 \cdot 10^4$, respectively (Tab. 3 - Supplementary materials). At the Kilian level, values drop to $170.51 \cdot 10^4$, then gradually increase and at 8.90 m the Ba/Al ratio records its maximum value of $2244.99 \cdot 10^4$. The remarkable enrichments of Ba respect the AS value, particularly from 6.30 m upward (Fig. 4.6), could reflect higher marine primary productivity, presumably

driven by the higher nutrient delivery to the ocean suggested by the detrital proxies. The lower values of Ba/Al ratios in coincidence of the Jacob and Kilian sub-events, however, could reflect the complete depletion of SO_4 within the black shale sequences, resulting in an undersaturation of pore water with respect to barite ($BaSO_4$). This may have promoted the remobilization of biogenic barium, while authigenic barite may precipitate at the top of the sulfate-depletion zone, forming diagenetic barite fronts within or above the TOC-rich strata (e.g., von Breymann et al., 1992; Torres et al., 1996; Dickens et al., 2003; Sabatino et al., 2015).

The P/Al ratio shows a similar trend as Ba/Al, characterized by values drops at the Jacob and Kilian levels, higher variability from 6.00 m to 7.90 m, and increasing trend from the Kilian level to the top of the section.

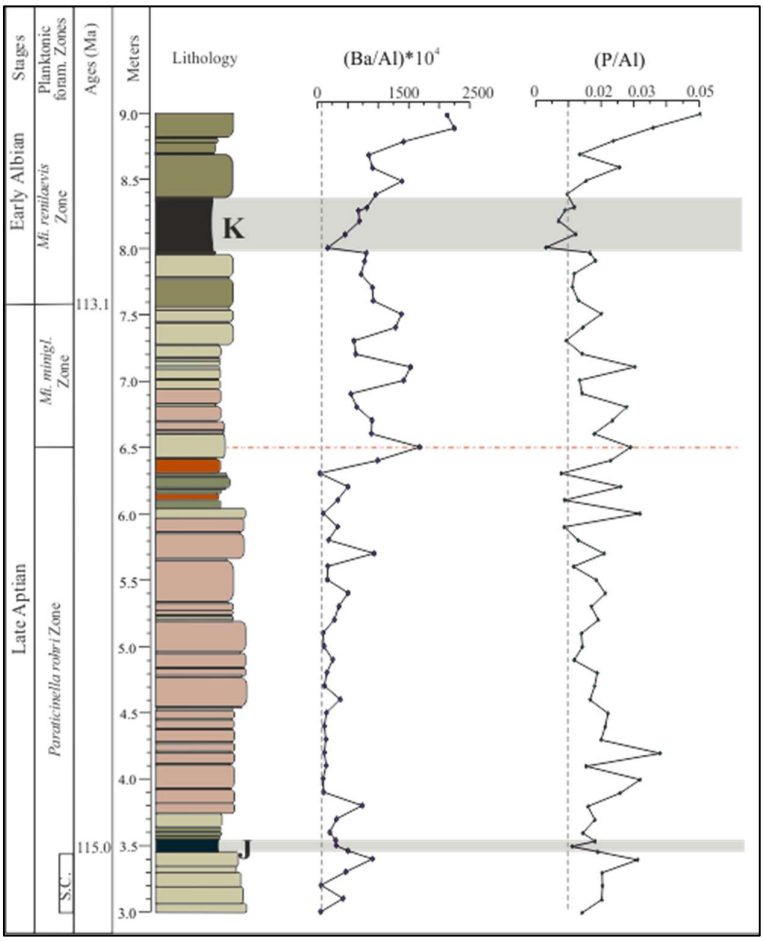

Fig. 4.6. Depth profile of Ba and P /Al from Poggio le Guaine section. The grey bands highlight the black shales levels of the Jacob (J) and Kilian (K) sub-events. Dashed red line marks the extinction level of *Pa. rohri*. Dashed grey lines marks the AS values (Wedepohl, 1971, 1991).

4.7 Mercury content

At Poggio le Guaine, mercury values around 8 $\mu g \cdot kg^{-1}$ are observed at the base of the section, followed by an enrichment trend starting at 3.20 m and culminating in correspondence of black shales of the Jacob level (3.46-3.56), where they rise to 237 $\mu g \cdot kg^{-1}$ (Fig. 4.7; Tab. 4 - Supplementary materials). Hg concentrations fall to values around 3.71 $\mu g \cdot kg^{-1}$ from ~3.70 to 5.90 m, with some mercury spikes around 7.16 and 11.83 $\mu g \cdot kg^{-1}$ at 4.10m and 5.70 m, respectively. A slight increasing trend from 4 to 14 ppb starts at ~6.00 m, followed by two evident peaks at 7.30 m and 7.80 m (~75 $\mu g \cdot kg^{-1}$ and 45.96 $\mu g \cdot kg^{-1}$, respectively). In the Kilian level (7.96 – 8.38 m), mercury contents reach 141.52 $\mu g \cdot kg^{-1}$, and then decrease to a mean value of ~22.53 $\mu g \cdot kg^{-1}$ (Fig.4.7 – Tab 4 - Supplementary materials).

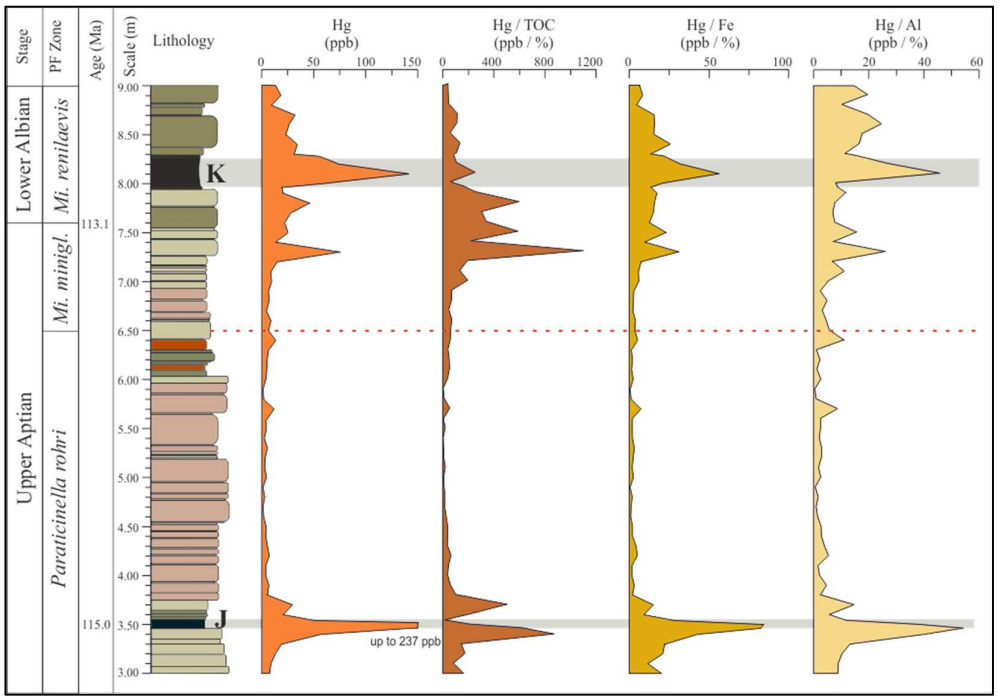

Fig. 4.7. Hg concentrations, total organic carbon (TOC) and Hg/TOC, Hg/Fe, Hg/Al depth profiles along PLG section. The grey bands highlight the black shales levels of the Jacob and Kilian sub-events. Dashed red line marks the extinction level of *Pa. rohri*.

The Hg concentrations have been normalized against TOC, Fe and Al, in order to investigate the role of organic-matter scavenging and/or adsorption onto clay minerals or hydrous iron oxides in the sequestration of Hg in sediment. At the bottom of the section, the Hg/TOC profile shows high values of ~ 141 with a double spike centred at 3.40 m and 3.70 m, respectively below and above the Jacob level, because of the higher TOC values in black-shales (up to 3.53 wt%). The absence of

a Hg/TOC peak in coincidence of the Jacob level suggest that the Hg enrichment in this horizon is strongly related by organic matter deposition. Then ratio gradually decreases to the value of 2.15 (at 5.31 m) and start to rise at ~6.00, with three main spikes 0.66cm, 0.46cm and 16 cm below the Kilian level (Hg/TOC of 1098.95, 587.67, and 596.96 $\mu g \cdot kg^{-1}$/wt%, respectively). In analogy with the Jacob level, the high TOC of black shales of the Kilian level (ca 1.0 wt%) results in a less pronounced peaks of the Hg/TOC ratios (higher value of 253.46). In the upper part of the section, values range between 132.78 and 39.59 $\mu g \cdot kg^{-1}$/wt%.

Hg/Fe and Hg/Al are rather well correlated with the overall Hg contents, and intervals of maxima in Hg/Fe and Hg/Al ratios correspond to samples with relatively high Hg contents. This is the case of prominent peaks at 3.50 m (Jacob level), 3.70 m, 5.70m, 6.40m, 7.30m, and 8.10 m (Kilian level) (Fig. 4.7, Tab 4 - Supplementary materials). Hence, the Hg contents along the target interval do not seem to be primarily controlled by sulphide precipitation and/or clay contents, as alternatively evident in the black shales levels of the Kilian sub-event (Fig. 4.7).

4.8. Biomarkers identified and their distribution in Poggio le Guaine section

Gas chromatograms obtained by GC/MS of apolar fractions display a full suite of saturated hydrocarbons belonging to *n*-alkanes, regular and irregular acyclic isoprenoids, aryl isoprenoids, steranes and hopanes. All the detected specific compounds are listed in Table 5 (Supplementary materials) with additional information such as the characteristic mass chromatograms (m/z), abbreviations and the biological precursor presumed.

The Most Abundant Compound (MAC) in each analysed sample is listed in Table 6 (Supplementary materials). The OM extracted from limestones from 0.00 m up to 3.00 m records the C_{31}-alkane as the most abundant organic compound with mean relative concentrations of 134.5 µg/g TOC. The only exception is one sample at 1.80 m where TMI is more abundant. The black shales of the Jacob level (3.46 – 3.56 m) are dominated by significant amounts of pristane (mean value of 604.0 µg/g TOC), with main peak of 1105.2 µg/g TOC at the median horizon of the black-shale interval (3.51 m). Restoration of carbonate deposition is marked by the re-establishment of *n*-alkanes as most abundant compounds in sediment extracts, with the short-chain *n*-C_{18} dominant between 4.14 and 7.96 meters (concentrations of 201.86 µg/g TOC). The 40 cm-thick black shales interval of the Kilian sub-event

(samples from 7.97 to 8.38 m) shows a patchy composition with alternation of *n*-C_{16}, *n*-C_{18}, *n*-C_{31}, and pristane, as most abundant compounds. Above the Kilian level, both limestones from 8.39 m to 10.42 m and black shales of Monte Nerone level (11.44 - 13.09 m) are dominate mainly by *n*-alkanes with 16 and 18 carbon atoms, with concentrations ranging between 28.6 and 532.2 µg/g TOC. Black shales from the Paquier level record higher amounts of pristane, which vary from 68.3 to 483.7 µg/g TOC, whereas Leenhardt interval shows major abundances of short-chain C_{16}- *n*-alkanes (up to 758.42 µg/g TOC).

4.9 Biological Source of Organic Matter

Biomarkers (molecular fossils) can provide key information about climate (e.g. sea surface temperature), biogeochemistry (e.g. redox state of the ocean), and evolution of life (e.g. first appearance of steranes derived from algae). In many cases their carbon skeleton is identical or slightly altered relative to the structure of their precursor biolipids generated by living organisms (Peters et al., 2005).

Here a range of biomarkers has been used to determine the dominating biological source of hydrocarbons and changes in water column redox state in sediments from the Poggio le Guaine section (Italy).

4.9.1 *N-alkanes parameters*

N-alkanes (or n-paraffins) are saturated hydrocarbon with a linear arrangement of carbon atoms and with general formula C_nH_{2n+2}. Most of *n*-alkanes isolated from marine sediments typically are derived from the degradation of bacterial cell membranes, algal algaenans and vascular plant waxes (cutans). More specifically, the aquatic range of *n*-alkanes comprises short-chain homologues with 16 to 22 carbon atoms that typically originate from aquatic algae and cyanobacteria (Blumer et al., 1971; Gelpi et al., 1970; Han and Calvin, 1969; Brassell et al., 1978; Peters et al., 2005). The long chain (*n*-C_{23}-C_{35+}) *n*-alkanes are characteristic biomarker for contributions from terrestrial plants, (Eglinton and Hamilton, 1967).

The apolar fraction of the analysed PLG extracts display full site of saturated hydrocarbon between C_{16} and C_{35} n-alkanes (Fig. 4.8). For most samples, the n-alkane distribution is dominated by the aquatic-derived *n*-C_{16} to *n*-C_{18} homologous, except for sediments from 0.00 to 3.00 m and from 7.31 to 8.99 m, where the most

abundant *n*-alkane is the long-chain *n*-C_{31} homologue, biomarkers belonging to the terrestrial range ($C_{max\text{-}aquatic}$ and $C_{max\text{-}waxes}$; Tab. 7 - Supplementary materials). This suggests the presence of land-plant derived input in the sedimentary environment during these intervals.

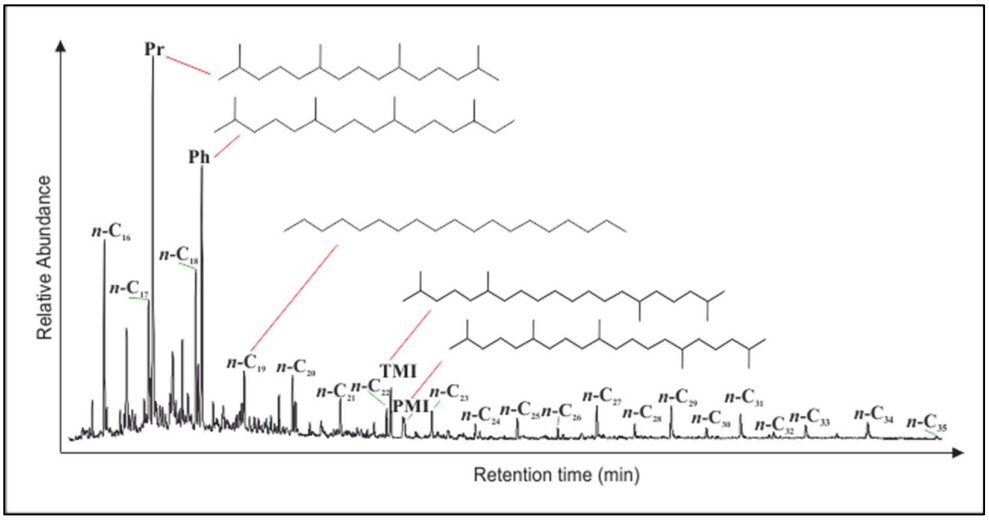

Fig. 4.8. Partial GC-MS gas-chromatogram (*m/z* 71.1) of apolar fraction from sediment extract of black shales samples of PLG section. Abbreviations are: *n*-C_x for *n*-alkanes with x carbon atoms; Pr: pristane; Ph: phytane.

The ratio of long- to short-chain alkanes (**L/S**) is a simple parameter that reflects relative contribution of aquatic/marine and terrestrial n-alkanes, and can be calculated by the following formula:

$$L/S = \frac{(nC_{25} + nC_{31} + nC_{33})}{(nC_{17} + nC_{18} + nC_{19})}$$

The proportion of land-plant material in Poggio le Guaine sediments varies through time. Precisely, the lower part of the section, from the 0.00 m to the onset of Jacob black shale interval at 3.46 m, is characterised by major contributions of terrestrial organic matter, highlighted by high values of the L/S ratios (mean value ca. 9.55, Tab. 7 - Supplementary materials). Conversely, from 3.46 m to the top of the section, L/S ratios significantly decrease to mean values of about 0.79, due to the higher concentrations of short-chain *n*-alkanes relative to long-chain counterpart, suggesting the interruption of terrestrial inputs and a primary role of marine sources during the deposition. Slight increases of L/S ratios are recorded below and above the Kilian level, and in the black shales of the Monte Nerone interval.

The **terrigenous / aquatic ratio** (**TAR**) is the n-alkanes parameter more commonly used to provide evidence of the organic matter sources (Bourbonnier and Meyers, 1996; Peters et al., 2005). This ratio correlates odd- long-chain and odd- short-chain *n*-alkanes in analogy to the L/S ratio, and it is expressed by the formula:

$$\mathrm{TAR} = \frac{(nC_{27} + nC_{29} + nC_{31})}{(nC_{15} + nC_{17} + nC_{19})}$$

TAR ratio in the analysed PLG sediments shows strong predominance of long-chain *n*-alkanes in the basal tree meters and low-medium values, ranging between 0.39 – 5.45, throughout the rest of the section (Fig. 4.9; Tab. 7 - Supplementary materials).

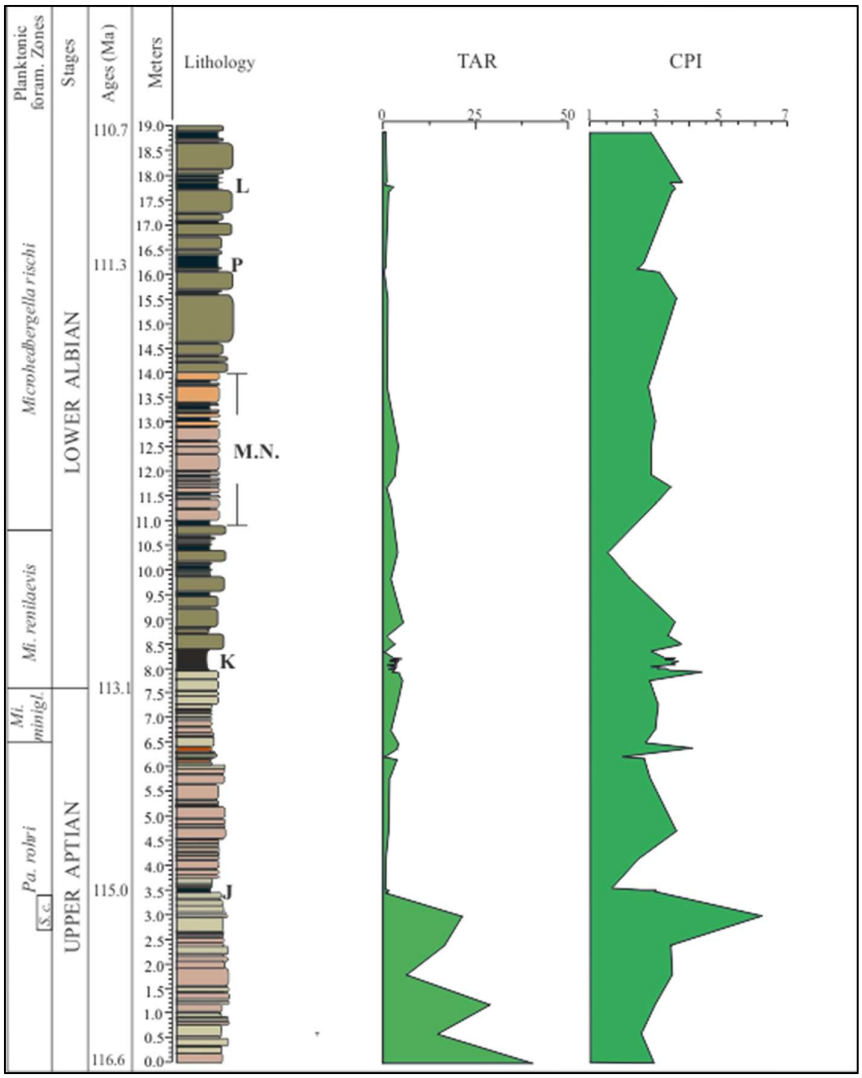

Fig. 4.9. Plots of TAR and CPI *n*-alkanes ratios along the stratigraphic succession of PLG. J = Jacob sub-event; K = Kilian sub-event; M.N. = Monte Nerone black-shales interval; P = Paquier sub-event; L = Leenhardt sub-event.

The **Carbon Preference Index** (**CPI**) (Bray and Evans, 1961) is a mathematical expression of the odd over even predominance between *n*-C_{24} and *n*-C_{34}, and it is expressed as:

$$\mathrm{CPI} = \frac{1}{2}\left(\frac{C_{25}+C_{27}+C_{29}+C_{31}+C_{33}}{C_{24}+C_{26}+C_{28}+C_{30}+C_{32}} + \frac{C_{25}+C_{27}+C_{29}+C_{31}+C_{33}}{C_{26}+C_{28}+C_{30}+C_{32}+C_{34}}\right)$$

Long-chain *n*-alkanes from land plant originating material usually show a significant odd to even carbon number predominance (usually dominated by C_{27}, C_{29} or C_{31} homologues) with CPI values in non-degraded plant material normally between 5 and 10 (Eglinton and Hamilton, 1967; Rielley et al., 1991; Commendatore et al., 2012; Kanzari et al., 2014). For PLG section the values range between 1.56 and 4.37, and only a sample at 3.00 meters shows a CPI value >5 (Fig. 4.9, Tab. 7 - Supplementary materials). The *n*-C_{16}-C_{22} derivates from marine OM tend to have no carbon number preference or slight preferences for even numbers. However, as CPI decreases with maturity, high values could indicate low maturity and/or terrestrial plants input, and then sediments with CPI ≤ 1 may result from the lack of terrestrial input and/or thermal maturity.

4.9.2 Isoprenoids

4.9.2.1 Acyclic isoprenoids

Acyclic isoprenoids are single isoprenoids concatenated to form long chains widely used in organic geochemistry studies. They were among the earliest lipids on Earth and many isoprenoids have proven to be useful biomarkers to determinate the biological source of organic matter in sediments and crude oil (Volkman, 2014). Acyclic isoprenoids may be connected in a regular head-to-tail manner or an irregular tail-to-tail one. Compounds belonging to the first group of linear isoprenoids found in PLG extracts are Pristane and Phytane, whereas in the realm of the irregular tail-to-tail isoprenoids, the acyclic C_{24} 2,6,15,19-tetramethylicosane (TMI) and C_{25} 2,6,10,15,19-pentamethylicosane (PMI) were detected. Regular head-to-tail isoprenoids have low biological specificity as they originate from multiple sources in addition to the phytol side chain of chlorophyll (Illich, 1983; Peters et al., 2005). Irregular tail-to-tail isoprenoids seem to be, on the contrary,

synthetized exclusively by Archaea, and they have excellent potential as biomarker (Chappe et al., 1979; Ward et al., 1985; Stefanova, 2000, Barber et al., 2001).

Pristane and Phytane

Pristane (2,6,10,14-tetramethylpentadecane) and phytane (2,6,10,14-tetramethylhexadecane) are regularly branched C_{19}- and C_{20}-isoprenoids primarily derived from phytol sidechain of the chlorophyll *a* in photoautotrophic organism (e.g. cyanobacteria) (Didyk et al., 1978; Volkman and Maxwell, 1986; Peters et al., 2005) and can be used as biomarkers for phytoplankton. However, other primary sources have been proposed as bacteriochlorophyll *a* and *b* of phototrophic bacteria (e.g. purple sulphur bacteria), tochoferls, and, only for phytane, the phytanyl ether lipids of archaea or other from archaeal membrane lipids (Brassel et al., 1983; Goossens et al., 1984; Risatti et al., 1984; Peters and Moldowan, 1993; Koopmans et al., 1999; Greenwood and Summons, 2003; Brocks and Summons, 2004; Peters et al., 2005). These multiple possible primary sources lead bias in their use as biologic-source indicators and, consequently, to infer the redox conditions in the depositional environment.

Generally, in oxic conditions, phytol would be oxidised to phytenic acid, yielding Pr after decarboxylation. In the absence of oxygen, i.e. in anoxic condition, phytol would be dehydrated, yielding phytadienes which eventually would be hydrogenated to Ph. Hence, the amounts of pristane and phytane reflect the oxic-anoxic setting and allow the use of Pr/Ph ratio as indicator of depositional environment of sedimentary organic matter. Pr/Ph ratios substantially < 1.0 were ascribed to reducing and stratified conditions, whereas Pr/Ph ratios > 3.0 were ascribed to oxidizing depositional environments (Didyk et al., 1978; Hunt, 1996). Values between 1 and 3 indicate alternating oxic and anoxic conditions. Moreover, empirical observations have also suggested that specific depositional environments and lithologies are associated with specific values for the Pr/Ph ratio (e.g. Hughes et al., 1995). Values <1 have been associated with marine carbonates, values between 1 and 3 with marine shales, and values >3 with non-marine shales and coals (oxidizing conditions) (Peters et al., 2005). Lastly, the Pr/Ph ratio is positive affected by thermal stress (e.g. Alexander et al., 1981; ten Haven et al., 1987).

Pr and Ph were detected along the entire succession of Poggio le Guaine (Figs. 4.8, 4.10). In carbonate levels Pr and Ph concentrations are very low and range

around the mean value of 11.5 and 10.7 µg/g TOC, respectively (Tab. 8 - Supplementary materials). An abrupt increase of Pr and Ph content is recorded in the black shales of the Jacob level, where Pr shows the highest concentrations among all the identified compound (1105.2 µg/g TOC at the middle level of Jacob level), suggesting a strong presence of cyanobacteria and/or purple sulphur bacteria in the depositional environment. These enrichments are recorded also in the Paquier black shales, where the Pr is the most abundant compound in the apolar fractions with concentration up to 483.7 µg/g TOC. The predominance of Pr respect Ph leads to moderate to high Pr/Ph ratios, especially in black-shales, where ratios reach the value of 3.53 (at 3.55 m – Jacob level). The higher concentrations of Pr in black shales cannot be interpreted as exclusive products of decarboxylation of phytol, which preferentially produces Ph under reducing conditions. Probably, additional source of Pr acted during deposition of black shales and therefore the Pr-signal should not be considered as exclusively linked to the oxic state of the depositional environment.

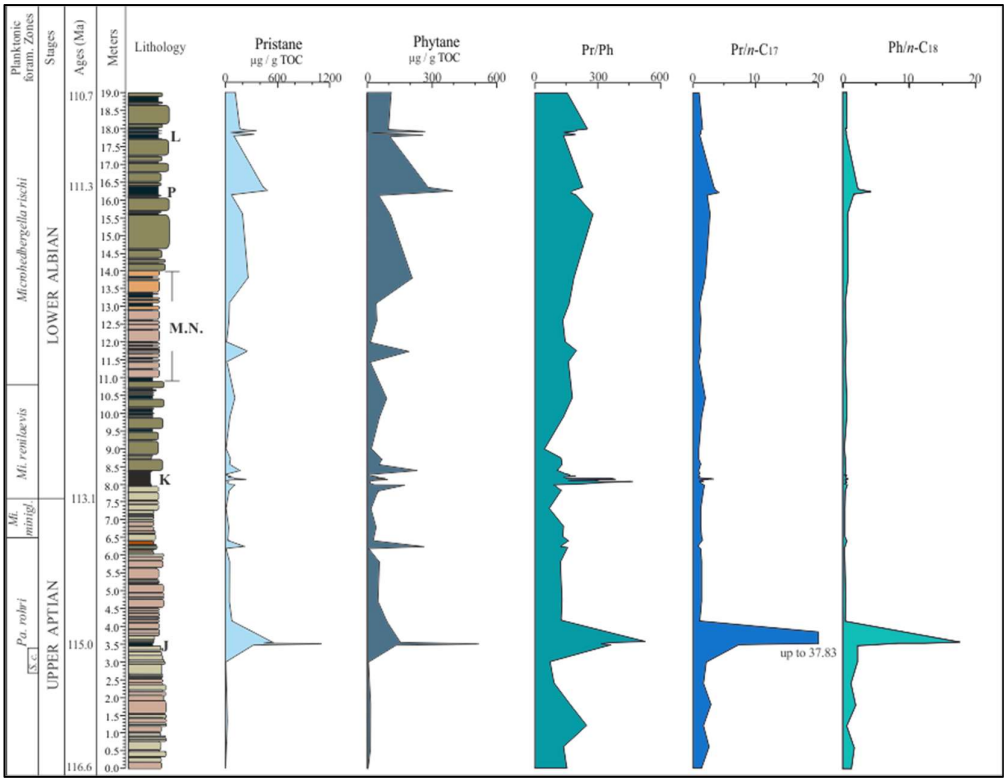

Fig. 4.10. Plots of pristane and phytane concentrations, Pr/Ph, Pr/*n*-C_{17} and Pr/*n*-C_{18} along the PLG section. K = Kilian sub-event; M.N. = Monte Nerone black-shales interval; P = Paquier sub-event; L = Leenhardt sub-event.

Redox conditions at the time of sediment deposition and the type of kerogen (I, II, III a) in sedimentary organic matter can be inferred from scatter log plots of Pr/*n*-C_{17} versus Ph/*n*-C_{18} (Lijmbach, 1975; Obermajer et al., 1999). Kerogen is the portion of OM present in sedimentary rocks that is insoluble in ordinary organic solvents. The chemical and physical characteristics of a kerogen are strongly influenced by the type of biogenic molecules from which the kerogen is formed. Hence, based on the chemical characteristics and the nature of the organisms from which it derives, kerogen can be identified as i) Type I, derived principally from lacustrine algae; ii) Type II, from several very different sources, including marine algae, pollen and spores, leaf waxes, fossil resin, and contributions from bacterial-cell lipids. Most Type II kerogens are found in marine sediments deposited under reducing conditions. iii) Type III kerogens, composed of terrestrial organic material that is lacking in fatty or waxy components (Tyson, 1995; Hantschel and Kauerauf, 2009).

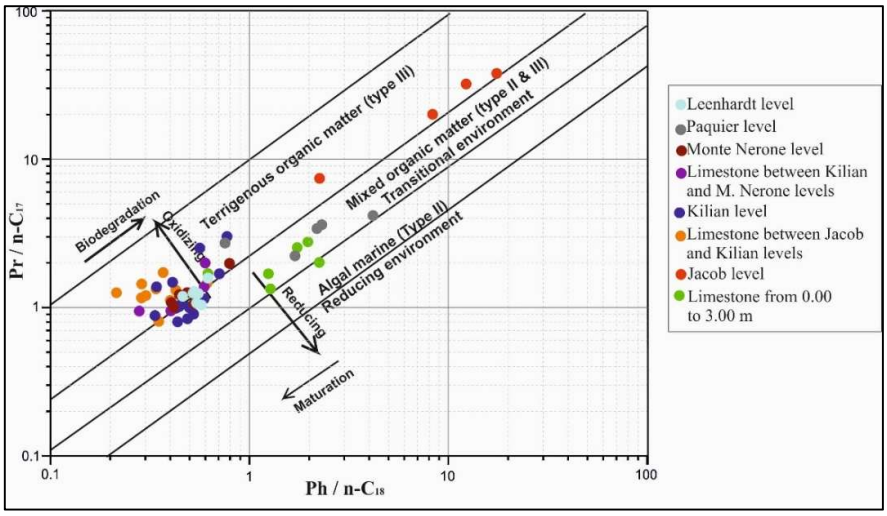

Fig. 4.11. Scatter log plots of Pr/*n*-C_{17} versus Ph/*n*-C_{18}

Pr/*n*-C_{17} vs. Ph/*n*-C_{18} ratio in apolar fractions of PLG section indicates that kerogen in the samples analysed can be classified as type III and II (Fig. 4.11). Most of the samples contain OM mainly originated from terrestrial plants and humic substances (Tissot and Welte, 1978), whereas the limestones from 0.00 to 3.00 m and the Paquier black shales shows contents of kerogene type II, originating from mixtures of zooplankton, phytoplankton, and bacterial debris in marine sediments.

PMI and TMI

C_{25} 2,6,10,15,19-pentamethylicosane (PMI). This C_{25} acyclic isoprenoids is considered diagnostic marker for Archaea. This compound has been detected in various cultured organism, microbial communities and sediments comprising methanogenic Archaea (e.g. Brassell et al., 1981; Koga et al., 1993; Risatti et al., 1984; Schouten et al., 1997; 2001a,b,c;) and methanotrophic Archaea in anaerobic consortia with S-reducing bacteria (e.g. Elvert et al., 1999; Thiel et al., 1999; Pancost et al., 2000; Hinrichs et al., 2002; Brocks and Summons, 2004). PMI is particularly abundant in *Methanosarcina barkeri*¸ of which is the main free lipid (Holzer et al., 1979; Pancost et al., 2001).

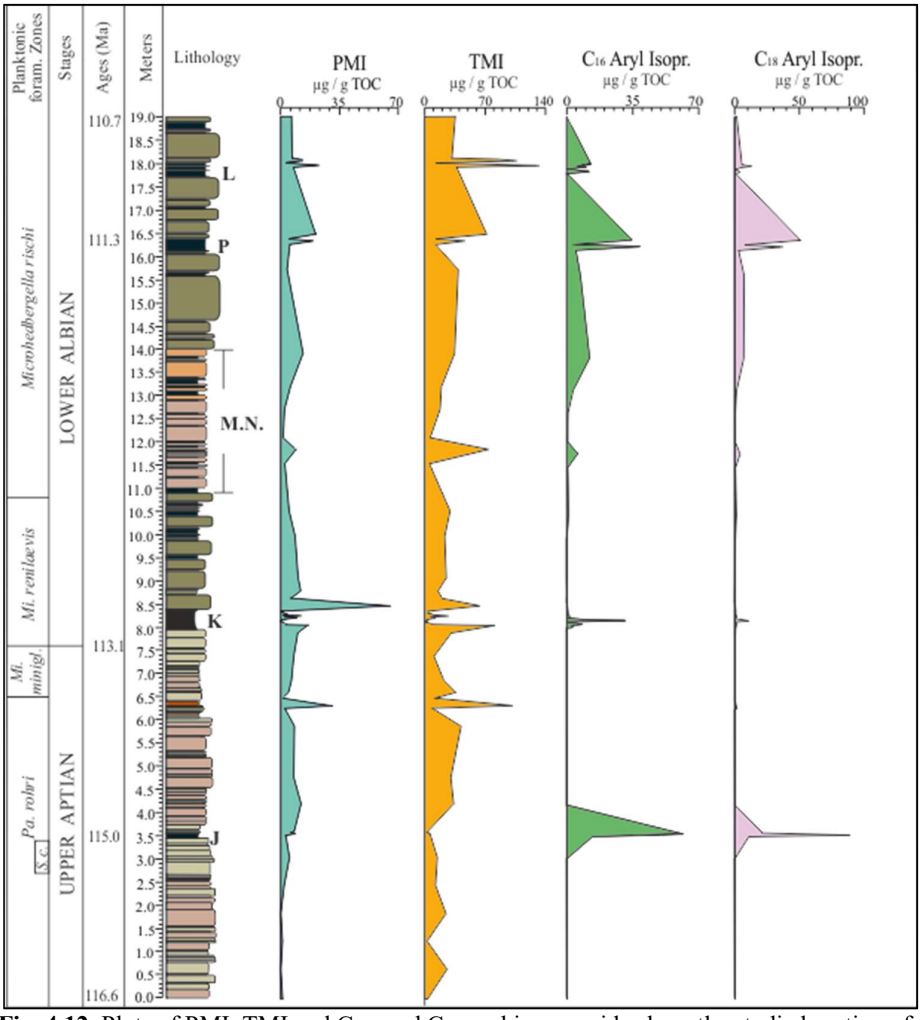

Fig. 4.12. Plots of PMI, TMI and C_{16}- and C_{18}-aryl isoprenoids along the studied section of PLG. K = Kilian sub-event; M.N. = Monte Nerone black-shales interval; P = Paquier sub-event; L = Leenhardt sub-event.

All late Aptian – early Albian sediments of Poggio le Guaine contain PMI, with concentration ranging around the mean value of 7.77 µg/g TOC (Figs 4.8 and 4.12 Tab 9 - Supplementary materials). Remarkably, small amounts of PMI (ranging

between 1.12 and 30.38 µg/g TOC) are recorded in marly limestones of the lower part of the section, in the interval between the Jacob and Kilian events, and between the Kilian and Monte Nerone black-shales, with a weak peak at 6.25 m (Fig. 4.12, Tab. 9 - Supplementary materials). Significant amounts of PMI are recorded at black shale levels, with most prominent peak at the Kilian sub-event (up to 64.99 µg/g TOC), and a less intense excursion corresponding to the Leenhard sub-event (up to 22.83 µg/g TOC) (Fig. 4.12 Tab. 9 - Supplementary materials). Black shales of Jacob sub-event record lower concentrations of PMI (max concentration 9.15 µg/g TOC) suggesting lower anoxia levels compared to the other sub-events of OAE 1b. This is a very interesting finding, since the continued presence of PMI provides a reliable evidence of methanogenesis during deposition, even if concentrations are very low in some tract.

C_{24} 2,6,15,19-tetramethylicosane (TMI). TMI, first discovered by Vink et al. (1998), is rarely found in natural archives. To date, TMI has only been reported before from saturated hydrocarbon fractions and in kerogen extracted from laminated black shales and massive marls of the Paquier and Kilian levels (OAE1b) in the Vocontian Basin (SE France), the Ionian Basin (NW Greece), and at the ODP Site 1049C (North Atlantic Ocean), whereas it is absent either in underlying and overlying levels or in any other non-contemporaneous black-shale horizon (Vink et al., 1998; Kuypers et al., 2001, 2002; Okano et al., 2008; Tsikos et al., 2004). There are no modern analogues for this isoprenoid nor any evidence about its biological precursor. Nevertheless, because its structure and carbon isotopic composition are similar to those of PMI, TMI is widely considered as a methanogenic and/or methanotrophic archaeal compounds (Vink et al., 1998; Kuypers et al., 2001, 2002; Brocks and Summons, 2004; Peters et al., 2005; Okano et al., 2008).

TMI was detected on the basis of their corresponding mass spectra and characteristic retention times (Vink et al. 1998). It is recorded in all samples of Poggio le Guaine section, in both limestone and black shales levels (Figs. 4.8, 4.12-4.13), although highest levels are recorded in the black shales intervals.

This is surprising as this is the first time that TMI is detected in sediments which do not belong to the Kilian and the Paquier black shales levels (Vink et al., 1998; Kuypers et al., 2001, 2002; Okano et al., 2008). The GC-MS chromatograms in fig.

4.13 clearly shows the occurrence of TMI peak in the apolar fraction from limestone sample at 4.70 m.

TMI shows similar trend to that of PMI, but slightly higher concentrations. Argillaceous limestone levels from 0.00 to 3.00, from 4.15 to 7.81, and from 8.55 to 9.88 meters record TMI content of ~25 µg/g TOC, with a modest increase up to 101.39 µg/g TOC corresponding to the sample 6.25 m, as PMI. The strongest TMI signal is recorded at the black shales of the Leenhardt sub-event, with a prominent peak up to 132.11 µg/g TOC, after which TMI content decreases to the mean value of 33.21 µg/g TOC (Tab. 9 - Supplementary materials).

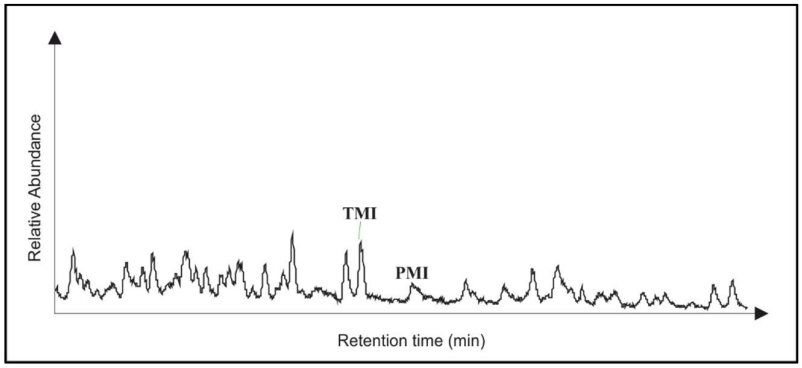

Fig. 4.13. Partial GC-MS gas-chromatogram (*m/z* 71.1) of apolar fraction from sample 4.70 m of the PLG section.

Ultimately, patterns of PMI and TMI along the Late Aptian / Early Albian Poggio le Guaine section provide evidence of the leading role of Archaea in the biochemical cycle of carbon during the OAE 1b, with temporary expansion of archaeal biomass concomitant to the black-shales deposition.

4.9.2.2 Cyclic aryl isoprenoids

Aryl isoprenoids are a large range of diagenetic and catagenetic products of isorenieratene, a photosynthetic pigments aromatic carotenoid that is considered to be uniquely biosynthesized by brown-coloured photosynthetic green sulphur bacteria (Chlorobiaceae) (Summons & Powell 1987; Sinninghe Damsté et al., 2001; Liaaen-Jensen, 1978; de Wit and Caumette, 1995). Green sulphur bacteria are phototrophic anaerobes that require both light and H_2S for growth. They thrive when the euxinic zone reaches the photic zone in the water column, creating the optimal habitat that offers a combination of lights and H_2S availability. Hence, presence of Chlorobiaceae-derived aryl isoprenoids in sediments and oils extracts

allows to evaluate the redox conditions in the depositional source rock environments (Summons and Powell, 1986, 1987; Clark and Philp, 1989; Yu Xinke et al., 1990; Fowler, 1992; Requejo et al., 1992; Hartgers et al., 1994a,b; Koopmans et al., 1996a). However, Koopmans et al. (1996b) found that aryl isoprenoids may also derivate from aromatisation of β-carotene, a carotenoid ubiquitous in higher plants, algae and some Bacteria. Their results indicate that mere identification of aryl isoprenoids, without determination of their $\delta^{13}C$ values, cannot be used to assess the presence of Chlorobiaceae, and, thus, photic zone euxinia in the depositional environment.

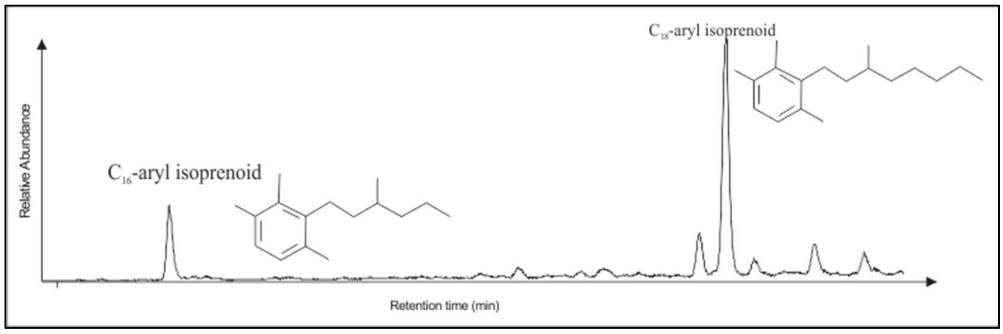

Fig. 4.14. Peaks of C_{16}- and C_{18}-aryl isoprenoids in the partial GC/MS gas-chromatogram (*m/z* 133.1) of apolar fraction from sediment extract of black shales samples of PLG section.

In this study, only C_{16}- and C_{18}- aryl isoprenoids were found (Figs. 4.12, 4.13, Tab. 9 - Supplementary materials). Carbonate levels are devoid of aryl isoprenoids, whereas all the black-shales levels along the investigated section record C_{16}- and C_{18}-aryl isoprenoid concentrations ranging around the mean value of ~6.40 µg/g TOC. Abrupt and brief increases are detected just in the Jacob and Paquier levels, where C_{16}- and C_{18}- concentrations rise to 61.67 and 88.97 µg/g TOC, and to 38.50 and 50.96 µg/g TOC, respectively. These patterns point to episodic expansion of euxinia to the photic zone during the late Aptian – early Albian interval in the western Tethys realm.

4.9.3 Steranes

Sedimentary steranes derive from sterols that are present in cell membranes of a wide variety of eukaryotes, mainly algae and higher plants (Mackenzie et al., 1982). Sterols are essential lipids that control membrane permeability and rigidity. Even if sterols are widespread among eukaryotes, a large number of steranes is diagnostic for certain taxonomic groups (e.g., Volkman, 2003). The conversion of sterols to steranes occurs without loss or gain of carbon atoms. Hence, the sterane

carbon number distribution will reflects the carbon number distributions of the sterols of the organism active in the depositional environment (Grantaman and Wakelfield, 1988). Steranes with 21 and 22 carbon atoms are known (Wingert and Pomerantz, 1986) although those with carbon numbers ranging from 26 to 30, and especially those with 27, 28 and 29 carbon atoms, are more frequently reported in crude oils and source rocks extract. (Seifert and Moldowan, 1978, 1979; Mackenzie et al., 1982; McKenzie et al., 1983). C_{27} sterols are typical of zooplankton and red algae, C_{28} sterols dominate in phytoplankton (green algae e diatoms), and C_{29} sterols occur in higher plants and some strains of brown or green algae (Huang and Meinschein, 1979).

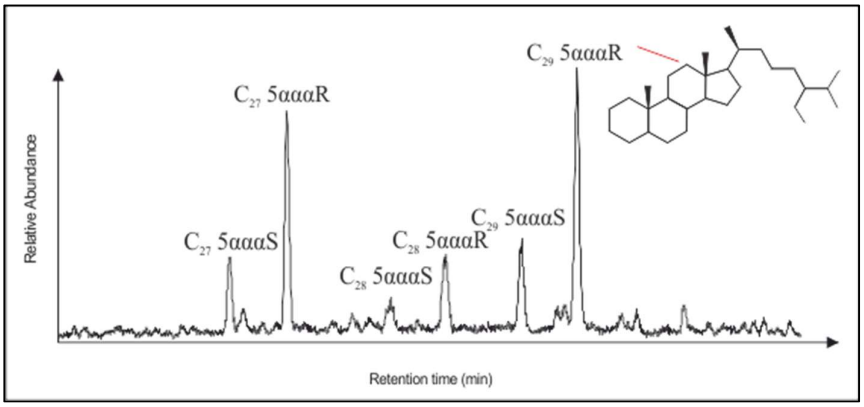

Fig. 4.15. GC/MS gas-chromatograms (*m/z* 217.1) showing the peaks relative to C_{27}, C_{28} and C_{29} 5ααaS-R isomers.

In Poggio le Guaine sample extracts, the 5α,14α,17α(H)-20R (5ααaR) isomers of 3 steranes, cholestane (C_{27}; M^+=372), 24-methylcholestane (C_{28}; M^+=386), e 24-ethylcholestane (or stigmastanes) (C_{29}; M^+=400), were identified in all black-shales samples (Fig. 4.15), albeit with very low concentrations (highest concentration 13.18 µg C_{29} / g TOC at 10.82 m, few cm below the Monte Nerone black-shale interval; Tab 10 - Supplementary materials). Limestones and calcareous marls from 0.00 to 3.00 m, 4.14 to 7.90 m and from 8.39 to 8.98 m, are devoid of steranes or have concentrations minor of 1.00 µg / g TOC, except for just two samples at 5.80 and 6.18 m. Steranes relative abundances are reported in Table 10 (Supplementary materials), which shows that C_{27} and C_{29} steranes are more abundant than C_{28}. Minor amounts of C_{27}, C_{28} and C_{29} 5ααaS isomers were also detected (Fig. 4.15, Tab 10 - Supplementary materials), whereas no 14β, 17β(H)- isomers or 5β,14α,17α(H)-20R configurations were found.

The source-specificity of C_{27}, C_{28}, and C_{29}-steranes is the base of using their abundances (expressed as %) on a ternary diagram to differentiate ecosystems. Figure 4.16 displays homogenous planktonic-marine organic facies for most of PLG samples, with only minor deviations towards terrestrial input shown by extracts from argillaceous limestones from the interval between the Jacob and the Kilian levels.

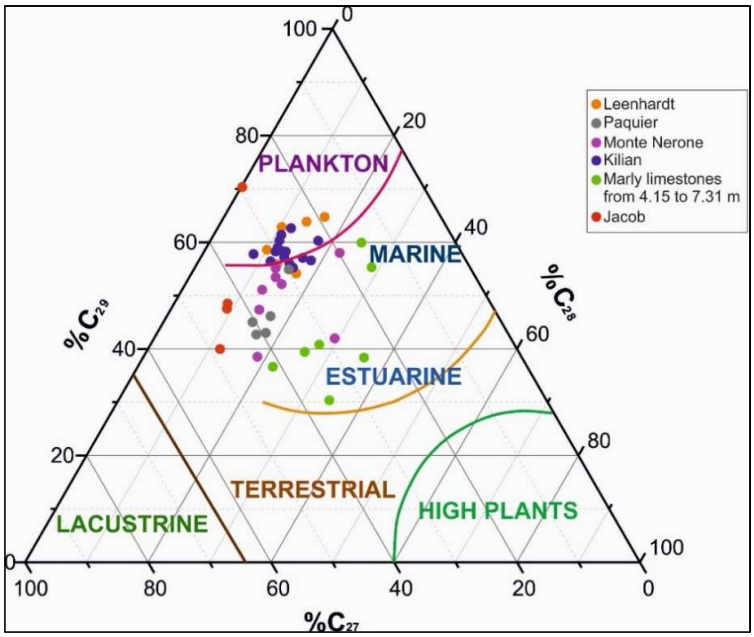

Fig. 4.16. Ternary diagram showing the relative abundances of C_{27}, C_{28}, C_{29} regular steranes in the apolar fractions of Poggio le Guaine section determined by gas chromatography / mass spectrometry (M+ → 217).

4.9.4 Hopanes

Hopanes are general biological source indicator. They are pentacyclic triterpenoids commonly containing 27-35 carbon atoms derived from cell membranes of prokaryotes. The major precursors include bacteriohopanetetrol and related bacteriohopanes produced mainly by heterotrophic bacteria and phototrophic cyanobacteria (e.g., Ourisson et al., 1987; Ourisson and Rohmer, 1992). Hopanes with more than 30 carbon atoms are commonly called **homohopanes**, where the prefix homo- refers to additional methylene groups attached to C_{30} hopane.

Full range hopane series from C_{29} to C_{32} is present in trace to substantial amount in the apolar fraction (Fig. 4.17, Tab. 11 - Supplementary materials). All αβ, βα,

and ββ stereochemical arrangement are displayed along with 22S- and 22R-stereoisomers. Table 5 (Supplementary materials) provides the list of the hopanes identified in all samples except in the basal three meters of the section (0.00 - 3.00 meters) and in the 1.17m-thick interval before the Kilian event (from 8.71 to 9.88 m). C_{31} αβ- and βα- homohopane is the prominent compound in most of the studied samples, with 22R-isomers dominating over the 22S-isomers but subordinate to ββ-hopanoids (Tab. 11- Supplementary materials). Highest concentrations of C_{31}-homohopane are recorded in the black shale levels from the Jacob (highest concentration of 36.36 µg/g TOC), the Kilian (35.26 µg/g TOC), and Paquier (60.79 µg / g TOC) sub-events, suggesting temporary pulses of bacterial input and/or bacterial reworking during early diagenesis.

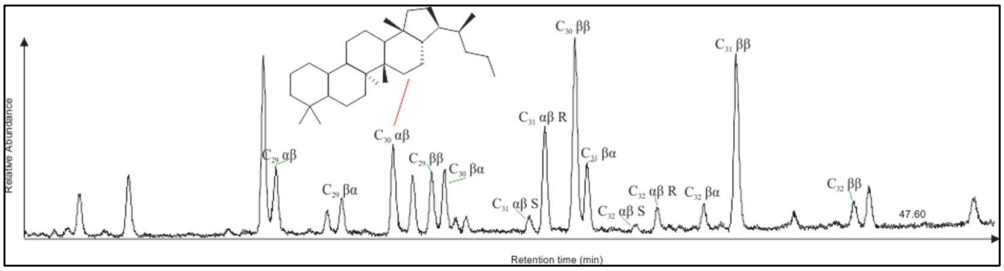

Fig. 4.17. Mass chromatogram (*m/z* 191.1) showing the full range hopane series C_{29} to C_{32} detected in the apolar fraction of sediments extracts of PLG section.

4.10 Thermal Maturity Parameters and Their Use

The use of biomarkers as thermal maturity parameters is based on the structural modifications of compound by stepwise transformations from biological precursor molecules to geochemical fossil thermodynamically more stable through sequences of enzymatic reactions. Generally, biological molecules have a so-called "biological configuration", that is the particular structural arrangement of atoms (stereochemistry) that confers the best functionality to the living organism. However, such biological configuration is no thermodynamically stable, and therefore the diagenetic pathways operates on a sequential structural rearrangement toward more stable molecules having the so-called "geological configurations". The stereochemical transformations are progressive and proportional to time and temperature of sedimentary burial. The concept of "thermal maturity" hence refers to the extent of thermal alteration and intensity of stereochemical transformations between the "biological molecules" and "fossil molecules" end-members. Peters et al. (2005) defines "immature" the organic matter affected by diagenesis, including

biological, physical and chemical alteration, but without a pronounced effect of temperature. “Mature” organic matter has been affected by catagenesis, that is equivalent to the oil-generative window. Finally, “postmature” is the organic matter heated to such high temperatures that it has been reduced to a hydrogen-poor residue capable of generating only small amounts of hydrocarbon gases.

In this study, the following thermal maturity proxies were considered: Pr/n-C17 and Ph/n-C18 ratios, Steranes 20S/(20S+20R) isomerization, 22S/(22S+22R)-homohopanes, moretane vs hopane ratios, ββ/(ββ+αβ+βα)-hopane, and ββ/(ββ+αβ+βα)-homohopane ratios.

4.10.1 Pr/n-C_{17} and Ph/n-C_{18}

The isopreniods / n-alkanes (Pr/*n*-C_{17} and Ph/*n*-C_{18}) ratios provide valuable information on biodegradation, maturation and diagenetic conditions, as by increasing maturity *n*-alkanes are generated faster than isoprenoids in contrast to biodegradation (Waples; 1985; Peters et al., 2005). Isoprenoid hydrocarbons are generally more resistant to biodegradation than normal alkanes, and therefore the ratio of the pristane to its neighbouring *n*-alkane C_{17} is provided as a rough indication to the relative state of biodegradation. This ratio decreases as weathering proceeds.

Pr/*n*-C_{17} and Ph/*n*-C_{18} ratios along Poggio le Guaine section shows mean values of 1.41 and 0.60, respectively, and prominent peaks in correspondence of Jacob level (Fig. 4.10, Tab. 8 - Supplementary materials), indicating significant abundances of isoprenoids respect to *n*-alkanes, and consequently low maturity and/or low biodegradation of organic matter.

4.10.2 Steranes 20S/(20S+20R) isomerization ratio

During diagenesis and catagenesis the biological stereospecificity of sterols, particularly at C-5, C-14, C-17, and C-20, is usually lost and a diverse range of isomers is generated. In the first three stereocenters, that are the conjunctions points between rings in the tetracyclic system, hydrogen atom can be below or above the plane formed by the four rings, and these positions are referred as α and β respectively. Hence, the term αββ-sterane is commonly used as short-hand to denote steranes with the 5α(H),14β(H),17β(H) configuration, while ααα-sterane refers to those with 5α(H),14α(H),17α(H) stereochemistry.

C-20 stereocenter is not a conjunction point of rings and two main sterane isomerisation reactions have been described (Mackenzie et al., 1980, 1981, 1982, 1983, 1984; Mackenzie and McKenzie, 1983). The first is the isomerisation of "normal" 5α(H),14α(H),17α(H)-20R steranes, that is the only configuration at C-20 that occurs in steroid precursors in living organism and consequently occurs as the most prominent steranes of very immature sediments. As the maturity increases, isomerisation at the chiral carbon-20 takes place gradually converting C20-R steranes in a mixture of R- and S-sterane configurations. The increase of the 20S isomer concentrations relative to the 20R isomers continues until an equilibrium condition is reached [20S / (20S + 20R) ~ 0.55], after which the relative isomer concentrations remain the same although source rock maturity may continue to increase. The steranes isomerization ratios are often reported for the C_{29} compounds, even if all C_{27}, C_{28} and C_{29} 20S/(20S+20R) ratios have equivalent potential as effective maturity parameters. Moreover, comparison of 20S/(20S+20R) ratios of steranes with different carbon number can be useful to verify if these biomarkes are all indigenous, as different ratios suggest that they experienced distinct thermal histories, and therefore some them results from contamination.

The C_{29} 20S / (20S+20R) ratios is considered to be independent of organic matter input and therefore an effective maturity parameter for oils and some source rocks extracts (Peters et al., 2005). This ratio in PLG extracts shows values far below the equilibrium threshold (~ 0.55), generally around of 0.29, except for three samples (4.71, 9.88 and 17.92 m) where values are ≥ 0.45 (0.48, 0.45 and 0.45, respectively) (Tab. 12 - Supplementary materials). C_{27} and C_{28} 20S / (20S+20R) ratios show general trends similar to that of C_{29}, thus indicating a comparable thermal history and excluding any contamination from non-indigenous organic matter.

4.10.3 Hopanes parameters

The biological configuration of hopanes precursors, which show the biological 17β,21β(H)-stereochemistry, is nearly flat to allow bacteriohopanetetrol to fit into the lipid membrane structure (Rohmer, 1987). Because this stereochemical arrangement is thermodynamically unstable, diagenesis and catagenesis of bacteriohopanetetrol result in transformation of the 17β,21β(H)-precursors to the

17α,21β(H)-hopane and 17β,21α(H)-hopanes, where notations α and β indicate if the hydrogen atoms are below or above the plane of the rings, respectively. Compounds in the βα series are also called **moretanes**. Hopanes and homohopanes with a ββ configuration are usually absent from petroleum and sedimentary rocks that have undergone mild diagenesis because it is thermally unstable. Conversely, hopanes with αα stereochemical arrangement are not natural products and it is unlikely that they occur above trace levels in petroleum (Bauer et al., 1983). Likewise, bacteriohopanetetrol holds the biological 22R configuration, which is an extended side chain with an additional asymmetric centre at C-22. Experiencing diagenesis and catagenesis processes, 22R arrangement gradually converts to an endpoint mixture of 22S and 22R αβ-homohopanes (Seifert and Moldowan, 1980), which results in two peaks for each homolog (22R and 22S) on the mass chromatograms for these compounds.

As stated above, apolar fractions of Poggio le Guaine section display all αβ, βα, and ββ stereochemical arrangement of hopanes, along with 22S- and 22R-stereoisomers, suggesting low thermal maturity and degradation of the organic matter.

All the maturity-sensitive stereoisomers and configurations of hopane series allow to use the moretane/hopane and 22S/(22S+22R) ratios as thermal maturity indicators.

Isomerization of terpanes. since the 22R configuration of biological hopane precursor is converted gradually to a mixture of 22R and 22S stereoisomers, the proportion of 22R and 22S can be calculated for any of all the homohopanes to infer the thermal maturity of OM. The 22S/(22S+22R) ratio rises from 0.00 to ~0.60 (0.57-0.62 = equilibrium) during maturation (Seifert and Moldowan, 1980). Ratios in the range 0.50-0.54 suggest that samples have barely entered oil generation, while ratios in the range 0.57-0.62 indicate that the main phase of oil generation has been reached or surpassed (Peters et al., 2005). After reaching equilibrium at the early oil-generative stage, no further maturity information is available because the 22S/(22S+22R) ratio remains constant.

In Poggio le Gauine saturated hydrocarbon fraction, both C_{31} and C_{32} 22S/(22S+22R)-homohopanes ratios shows values far lesser than equilibrium range (Tab. 13 - Supplementary materials), meaning that most of the sediments never

entered oil generation phase. Exceptions are sediment from 1.80 to 2.40 meters, and from 4.71 to 6.53 meters, that show ratios ranging between 0.51 to 1.00, indicative of high thermal maturity.

Moretane / hopane ratio. As stated above, the 17β,21α(H)-moretanes are thermally less stable than the 17α,21β(H)-hopanes, and abundance of the C_{29} and C_{30} moretanes decrease relative to the corresponding hopanes with thermal maturity. During burial, the ββ-hopanes readily convert to βα-(moretane) and αβ-hopane configuration. At low temperature, the conversion on these compounds back to ββ-hopanes is not possible. At higher temperatures, the conversion of moretanes back to αβ-hopane become possible through a ββ-hopane intermediate. However, the high energy barrier allows little conversion of αβ-hopanes to ββ-hopanes, resulting in an equilibrium mixture favouring αβ-hopanes over βα-moretane by ~20:1. The ratios of ββ/(ββ+αβ+βα) and of moretanes to their corresponding hopanes, then decreases with thermal maturity. Moretane / hopane ratios range from ~0.8 in immature bitumes to <0.15 in mature source rocks and oil to a minimum of 0.05 (Mackenzie et al, 1980; Seifert and Moldowan, 1980).

In PLG extracts, moretane/hopane ratios reflect low thermal maturity with values generally greater than 0.15, except for some level in the carbonate interval from 4.15 to 6.53 m that, again, records higher maturity degree (C_{29}- and C_{30}- moretane / hopane ratios of ~0.10) (Tab. 13 - Supplementary materials). Table 13 (Supplementary materials) shows the abundances of the ββ- hopanes and -homohopanes respect to total of hopanes (or homohopanes) expressed in per cent. The results clearly show that the ββ- isomers are major contributor among all isomers (average contribution 43.76%) and hence confirm low thermal maturity and degradation of the organic matter extracted.

Chapter 5
Results from DSDP Site 511

5.1 Identification of bioevents and comments on the faunal assemblages

The microfaunal assemblages observed in the samples from the late Aptian – early Albian succession of the DSDP Site 511 are remarkably well-preserved and typical of upper-bathial depths. In addition to planktonic and benthonic foraminifera, and Radiolaria, washed residue contains several ostracods, abundant pelecypods (unbroken or fragments), siliceous sponge spicules, fragments of calcareous algae, bryozoans, and echinoids. Most of samples are dominated by benthic foraminifera (both agglutinated and throchospiral calcareous), which shows high genera diversity and often glassy (i.e., optically translucent) shells. The planktonic foraminifera are poorly represented and show low species diversity. Their abundances are always subordinate to those of benthic foraminifera and radiolarian, and specimens > 200 μm are from few to rare even in the Aptian strata.

The lower biozone identified at the DSDP Site 511 correspond to the *Hedbergella trocoidea* Partial Range Zone, and includes common occurrence of *Hd. aptiana* and *Hd. infracretacea*, and subordinate *Hd. trocoidea*, *Hd. excelsa* and *Hd. gorbachikae*. Planktonic foraminifera record a drastic drop in abundance from 43.14% to 0.36% at 482.80 mbsf, followed by a brief increase to 24.65% at 492.10 mbsf (Fig. 5.1, Tab. 14 - Supplementary materials). The benthic foraminifera dominate the microfaunal assemblages, with abundances up to 91.50%. The Radiolaria shows mean abundances of 12.72% with a prominent peak 492.80 mbsf where they temporary reach the 60% of the total assemblage.

The upper boundary of the *Hedbergella trocoidea* Zone is marked by the LO of *Pa. rohri* (= *Paraticinella eubejaouaensis* of Huber and Leckie, 2011, and *Ticinella bejaouaensis* of Robaszynski and Caron, 1995) at 492.10 mbsf. Huber and Leckie (2011) reported this bio-event at 491.23 mbsf merely because of the lower resolution adopted by the authors respect those of this study. The *Pa. rohri* Taxon-range Zone comprises total range of *Pa. rohri* that, at the DSDP Site 511, spans from the LO of Pa. rohri at 492.10 mbsf to the HO of this taxon at 486.20 mbsf. This biostratigraphic interval records the co-occurrence of few specimens of *Pa. rohri*, *Pa. transitoria*, *Hd. trocoidea*, *Hd. infracretacea*, *Hd. gorbachikae*, and more

common *Hd. aptiana*, *Hd. excelsa*, *Hd. ruka*, and *Hd. praelippa*. The planktonic foraminiferal abundances are low throughout the biozone, ranging around the mean value of 6.83%. Benthic foraminifera are more abundant in the lower part of the biozone, with mean percentages between the 50 and 60%, whereas from 487.41 mbsf to the top Radiolaria account on average for the 60% of the total assemblages (Tab. 15 - Supplementary materials). The LO of *Mi. miniglobularis* is recorded at 486.71 mbsf, and hence this taxon co-occurs with *Pa. rohri* for a short interval, which is similar to observations made at PLG (Fig. 5.1).

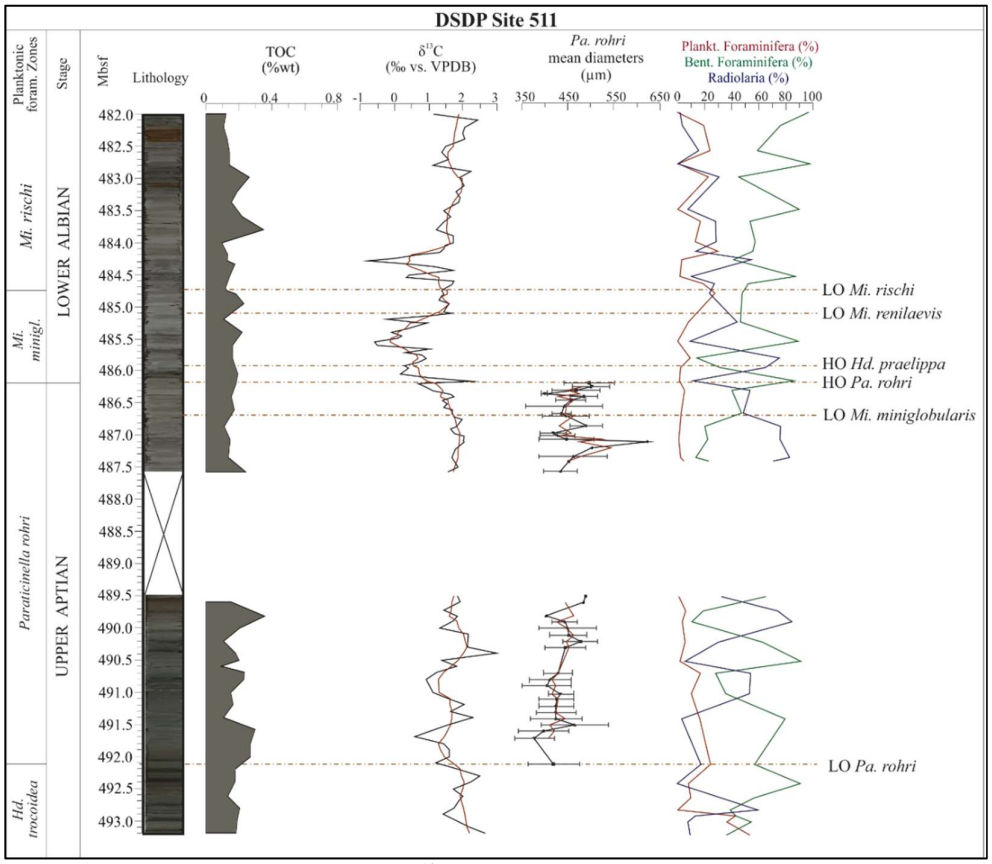

Fig. 5.1. Depth profiles of TOC content, $\delta^{13}C$, mean diameters of *Pa. rohri* and relative abundances of planktonic, benthic foraminifera and Radiolaria at DSDP Site 511. Orange dashed lines marks major bioevents. Key to planktonic foraminiferal abbreviations: *Pa. = Paraticinella*, *Mi. = Microhedbergella*, *Hd. .= Hedbergella, minigl. = miniglobularis*

The last specimen of *Pa. rohri* is found at 486.20 mbsf, almost in agreement with Huber and Leckie (2011) who place the HO of this species at 486.16 mbsf. The extinction horizon of *Pa. rohri* coincides with a major change in the planktonic foraminifera assemblages resulting in the abrupt and dramatic decrease of tests size, although the relative abundances do not show significant deviation from the mean

value of 3.55%. The extinction of *Pa. rohri* is, in fact, concomitant to the definitive disappearance of the large-sized late Aptian planktic species, dimensions of which range 200-500 μm, whereas species occurring within the overlying levels average 80-100 μm. The *Mi. miniglobularis* Interval Zone represents the biostratigraphic interval from the HO of *Pa. rohri* to the LO of *Mi. rischi* (Fig. 5.1). Species diversity is very low, with only *Mi. miniglobularis* and *Hd. praelippa* occurring up to 485.95 mbsf, where the latter records its HO. Then *Mi. miniglobularis* co-occurs with small microperforate hedbergellids that Huber and Leckie (2011) consider as gradual evolutionary transition from the nominate taxon to *Mi. renilaevis*, whose LO is identified at 485.11 mbsf. Benthic foraminifera and Radiolaria account for the 86% of the total assemblages alternating in dominating during short intervals (Fig. 5.1).

The LO of *Mi. rischi* is identified at 484.75 mbsf, in agreement with Huber and Leckie (2011). However, this taxon is rare to few in relative abundance and is sporadic in its stratigraphic occurrence. The *Mi. rischi* Partial-range Zone comprises the biostratigraphic interval from the HO of the nominate taxon to the top of the studied succession. The relative abundances of planktonic foraminifera tend to increase slightly, also reaching peaks of 30% and 24% (at 484.15 mbsf and 482.60 mbsf, respectively). From 484.15 mbsf benthic foraminifera dominate the assemblages with percentages ranging from 45% to 97.88%, whereas Radiolaria progressively decrease in number upward (Tab. 14 - Supplementary materials).

5.2 Test size variations in *Pa. rohri*

The *Pa. rohri* Taxon-range Zone spans from 492.10 mbsf to 486.20 mbsf, with total thickness of 5.96 meters (Fig. 5.1). Planktic foraminifera occur as the 6.83% of the total assemblage through the Aptian biozone. Consequently, the nominated taxon is difficult to find, and it is recorded sporadically and in low amount. It should be noted that the discontinuous occurrence of *Pa. rohri* could have possibly led uncertainty of the boundary assignment above and below its recorded range.

The mean size of *Pa. rohri* throughout the biozone is 448.40 μm, ranging from the minimum of 376.06 μm to the maximum diameter of 623.70 μm (Tab. 15 - Supplementary materials).

The first specimens of *Pa. rohri* occurring at 492.10 mbsf shows mean test size of 417.94 μm. After a brief decreasing phase to 376.06 μm, mean diameters record a long-term increasing trend culminating at 489.50 mbsf with the mean value of

487.64 μm. Some brief size reduction is recorded at 490.89 mbsf and 489.81 mbsf. *Pa. rohri* populations show moderate to high size-variability (mean standard deviation of ± 45.9 μm) throughout this interval. The wider dimensional range is shown by the specimens picked at 490.00 mbsf, whose diameters range between 341.38 μm and 549.70 μm. Unfortunately, the not-recovered sediments from 489.50 mbsf to 487.50 mbsf does not allow the reconstruction of the dimensional changes through this 2 m -thick interval.

From 487.57 mbsf upward, the mean diameters show a strong increasing trend culminating at 487.11 mbsf with the value of 623.70 μm, the largest dimension recorded throughout the section. The overlying samples up to 486.39 mbsf yields smaller specimens of *Pa. rohri* with mean size of 444.75 μm. The brief interval prior its extinction is marked by an increase of 20% in size and the last specimens of *Pa. rohri* occurring before its extinction show diameters of about 500 μm (Fig. 5.1, Tab. 15 - Supplementary materials).

5.3 Carbon isotope data

Carbon isotope values vary between -0.78‰ and +2.99‰ through the late Aptian – early Albian sedimentary succession of DSDP Site 511 (Fig. 5.1, Tab. 14 - Supplementary materials). In the *Hd. trocoidea* Zone, the $\delta^{13}C$ value range from 1.42‰ to 2.65‰. The lower part of *Pa. rohri* is characterized by wider short-term shift of $\delta^{13}C$ values, which range between 0.59‰ and 2.99‰ (492.1 - 489.5 mbsf). From 489.50 to 487.50, the $\delta^{13}C$ is interrupted because of the not recovered interval. This is followed by a gradual negative trend of the $\delta^{13}C$ values, up to -0.59‰ at 485.54 mbsf, interrupted by an abrupt increase (2.25‰) coinciding with the extinction level of *Pa. rohri*. From 485.5 mbsf the carbonate $\delta^{13}C$ values increase and the horizon at 485.14 mbsf is marked by an abrupt increase up to 1.06‰, followed by a nearly constant vertical trend up to slightly above the lower boundary of the *Mi. rischi* Zone. At 484.50 mbsf the $\delta^{13}C$ decrease to the value of 0.42‰, followed by a prominent negative spike of -0.78‰ at 484.286 mbsf. Then the $\delta^{13}C$ curve gradually returns to positive values and display a relatively increasing trend interrupted by a weak negative shift of ~1.11‰ at 482.795 mbsf.

5.4 Total Organic Carbon Content

The late Aptian – early Albian interval of the DSDP Site 511 does not show significant TOC contents, with values ranging between 0.17% and 0.36%, confirming the absence of black-shale levels in this section (Fig. 5.1, Tab. 14 - Supplementary materials). Only some interval shows weak enrichment compared to the background value of 0.17%, as from 492.00 mbsf to 491.59 mbsf, at 489.81 mbsf, 483.80 and 482.98 mbsf (TOC content of ~0.28‰, 0.36‰, 0.35‰ and 0.26‰, respectively). Moreover, there is no correspondence between higher TOC values and darker-coloured sedimentary horizons.

Chapter 6
Discussions

6.1 The emplacement of the Southern Kerguelen Plateau as trigger for the OAE 1b

The climatic impact triggered by the emplacement of Large Igneous Provinces (LIPs) during the Earth's history has long been a topic of intense interest and of considerable research effort. The volcanic activity linked to LIPs is now recognised as an important trigger for major environmental and climatic changes as the OAEs, with relevant impact on the ocean-atmosphere system by injecting large amount of gases and particulate that alter the structure and chemistry of atmosphere and oceans (Coffin and Eldholm, 1994; Ernst, 2014, Erba, et al., 2015). In particular, enhanced volcanic and hydrothermal activity associated with LIPs i) increase atmospheric pCO_2 and temperature, leading to enhanced chemical weathering intensified by increased runoff and input of terrestrial nutrient fluxes to the oceans, ii) increase input of reduced trace metal fluxes, and iii) induce oxygen depletion and possibly inject extra-input of micronutrients producing enhanced primary production (e.g., Adams et al., 2010; Frijia and Parente, 2008; Kerr, 1998; Kuroda et al., 2007; Sinton and Duncan, 1997; Turgeon and Creaser, 2008).

6.1.1 The Southern Kerguelen Plateau

The Kerguelen Plateau is one of the largest ingenuous province in the world, consisting on ~2.5×10^7 km^3 –wide submarine structure of mafic crust in the Southern Indian Ocean, on the Antarctic plate (Coffin et al., 2002)

Knowledge of this province is extensive thanks a huge number of available seismic reflection data, piston coring and drilling results of Ocean Drilling Program (ODP) Legs. Evidence from basalts and overlying sediments combined with results of subsidence modelling, has shown that much of the igneous crust of the Southern (SKP) and Central Kerguelen Plateau (CKP) was erupted in a subaerial environment (Mohr et al., 2002). Moreover, portions of the SKP remained subaerial for as much as ≥ 50 Ma after volcanism ceased.

Compared with most other LIPs, which formed typically within a few million years, Kerguelen had an unusual and complex emplacement history (Frey et al., 2000; Duncan, 2002).

Geochronology of the uppermost igneous crust of the Kerguelen Plateau suggests that its older southern portion (the SKP) formed over a prolonged period, with a major peak in magmatic output from *ca*. 119 to *ca*. 110 Ma (Coffin et al., 2002; Duncan, 2002; Frey et al., 2003). The volcanism was linked to the onset of the sea-floor spreading between India, Australia and Antartica plates (Houtz et al., 1977; Operto e Charvis, 1995; Frey et al., 2002). Over its geological history, the SKP activity correlates, in time and place, with the southward movement of the Kerguelen hotspot interacting with the overlying lithosphere (Frey et al., 2002). In contrast, the Northern Kerguelen Plateau (NKP) is appreciably younger, having been erupted largely in the late Eocene-early Oligocene, with minor volcanism continuing up to the present on Kerguelen Island.

On the basis of $^{40}Ar/^{30}Ar$ ages measurements of magmatic rocks, Coffin et al. (2002) estimated that the magma output rate increased by several orders of magnitude (to ~0.9 km^3/y), during the emplacement of the SKP and the structurally linked Rajmahal LIP. There is a general correlation between the size of the LIP and the amplitude of the associated climatic perturbation, and that is why the South Kerguelen is considered a direct responsible for the end of late Aptian cold-house phase and the restoration of the normal greenhouse state (Bodin et al., 2015).

6.1.2 Mercury chemostratigraphy as a powerful tool for recognising worldwide LIP impact

Since very recently, the mercury chemostratigraphy has been considered as a powerful proxy for distal volcanic activity, offering the possibility to evaluate the potential relationship between major environmental perturbations and LIP activity (Nascimento-Silva et al., 2011; Sanei et al., 2012; Sial et al., 2016). Volcanic and submarine hydrothermal emissions are the major contributors of natural Hg in the ocean-atmosphere system. The enrichments of this element are generally used to trace increased volcanic activity in both proximal and distal sites, because of its emission in the form of gaseous elemental mercury (Hg^0), which is globally distributed due to a rather long atmospheric residence time (0.5-2 y) (Lindberg et al., 2007; Ariya et al., 2008). After a gas-phase oxidation to reactive and soluble

Hg^{2+} by halogen, ozone and other radicals, Hg is deposited in continental and marine environment by precipitations. In the aquatic realm, most of Hg is scavenged and deposited in the sediments by organic matter, where biotic or abiotic reactions may form mercury sulphide poly-complexes (HgS) or methylmercury (MeHg) (Sanei et al., 2012; Grasby et al., 2013; Percival et al., 2015). Also, mercury can be also adsorbed on clays with subsequent transport deposition and burial in marine sediments (Font et al., 2016).

Hg anomalies attributed to LIP activity have been identified in marine sedimentary sequences spanning major mass extinction events, in association with second-order extinctions, and in strata that records several Mesozoic OAEs (e.g., Sanei et al., 2012; Grasby et al., 2015; Percival et al., 2015; Font et al., 2016; Jones et al., 2016; Sial et al., 2016; Thibodeau et al., 2016, 2017). Grasby et al. (2013) also demonstrated that background Hg levels appear constant over geologic time, showing that Hg spikes associated with LIPs are truly anomalous feature or the rock record.

The Hg record are low throughout the "target interval" of PLG section, generally <5 ppb (Fig. 4.7, Tab. 4 - Supplementary materials). However, in the Jacob and Kilian levels the Hg concentrations increased rapidly to 200 ppb, preceded and followed by gradual impoverishments. The Hg/TOC ratios well mirror with the Hg contents, and intervals of maxima Hg concentrations correspond to samples with relatively high TOC contents. Actually, after the normalization, positive excursions in Hg/TOC ratios persist, implying that most of the Hg enrichments cannot simply be explained only by TOC enrichments and corresponding fluctuations in primary productivity and redox conditions. Furthermore, normalizing Hg concentrations against Fe contents does not remove the trend observed in overall Hg contents, which suggests that iron-hydroxides and Fe-sulphides did not influence Hg sequestration (Pyle and Mather; 2003). The Hg/Al profile also correlates well with the overall Hg contents, suggesting that the Hg fluctuations are not primarily controlled by changes in detrital input and/or absorption onto clays mineral. Noteworthy, the onsets of the two major Hg anomalies parallel the decreasing segments of the $\delta^{13}C_{carb}$ curve and both culminate at the black shale levels of the Jacob and the Kilian sub-events (Figs. 4.2 and 4.7), suggesting a degree of temporal synchronicity between the global carbon cycling perturbation and the process promoting the Hg enrichments.

Based on previous works, in which anomalous enrichments in Hg were interpreted as indicative of an increase in volcanic activity (Sanei et al., 2012; Sial et al., 2013; Grasby et al., 2015; Percival et al., 2015; Font et al., 2016; Thibodeau et al., 2016; Charbonnier et al., 2017), data collected along the PLG section suggest a rapid increase in atmospheric Hg concentrations, likely associated with main pulse of volcanic activity that released massive amount of volcanic Hg into the atmosphere. The more realistic candidate for the main pulse in Hg contents to the atmosphere, and then in the studied sediments, seems to be the massive eruptions leading to the emplacement of the Southern Kerguelen Plateau (SKP). In the late Aptian time, in fact, volcanic activity on a massive scale constructed most of the SKP linked to the incipient Indian Ocean opening between India, Australia, and Antarctica at high southern latitudes (Coffin et al., 2002). The SKP volcanism was almost entirely subaerial and correlated with a period of excess of CO_2 (Retallack, 2001), although magma fluxes may have been an order of magnitude lower relative to other major LIP in the Earth history, as the Ontong-Java Plateau (Eldholm and Coffin, 2000). This difference might explain, at least partially, why greenhouse conditions were not fully reached, actually leading to the well-known "Late Aptian cold snap" (Price et al., 2012; McAnena et al., 2013, Erba et al., 2015). The SKP formed over a prolonged period, with a major peak in magmatic output from ca. 119 to ca. 110 Ma (Coffin and Eldhom, 1994; Coffin et al., 2002; Duncan, 2002; Frey et al., 2003). Thus, the multiple excursions observed in the Hg profile (Fig. 4.7) could reflect a multiple phase emplacement of the LIP.

6.2 The palaeoceanographic evolution of the OAE 1b

The mechanisms of black shale deposition are the focus of a long-standing controversy. The most accredited models to explain the widespread occurrence of this organic-rich layers refer to two end-members: the ocean stagnation model (STO) and the expansion of the oxygen minimum layer (OMZ) model. According to the first model, the high organic matter content in black shales is ascribed primarily to the elevated preservation efficiency of organic matter in the bottom of ocean, which was directly caused by oxygen deficiency resulting from seawater stagnation, strong vertical stratification and weak ventilation (e.g., Schlanger and Jenkyns, 1976; Bralower and Thierstein, 1984; Erbacher et al., 2001). In contrast, the second model stresses the importance of elevated primary productivity in the

surface ocean. The enhanced flux of organic matter sinking to the deep ocean increases the oxygen demand for degradation, until the overcoming of the oxygen supply and eventually causes the deep ocean to become anoxic (e.g., Pedersen and Calvert, 1990; Hochuli et al., 1999; Premoli Silva et al., 1999). However, some researcher considers a combination of both causes (e.g., Bralower et al., 1994; Bellanca et al., 1999).

Whatever the mechanism, both models involve continued and complete anoxia (and/or euxinia) until the oxygen content is restored by the reprise of bottom ventilation and/or the slowdown of the primary productivity. This produces to the recovery of benthic fauna and the reprise of OM degradation.

The OAE 1b apparently differs from the other Cretaceous OAEs. Its prolonged duration, the presence of multiple short-intervals of black shales deposition and the occurrence of highly specialized biota argue in favour of different mechanisms and feedbacks of the atmosphere-land-ocean system. This multi-episodic OAE seems related to i) several high-frequency short-term perturbations of the carbon cycle, ii) sudden increase of sea surface temperatures and iii) strengthening of density driven stratification of water column (Erbacher et al., 2001), suggesting similarity with the STO model. Moreover, the debate as to whether or not this multi-episodic event was completely anoxic is still open, whereas most of the studies would favour low oxygen conditions (Bralower et al., 1993; Holbourn et al., 2001).

It is now known that the late early-Cretaceous climate was far to be stable. Several brief global cooling and warming episodes (1 to 5 Myr-scale) have been identified during a generally extreme greenhouse climate (Weissert and Lini, 1991; Price, 2003; Weissert and Erba, 2004; Takashima et al., 2007), and basically, warming episodes are associated with accelerated water cycling, increased terrigenous influx (for example, siliciclastics and nutrients), rise of sea level and marine transgression (Weissert, 1990; Huber et al. 1995; Weissert et al., 1998; Clarke and Jenkyns, 1999; Wilson et al. 2002; Wortmann et al., 2004; Forster et al. 2007; Bornemann et al. 2008; Föllmi and Gainon, 2008; Mutterlose et al., 2009; Heldt et al., 2010; Herrle et al., 2010; McAnena et al., 2013).

This climatic transition reasonably punctuated the environmental forcing resulting in the multi-episodic OAE 1b, characterized by a rapidly changing oceanic system.

6.3 The late Aptian – early Albian record of PLG

The biological source of the organic matter of PLG samples has been evaluated based on the identification of several source-specific biomarkers and on their ratios. This allow to interpret the dynamics of the depositional environment based on the known physiological, biological, and environmental limitations of organisms from which the biomarkers originated (Peters et al., 2005).

6.3.1 Major contributors to the organic matter during the OAE 1b

The distributions of algal-, bacterial-, archaeal- and terrestrial- derived biomarkers through the PLG section suggest relevant variability of OM sources into the depositional basin during the late Aptian – early Albian interval (Fig. 6.1).

N-alkanes constitute a significant fraction of saturated hydrocarbons in almost samples. For most samples, the *n*-alkanes distribution is dominated by *n*-C_{16} and *n*-C_{18} (see MAC in Tab. 6 Supplementary materials), indicating a predominant marine source for the sedimentary OM. This is also supported by the significant amount of pristane and subordinate phytane identified through the section, and in particular at the Jacob, Paquier and Leehnardt levels and the marly interval from 13.95 m to 16.00 m.

However, the TAR ratio, which reflects the relative contribution of aquatic/marine and terrestrial *n*-alkanes, evidently shows the temporal variability in the proportion of land-plant material introduced in sediments during the deposition (Fig. 4.9, Tab. 7 Supplementary materials). The high molecular weight odd-numbered *n*-alkanes (*n*-C_{23} to *n*-C_{35}) associated with leaf waxes well occur in almost the samples, particularly in the lower 3 meters of the section, and, to a lesser extent, from 4.14 m to the Monte Nerone interval. Specifically, the sedimentary interval from 0.00 to 3.00 m is dominate by the *n*-C_{31} (mean concentration of 134.5 µg/g TOC) and all the long-chain *n*-alkanes account for ~76% of the total OM. This suggests intensive delivery of high amounts of terrestrial organic matter during the deposition. Nonetheless, the proportion of terrestrial relative to marine organic matter could be due to enhanced preservation of terrestrial relative to marine OM under oxidising conditions (Sinninghe Damsté et al., 2002; Słowakiewicz et al., 2015). The low amounts of OM in these levels (TOC of ~0.05%), the absence of more labile lipids as steranes and hopane stereoisomers, as well as the low concentrations of short-chain *n*-alkanes, suggest that OM degradation processes

were active on the ventilated oceanic floor, and can therefore alter the source signal of *n*-alkanes.

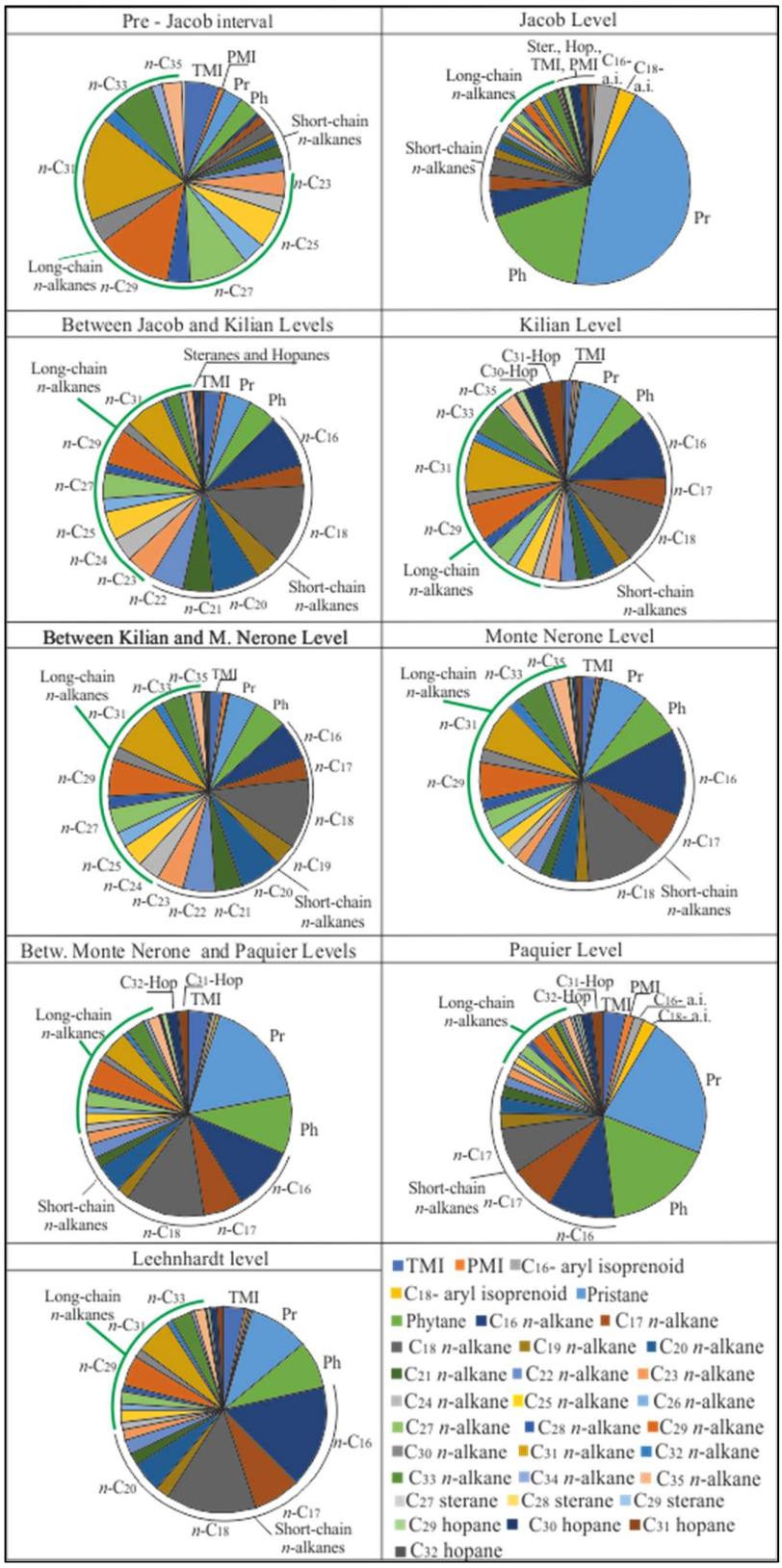

Fig. 6.1 Pie charts showing the mean biomarker composition of apolar fractions from the Poggio le Guaine section.

However, the active terrestrial input during late Aptian – early Albian interval is also supported by the Pr/*n*-C_{17} vs. Ph/*n*-C_{18} log plot and the steranes ternary plot (Fig. 4.11, 4.16). The former indicates prevailing terrestrial origin of the sedimentary OM extracted from most of the samples, in particular marly limestones between 4.15 m and 7.80 m, and Jacob, Kilian, Monte Nerone and Leenhardt black shales levels. Major marine algal contribution is suggested for the interval from 0.00 m to 3.00 m. The apparent contradiction with the results of the TAR ratio is probably related to the absence of the long-chain *n*-alkanes signal in this parameter. The distribution of C_{27} to C_{29} steranes, instead, emphasizes the mixed origin of the OM belonging to the sedimentary interval between the Jacob and Kilian sub-events, whereas support a mixed input of predominantly phyto- planktonic algae mainly during the Kilian and Leenhardt sub-events (Fig. 4.16).

6.3.2 Photic Zone Euxinia in Western Tethys Ocean during the late Aptian – early Albian OAE 1b

Trace metal and biomarker distributions through the PLG section suggests that fluctuating but frequently anoxic conditions were established during the deposition of black-shales levels. An efficient burial of OM under O_2-depleted conditions is indicated by high TOC contents, high abundances of biomarkers and high redox-sensitive proxies enrichments. Recent hypotheses about the OAEs occurrence, have invoked for OAEs the strong expansions of oceanic euxinia below the oxygenate surface layer, allowing the buildup of free H_2S through the water column concomitant with an upward excursion of the chemocline (Pancost et al., 2004; Kump et al., 2005). This presence of H_2S in the photic zone, termed Photic Zone Euxinia (PZE), can be inferred from the occurrence of aryl isoprenoids, which are diagenetic derivatives of isorenieratane, a pigment diagnostic for the presence of *Chlorobiaceae*. These are green sulphur bacteria that perform anoxygenic photosynthesis (Summons and Powell, 1986, Koopmans et al., 1996a; Sinninghe Damsté and Schouten, 2006), and thus require both light and H_2S for growth. However, Koopmans et al. (1996b) suggests extreme caution when using such biomarkers as indicators of PZE without any further constrain (as their $\delta^{13}C$ values),

since aryl isoprenoids may also originate from β-carotene, losing their redox-specificity.

Notably, at PLG section, the aryl isoprenoid concentrations became established following the development of reducing conditions in bottom waters, and rapidly disappear when oxic-suboxic conditions return (Fig. 4.12). This could reflect a marked shift in water-column redox state during the black shale deposition, likely associated with the intensification and vertical expansion of an intermediate-water oxygen minimum zone (OMZ) indicative of PZE. However, data of this study cannot resolve the PZE expansion and requires further investigations.

6.3.3 The methanogenic Archaea biomass in the Western Tethys Ocean during the OAE 1b

Many organic geochemical studies of OAE1b suggested that this multi-event was characterized by planktonic archaea as the main producers in sea waters (e.g., Kuypers et al., 2001, 2002; Tsikos et al., 2004; Okano et al., 2008; Trabucho Alexandre et al., 2011). The evidences consist in the occurrence of archaeal biomarkes such as TMI and PMI, as well as glycerol dialkyl glycerol tetraethers (GDGTs), in the Kilian and Paquier sediments from the southeast France (Vocontian Basin), the North Atlantic (ODP Site 1049) and the Ionian Basin (Tsikos et al., 2004). For the OAE 1b at PLG, Sabatino et al. (2015) speculated the expansion of marine archaea based on Rock-Eval parameters (mainly Hydrogen Index, HI), the $\delta^{13}C_{org}$ excursions and correlations with the well-constrained contemporary sedimentary sequences.

The biomarkers analyses carried out on the saturated hydrocarbon fractions extracted from Poggio le Guaine samples allow not only to confirm the occurrence of archaeal biomass during the OAE1b, but also to determine its temporal variability. The major archaeal lipids detected on PLG extracts are PMI and TMI, both considered reliable biomarkers for methanogenic archaea (Vink et al., 1998; Peeters et al., 2005; Kuypers et a., 2002; Pancost et al., 2000). They are present in considerable amounts throughout the section, not only in all the black shale intervals, but also in marly limestones and calcareous marlstones. This is surprising in many aspects. Firstly, this is the first time that TMI is detected in sediments which do not belong to the Kilian and the Paquier black shales levels (Vink et al., 1998; Kuypers et al., 2001, 2002; Okano et al., 2008). This probably relies on the

different lithological expressions of the OAE 1b event across basins, since previous authors studied sedimentary successions recording only the Paquier sub-event, as the ODP Site 1049 (Okano et al., 2008) or otherwise devoid of black shales levels correlated with all four sub-events of the OAE 1b.

The second, and perhaps most important aspect of the results of this study, is the detection of biomarkers diagnostic of methanogens in sediments documenting well-oxygenated depositional environment. Methanogenic Archaea are widely distributed in soils, wetlands, lakes, rivers, and marine environments (DeLong, 1992; McDonald et al. 1999, Takai and Horikoshi, 1999; Florin et al. 2000; Schouten et al., 2002; Galand et al., 2005; Bapteste et al., 2005; Knittel et al., 2005; Pouliot et al., 2009; Angel et al., 2012) and are responsible for a large fraction of organic carbon decomposition under anaerobic conditions (Kuntz et al., 2015). In early studies, archaeal habitats were thought to be limited shallow or deep-sea anaerobic sediments (Whitman et al., 1992) and deep-sea hydrothermal vents (Brock, 1978; Whitman et al., 1992). However, methanogens have been successfully isolated from plankton samples of oxic marine surface waters (Cynar and Yayanos, 1991; Hoef et al., 1997), suggesting the occurrence of potential anaerobic niches through the water column (De Long, 1992; De Long et al., 1994; Noble and Henk, 1998; Peters et al., 2005). From this perspective, the record of PMI and TMI throughout the PLG section suggests the continuous occurrence of methanogenic archaeal biomass during the whole OAE 1b. During interval of enhanced anoxic condition leading to the black shales deposition, methanogens thrive and can have ubiquitous presence throughout oxygen-depleted water mass. This would explain the highest abundance of PMI and TMI coinciding with the major anoxic sub-events. The weaker but permanent occurrence of both biomarkers during periods of relative oceanic equilibrium, on contrary, suggest the availability of ecological niches satisfying the anaerobic requirements of methanogens, which can be the deep sediments with oxygen-depleted pore water, but it is not possible to rule out the possibility that some water column methanogens inhabited transient anoxic microzones in a not well-ventilated water column (Karl and Tilbrook, 1994; Hoefs et al., 1997).

6.4 The PLG record of the late Aptian – early Albian regime shift

The high-resolution investigations conducted in this study on the "target interval" of PLG provide new insights on the evolution of anoxic conditions that led to the Jacob and Kilian black shales deposition, as well as the subsequent gradual restoring of normal oceanic conditions.

The Figure 6.2 reports the temporal subdivision of the sedimentary target interval in 5 major phases, based on the achieved multi-proxy dataset and conveying towards a multiple palaeoceanographic response of the Tethyan basin to specific climate dynamics evolving during the late Aptian / early Albian interval. Complete and detailed interpretation of data from the single intervals are presented in the following paragraphs. In nutshell, their key features can be summarised as follow: the first phase is characterised by an increasing environmental "pressure", likely triggered by an important interval of volcanic activity of the SKP, inducing a systematic shift toward more dysoxic/anoxic conditions in the deep ocean and culminating with the deposition of the black shales at the Jacob sub-event. The second phase appears as an interval of substantial and relative climate – oceanic equilibrium, emphasised by the lack of relevant anomalies in the geochemical and micropaleontological records. The third phase records a highly unstable time interval, both from an environmental and the biotic point of view. Inorganic geochemical proxies provide evidence of massive detrital input from land, which reasonably strongly affected the chemical structure of the water column. Moreover, at this interval the planktonic foraminifera experienced their first dramatic turnover, with an important extinction of almost all the large – sized Aptian taxa and the occurrence of few new species of small size. The fourth phase identified throughout the "target interval" records a new perturbation in the global carbon cycle, documented by the deposition of the 40 cm-thick black shale level of the Kilian sub-event. The Hg curve suggests the resumption of volcanic activity, probably linked to an early Albian phase of the SKP emplacement. Drastic shifts in the microfaunal assemblages occurred in coincidence of the organic-rich level, reflected also in the $CaCO_3$ content. The fifth and last phase documents enhanced detrital input and higher productivity.

The observed fluctuations resemble those of a system characterised by multiple-threshold instability where rapid transitions among different states (oxic – dysoxic – anoxic) linked to natural forcing shift lead to different responses of the system and multiple thresholds crossing. These observations well reflect the theory of the

ecological regime shift, that has become a fast-growing scientific discipline in the last decades. An ecological regime shift can be defined as the abrupt changes on several trophic levels (Lees et al., 2006) associated to a rapid, substantial and persistent reconfiguration in the state of communities / ecosystems (Scheffer et al., 2001, 2003; de Young et al., 2008). Commonly, the regime shifts are explored to investigate the response of modern ecosystems to anthropogenic activities and changing climate, and their impact on ecosystem services and human well-being (Carpenter et al., 2009; Millennium Ecosystem Assessment, 2005). The application of the regime shifts on the long-term history of the Earth is almost fragmentary although geological and paleontological records provide valuable insight on short burst of extinction and speciation, interspersed with longer periods of relative stasis when turnover of species is slower (Alroy, 2008; Hughes et al., 2013).

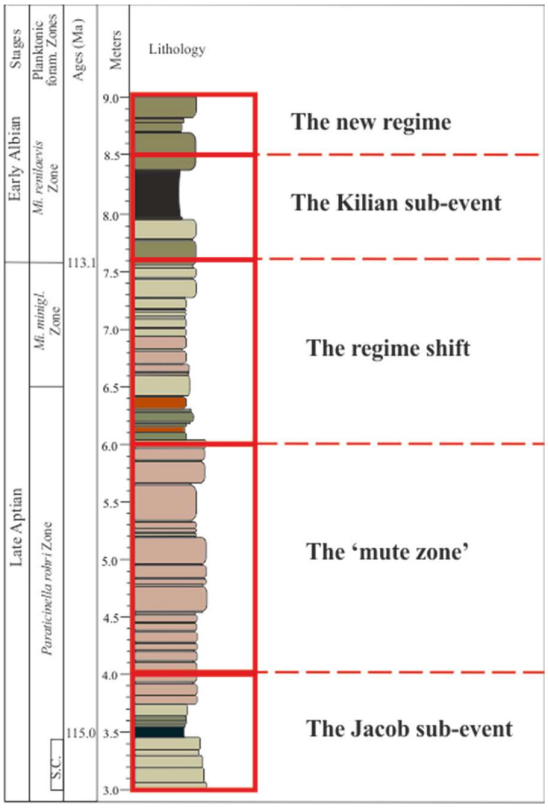

Fig. 6.2. The multiproxy-oriented division of the sedimentary target interval in 5 major phases on the basis of the inorganic and organic geochemical proxies.

The overall key features to detect in studies of ecological regime shifts are:

i) The external drivers of changes or shocks: major regional/global drivers influenced by any natural factors that directly or indirectly influence the ecosystem processes (feedbacks). Indirect driver operates diffusely affecting one or more direct drivers (Nelson et al., 2006, Andersen et al., 2009; Rocha et al., 2015). Examples of external drivers are climate change, volcanic activity, bolide impacts, invasive species after gateway opening, etc.

ii) Internal responses: transmission of the effects from the external drivers to ecosystems in pelagic realm, resulting in reinforcing structures and processes. The capacity of a system to absorb changes so as to still retain essentially the same function, structure, identity and feedbacks (Walker et al., 2004) is called resilience. The internal responses can mitigate (positive feedbacks) or exacerbate the pressure exerted by the external drivers. In the latter case, the negative feedback became the internal driver gradually eroding the resilience of the system (e.g. habitat fragmentation, biodiversity loss, etc.), pushing ecosystem closer to a global tipping point and making it more vulnerable to shocks and disturbances.

iii) Tipping point: is a critical value of an environmental driver for which small changes can produce a not reversible ecological regime shift (shift in variables). It is closely related to the concept of ecological threshold, with feedbacks that act to maintain a particular regime, and is the point at which there is an abrupt change in an ecosystem due to the loss resilience by the system. Hence, a perturbation must cross a threshold to cause a regime shift. However, May (1977) and Scheffer et al. (2001) point out that there is another type of threshold operating in a system, notably the dotted line or the unstable equilibrium separating the two regimes, mainly linked to a change in a parameter of the system. In this case, the system would respond more smoothly to changes.

iv) New regime or state: it consists on changes in feedbacks and consequently on the direction (the trajectory) of the new stable ecological equilibrium, incompatible with the previous (alternative stable states). After the rapid diversification, ecosystems experience a relative stasis.

This work tries to interpret from this perspective, the late Aptian – early Albian record of Poggio le Guaine. The conceptual matric of the ecological regime shift provides an excellent multi-dimensional approach to understand causal-effect relationship between environmental forcing and ecological response particularly in the pelagic community. Actually, the high resolution geochemical investigations of this study allow to reconstruct the complex system of internal feedback mechanisms, whereas the paleontological results provide insights on the impacts and responses on marine communities.

6.4.1 Evolution of the Jacob sub-event

Figure 6.3 groups together the major features of the 1-meter-thick interval straddling the Jacob black shale level, our first out five major phases of the late Aptian / early Albian OAE 1b. Here, the Hg anomalies reveal a major pulse in the volcanic activity linked to the emplacement of the SKP (see par. 6.1, this chapter), with injection of large amount of atmospheric CO_2.

In response, the oceanic system gradually shifts toward more dysoxic – anoxic conditions, as highlighted by several geochemical proxies. Particularly, progressive oxygen depletion in bottom waters appears well reflected in the gradual decreasing concentration of manganese in sediments. Oxic conditions favour equilibrium of the Mn^{3+} and Mn^{4+} hydroxides or oxides highly insoluble; conversely, reducing conditions favour reduction of Mn to the valence state Mn^{2+} characterised by formation of highly soluble complexes and high potential for moving to the overlying seawater (Quinby-Hunt and Wild, 1994; Tribovillard et al., 2006). Concomitant Mn impoverishment, enhancement of other redox-sensitive TM (as V, Ni, Zn, etc), change in trace metal ratios (as V/Cr, V/(V+Ni) (Hatch and Leventhal, 1992; Jones and Manning, 1994)) reliable proxies of oxygenated sediment conditions, and enhanced TOC contents seem clearly suggest incipient anoxic conditions, culminating with the deposition of the black shales of the Jacob sub-event. In particular, vanadium is considered a reliable proxy of sediment redox condition, being another element whose oxidation state can vary as a function of the prevailing redox potential. It occurs as highly soluble anionic species in oxic waters but is reduced to reactive or insoluble species under anoxic conditions (Morford and Emerson, 1999; Tribovillard et al., 2006). From the bottom of the "target interval" the V/Al curve shows a rising hyperbolic trend, reaching highest

enrichment at the Jacob level. This clearly indicates a progressive system-shift toward more euxinic sea-water conditions. The organic-rich black shales of the Jacob sub-event also document the occurrence of organic biomarker indicative of anaerobic methanogenic Archaea (TMI and PMI) and expansion of euxinia in the photic zone (C_{16}- and C_{18}- aryl isoprenoids), as well as large amount of pristane. As previously reported (Par. 4.9.2), this molecular fossil is usually considered as proxy of oxic conditions since it is readily produced by oxidation and decarboxylation of phytane. However, its higher occurrences in black shale levels seem to be attributable to primary sources as cyanobacteria or purple sulphur bacteria, and, to a lesser extent, to moderate oxygen content in the depositional environment.

All the evidences just mentioned suggest growing anoxia culminating with the carbonate crisis (well expressed by the decreasing trend in the $CaCO_3$ curve) and the black shale deposition of Jacob sub-event.

Detection of relatively higher Zr (proxy of the heavy fraction of continental input) concentration well reflects enhanced river runoff and associated stratification of the water column, culminating with the deposition of the Jacob level. A significant role of aeolian dust in this context is also well testified by the long- to short-chain *n*-alkanes ratio, that reveals an active source of higher plant waxes prior the Jacob level deposition, as also supported by the lightening of the carbon isotopic composition of the carbonate bulk. The Jacob deposition, however, marks the abrupt and definitive interruption of enhanced continental plant-waxes supply (fall of TAR ratios), probably reflecting a change from wet to dryer climatic condition that affects the vegetative growth on land and the intensity of wind.

The transitory anoxic conditions dramatically affect the planktonic communities, resulting in a temporary drop in planktonic foraminifera and Radiolaria relative abundances. The strengthening of water column stratification probably restricts the survival and adaptation of planktonic organisms to limited ecological niches. At the same time, the concomitant abrupt increase on benthic foraminifera abundance provides evidence of short-lived oxygenation events that would allow transient colonization even by bottom-living species. After the anoxic event, the restore of water mass mixing and oceanic ventilation enhance the primary productivity, as evidenced by the prominent peak of the Ba/Al proxy. However, this pulse on productivity appear to be adverse to the trophic requirements of planktonic foraminifera, that consequently records a new drops in abundance.

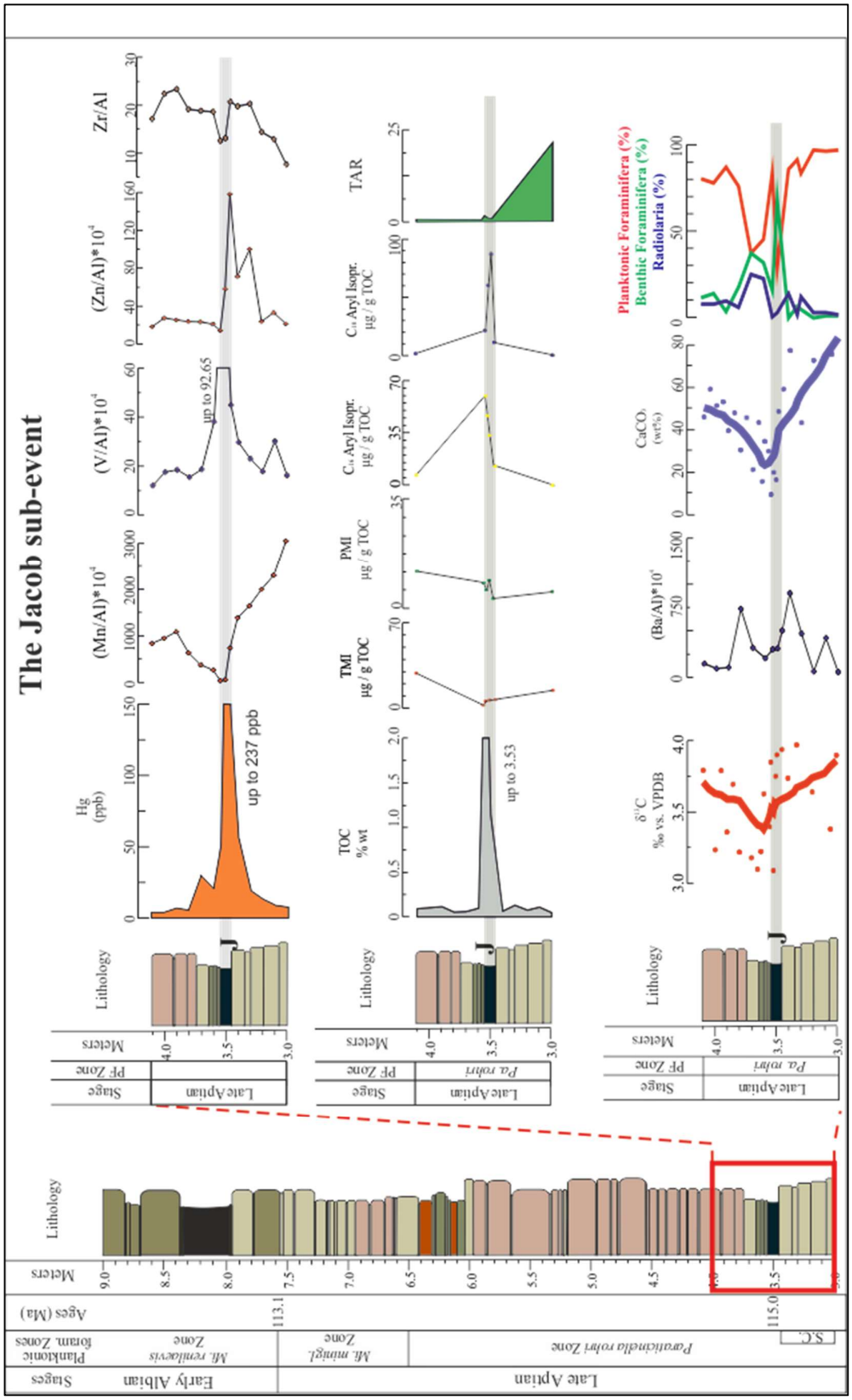

Fig. 6.3. Major inorganic and inorganic geochemical, and micropalaeontological features of the sedimentary interval encompassing the Jacob sub-event at Poggio le Guaine (3.00 – 4.10 m).

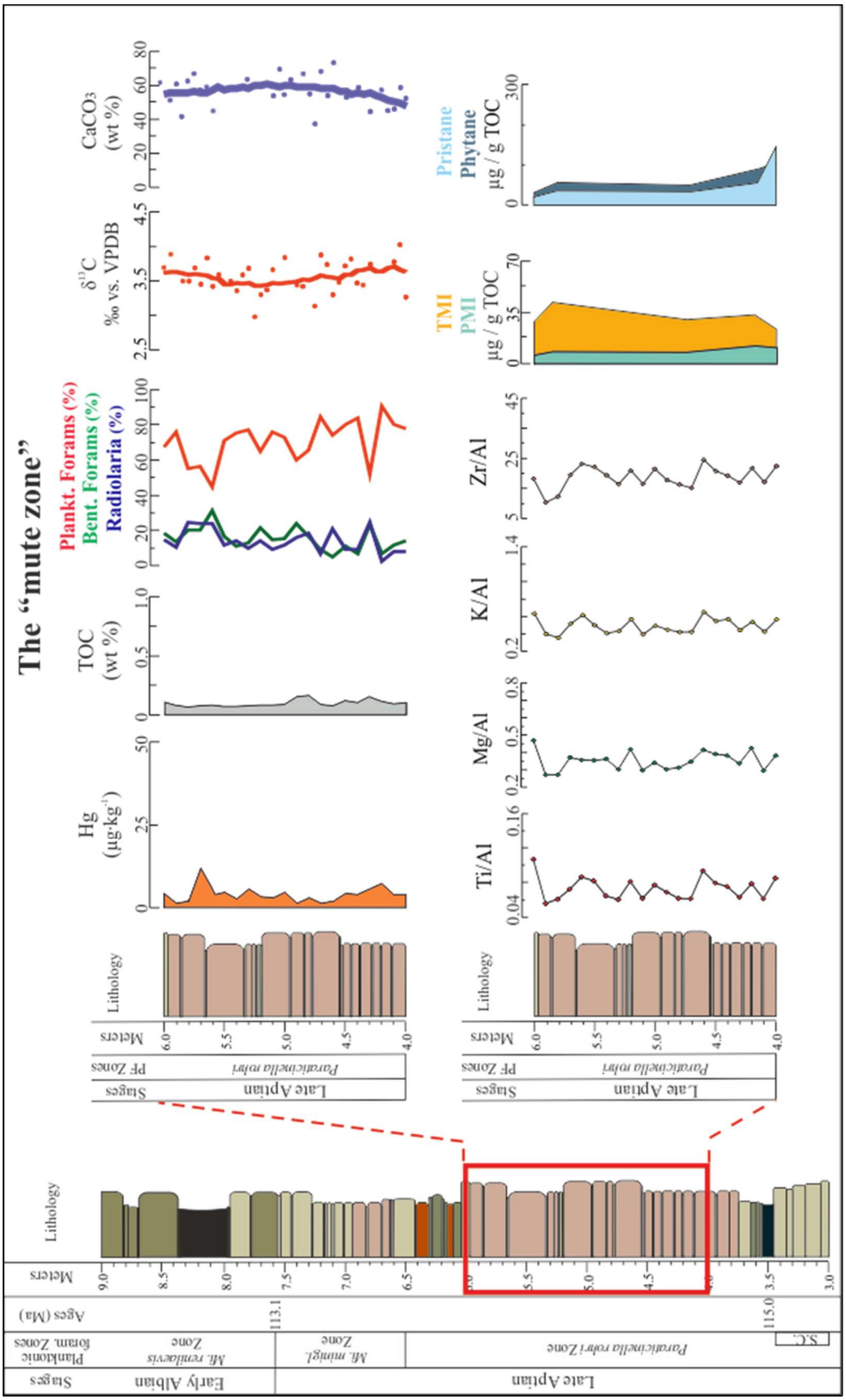

Fig. 6.4. Major inorganic and inorganic geochemical, and micropalaeontological features of the "mute zone" sedimentary interval at Poggio le Guaine.

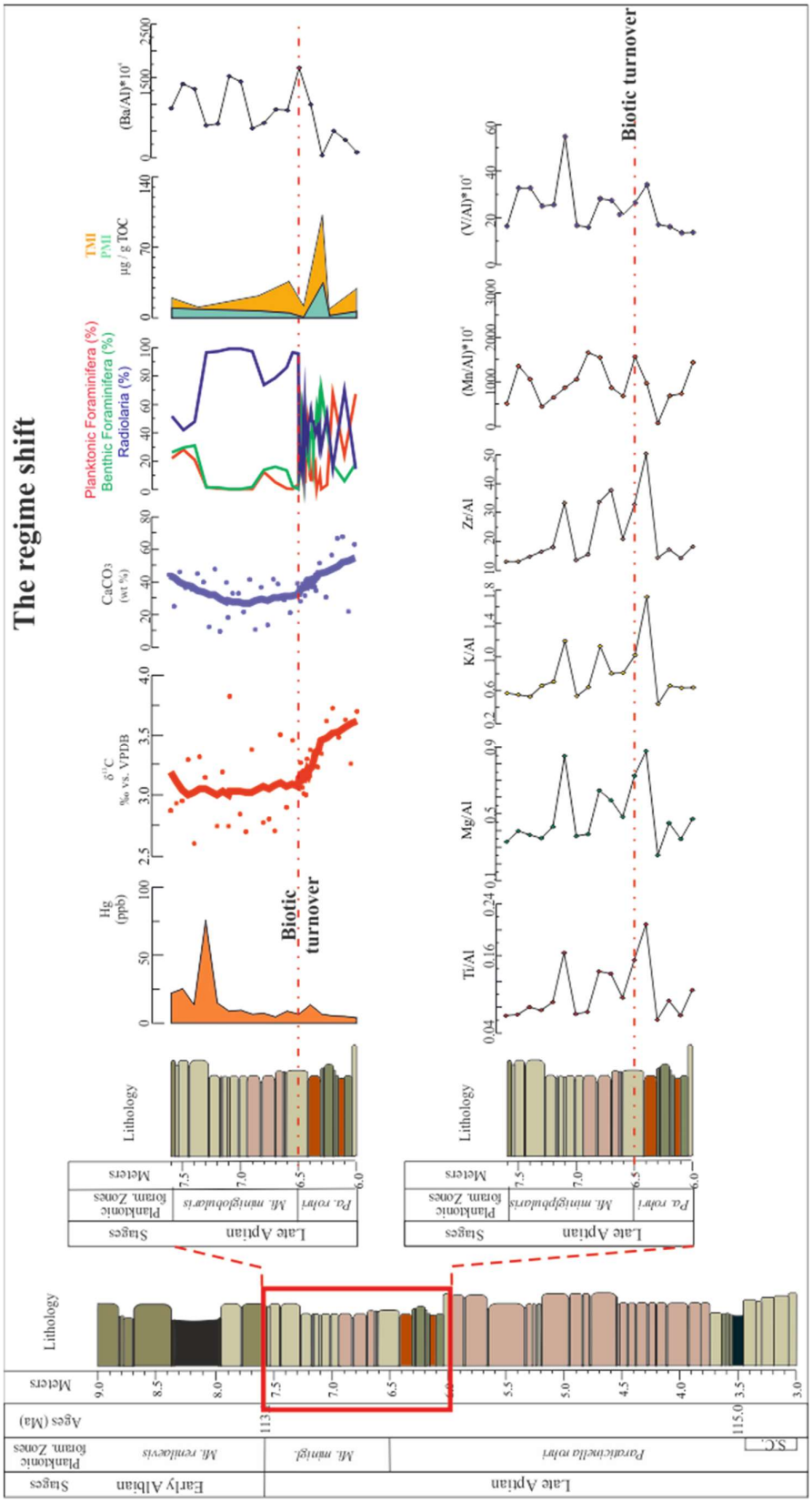

Fig. 6.5. Major inorganic and inorganic geochemical, and micropalaeontological features of the sedimentary interval encompassing the planktonic foraminiferal turnover at Poggio le Guaine.

6.4.2 The "mute zone"

After the Jacob sub-event, the interval from 4.00 m to 6.00 m sound as a "mute zone", where relevant geochemical anomalies or micropaleontological variability are extremely reduced in amplitude and frequency (Fig. 6.4). The mercury curve does not show significant enrichments, ranging around ~4 ppb, suggesting reduced volcanic activity linked to the emplacement of SKP. The oxygen levels at the bottom of the basin appear restored through the water column, and the planktonic foraminifera show higher abundances compared to that of benthic foraminifera and Radiolaria. Short-lived reductions in the percentage of PF correspond to small increase in the number radiolarian specimens.

The relatively stable pattern of proxies of detrital input (Ti, Mg, K, and Zr/Al) underline a temporary interruption of enhanced terrigenous input (riverine and aeolian) and potentially indicate dryer climatic conditions. The few biomarkers detected in significant amounts are *n*-alkanes from the aquatic range (*n*-C_{16} and *n*-C_{18} with concentrations of ~ 166 µg/g TOC), pristane and phytane (concentrations ≤ 0.1 µg/g TOC) and TMI (concentration < 90 µg/g TOC). The anomalous occurrence of the latter compound in sediments with "fully oxic" conditions could indicate anaerobic methanogenic archaeal activity below the water-sediment interface.

6.4.3 An interval of ecological regime shift

The interval between 6.00 and 7.60 m encompasses the planktonic foraminiferal turnover event (Fig. 6.5). It records the onset of a new interval of Hg increase, which possibly reflects a new resumption of the volcanic activity of the Southern Kerguelen igneous province. The Hg sedimentary content increases upward and at 7.30 m reaches the value of ~75 ppb, three time the background level. This increasing trend will continue up to the top of the "target interval". The main effect of the enhanced volcanic activity with injection of CO_2 in atmosphere produced a climatic shift toward wetter and warmer conditions, which once again strengthened the continental weathering and the wind intensity, in agreement with several authors who documented late Aptian – early Albian strong monsoonal activity (Barron et al., 1985; Oglesby and Park, 1989; Wortmann et al., 1999; Herrle, 2002; Herrle et al., 2003a,b; Bornemann et al., 2005; Hofmann et al., 2008; Wagner et al., 2008).

Stronger winds, in turn, could have increased the detrital supply, and consequently enhanced primary production in oceanic realms. The interval between 6.30 m and 7.10 m at PLG section actually records a relative increment of terrigenous input to the basin. Either riverine (Mg, K,) and aeolian (Ti, Zr) terrigenous proxies show three prominent peaks at 6.40 m, 6.70 m and 7.10 m, indicative of enhanced hydrologic cycle also highlighted by the lightening of the isotopic carbon ratios. This enrichment is also suggested by the enhancement in Cr, characterised by a strong affinity for the detrital fraction. Increase in concentration of other redox-sensitive metals as Mn, V, Fe, Ni, Cd, Cu, Zn, and Pb can be observed in this interval. Moreover, the three peaks of enrichment in the barium/Al curve highlights the productivity increase triggered by the pulses of detrital input, events slightly delayed compared to the peaks of other trace elements.

Ultimately, effects of sudden detrital discharges generally provide large nutrients supply in a short time. This destabilises the physical and ecologic equilibrium throughout the water column and lead to a regime shift toward eutrophic and mesotrophic conditions, low oxygen waters and weaker water mass stratification (Herrle et al., 2010).

The profound and relatively sudden changes of the ecosystem dynamics dramatically affect the planktonic and benthic communities. The highly spiky pattern of PF, BF and Radiolaria abundance curves clearly reflects how the ecosystem gradually shifted toward its ecological threshold, because of destabilizing feedbacks significantly eroding the resilience of marine biota. The massive terrigenous supply does not appear to be responsible for the short-term changes in faunal assemblages, as suggested by the slight lag between the two signals. It rather affected and/or complicated the attempt at survival of planktic foraminifera, destabilizing the physical niches and promoting the primary production. The extinction event of the Aptian planktonic foraminifera, coinciding with the HO horizon of *Paraticinella rohri* at 6.50 m, unequivocally marks the regime shift to an alternate stable ecological state. The new mesotrophic – eutrophic conditions, inhospitable for Aptian taxa, drive changes in the plankton community composition, promoting the blooming of opportunistic/disaster species and siliceous organism as Radiolaria.

Biomarkers are very scarce in this interval, since the degrees of oxygen in bottom water supported the effective degradation of the abundant organic matter,

preventing preservation. However, the low concentrations of TMI and PMI indicate archaeal presence, likely confined to deep sediments with pore-water are depleted in oxygen.

6.4.4 The Kilian sub-event

The higher sedimentary concentrations of mercury throughout the sedimentary interval between 7.60 and 8.50 meters, provide evidence of the persistence of the volcanic activity linked to an early Albian phase of the emplacement of the SKP (Fig. 6.6). This lead to a further upset of the basin system, recorded at 7.96 m: the Kilian black shale deposition marks a new phase of enhanced organic matter deposition and preservation.

The high atmospheric pCO_2 (volcanic – external drive) and the high rates of primary production (internal driver) resulting from the early regime shift, gradually push the oceanic system toward the impoverishment of the oxygen water levels, shown by the fall of Mn/Al ratio, and the small increase in redox-sensitive TMs, comparable to that of detrital proxies as Zr, Ti and K. Even if the geochemical signals are not as strong as at the Jacob level, the Kilian sub-event is marked by the sudden fall of the $\delta^{13}C$ values concomitant to the drastic drop of the $CaCO_3$ content. The productivity drops in correspondence of the bottom of the Kilian level, evidenced by the Ba/Al curve and, more broadly, by the dramatic fall of Radiolaria abundances, point toward the strengthening of water column stratification as reasonable driver of the Kilian anoxic sub-event. The small amount of organic biomarkers indicative of photic zone euxinia and archaeal biomass (namely C_{16}- and C_{18}- aryl isoprenoids, PMI and TMI) also sustain the anoxic conditions, although the rise of the benthic fauna (mainly agglutinated benthic foraminifera) is proof of episodic oxygenation of the bottom waters.

6.4.5 The new regime

The end of the organic-rich black shale deposition is marked by the restoring of the chemical equilibrium through the water column, highlighted by the geochemical proxies as the Mn/Al ratio, the $CaCO_3$ and $\delta^{13}C$ curve (Fig. 6.7). The wetter climatic conditions that are well established since the late Aptian (see. Par. 6.4.3), enhance the continental weathering and promote strengthened winds, resulting in larger terrigenous inputs evidenced by the significantly increasing trend of all the detrital-

proxies. The subsequent widespread nutrient availability result in eutrophic conditions promoting the blooming of siliceous organism as Radiolaria, which dominate over the calcareous foraminifera with mean abundances of about 70%. The depauperate planktonic foraminifera assemblages, composed only by small *Mi. miniglobularis* and *Mi. renilaevis* specimens, do not show deviations from the background abundance of 0-10%.

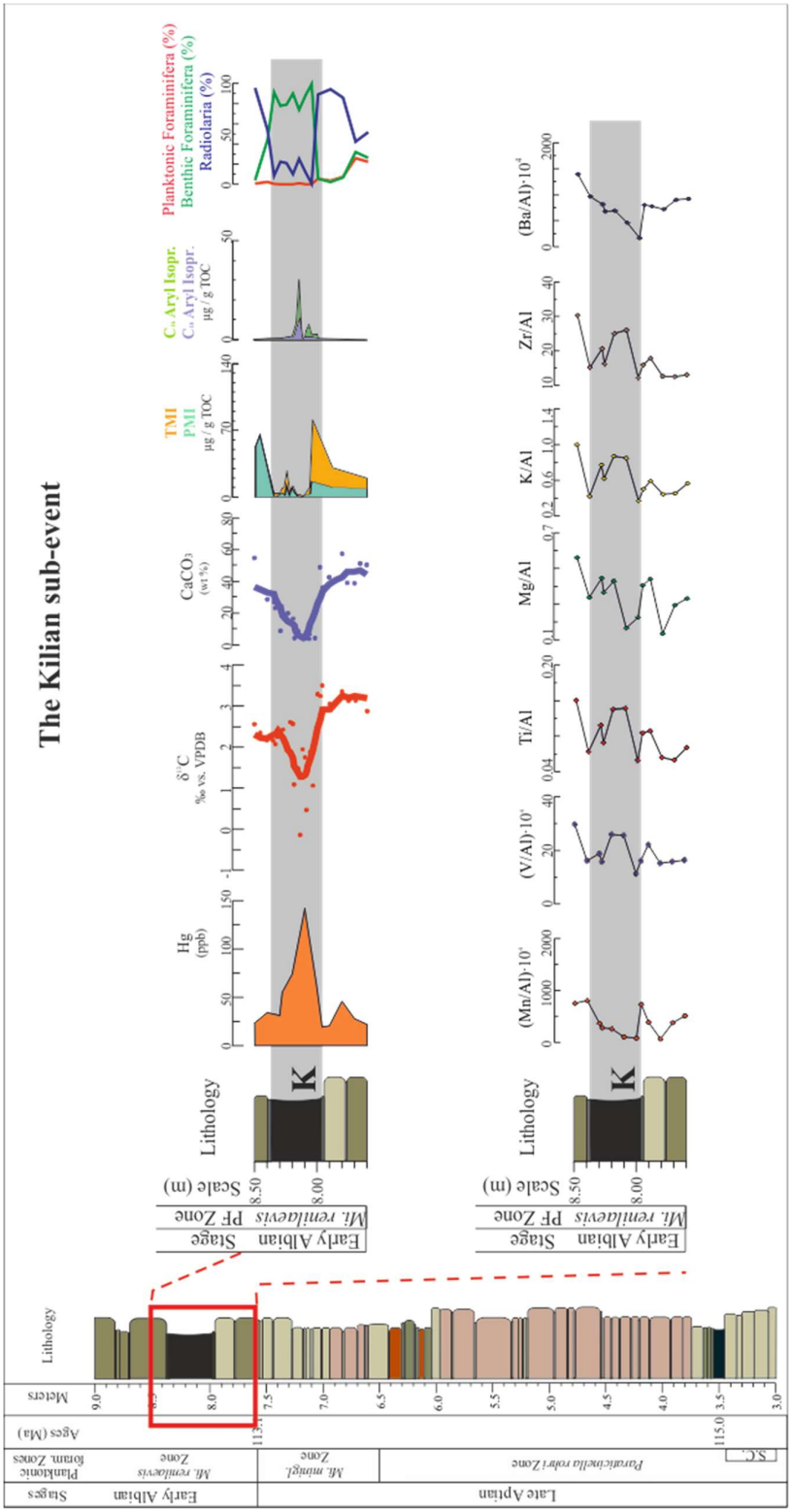

Fig. 6.6. Major inorganic and inorganic geochemical, and micropalaeontological features of the sedimentary interval encompassing the Kilian sub-event at Poggio le Guaine

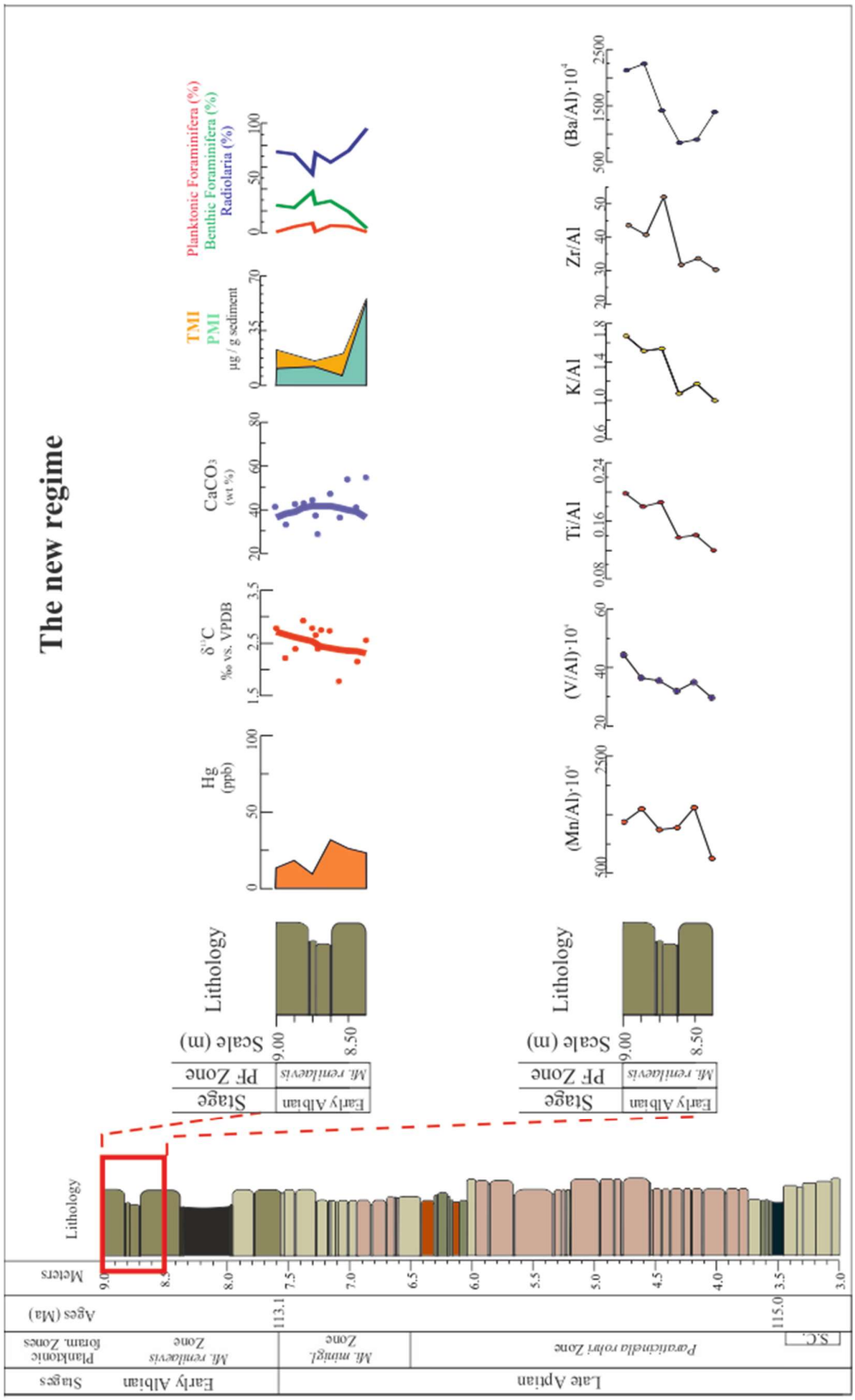

Fig. 6.7. Major inorganic and inorganic geochemical, and micropalaeontological features of the upper sedimentary interval at PLG section

6.5 The impact of environmental changes on planktonic community: a view on an ecological regime shift

Large environmental variations, as rapid climatic changes (cooling; greenhouse warming) and massive volcanic activity, significantly affected the atmosphere-oceanic system, resulting in changes in ice volume, temperature, seasonality, upwelling and hydrographic regimes, chemical and physical structure of water column. In the oceanic realm, these environmental changes influence the stability of pelagic ecosystems and their boundaries, and therefore could have a crucial effect on all planktonic groups, promoting long-term biotic stress that may exceed the threshold conditions for certain organisms (Keller and Pardo, 2004a; Keller, 2005; Pardo and Keller, 2008; Tantawy et al., 2009). Although the link between environmental pressures and evolutive changes is still poorly known, the body size is considered as a key indicator for the organism's health, since this morphological attribute has a fundamental impact on the ecology, evolutionary history and physiology of organisms (McKinney, 1990). Decreases in size have been described as transient phenomena, systematically associated with biologic extinctions (Aubry 2009). In fact, high environmental stresses promote the overall decrease on body size before the taxon extinction (pre-extinction dwarfing in Wade and Olsson,2009) and the size reduction of relict taxa after the extinction and before of the ri-diversification (Lilliput effect in Urbanek, 1993; Twitchett, 2006, Tantawy et al., 2009). This is the reason why dwarfism is considered a stress signal leading the organism to optimise the dimensions and the reproductivity capability for survival. Dwarfism has been often associated with mass events but it has been also documented in intervals of high biotic stress resulting in smaller extinction events and biotic crises, in an extensive range of organisms from both terrestrial and marine realms, from large mammals to invertebrates and to the smallest, single-celled microscopic organisms (e.g., Cordey et al., 1970; Harris and Mundel, 1974; Mancini, 1978; Hart and Ball, 1986; Leckie, 1987; Keller, 1989, 1993, 2003a, 2003b, 2004, 2005; MacLeod, 1990; Hart and Leary, 1991; Keller et al., 1997, 2004, 2007; Twitchett, 1999; MacLeod et al., 2000; Fürsich et al., 2001; Twitchett et al., 2001; Abramovich and Keller, 2003; Raia et al., 2003; Thomas, 2003; Coccioni and Luciani, 2004, 2005, 2006; Lockwood, 2005; Payne, 2005; Wheeley and Twitchett, 2005; Twitchett, 2006, 2007; Isozaki and Aljinovic 2009; Keller and

Abramovich, 2009; Morten and Twitchett, 2009; Mutter and Neuman, 2009; Tantawy et al., 2009; Wade and Olsson, 2009; Erba et al., 2010; Metcalfe et al., 2011; Yamaguchi et al., 2012). Many question remain unanswered regarding the causes of dwarfism, its duration and mechanisms. However, it appears that the ecological response to biotic stress is similar in all types of high-stress environments, varying only with the degree of environmental change, regardless of the particular causes that induced stress conditions (e.g., Wade and Twitchett, 2009).

6.5.1 The planktonic foraminiferal response to the OAE 1b at PLG section

The late Aptian – early Albian biotic turnover records a dramatic extinction event of the large-sized Aptian planktonic foraminifera taxa and the emergence of few new small-sized Albian species. In parallel to the selective extinction/disappearances of large species, that consequently results in the interspecific size reduction, planktonic foraminifera show also the intraspecific decreasing of the test size preceding extinction (pre-extinction dwarfing of Wade and Olsson, (2009), in contrast with the post-extinction dwarfing as in the Lilliput effect). Wade and Olsson (2009) claim that the terminal size reduction is an adaptive response to changing water column conditions. This survival strategy relies on early sexual maturity (progenesis), faster reproductive rates and larger numbers of offspring, which maximize survival test (Tantawy et al., 2009).

Dwarfism involves the large, morphologically complex, ornate, and specialized k-strategist Aptian taxa, which in comparison to smaller species tend to have slower reproduction rates, higher resource requirements, and therefore reduced population densities (Riveros, 2007). Planktonic foraminiferal assemblage from the aftermath of biotic turnover are almost entirely composed by small and thin *Mi. miniglobularis* specimens, accompanied by rare to few specimens of Aptian taxa, that soon become extinct. The ecological behaviour of *Mi. miniglobularis* seems that of disaster opportunist, since it occurs and thrives during a period of high but variable environmental stresses associated to anoxia, eutrophic waters, and intense volcanic activity (highlighted in previous paragraphs), when no other species blooms. Actually, Keller and Abramovich (2009) state that in the aftermath of major catastrophes often a single disaster taxon, generally small and unornamented, tends to dominate for a brief time, whereas it is rare or absent in normal

environments, exactly as *Mi. miniglobularis* and *Mi. renilaevis* after the late Aptian – early Albian turnover.

On the other hand, *Pa. rohri* perfectly symbolises the major features of Aptian taxa. It has generally larger test size (300-600 μm), numerous chambers (8-10), thick-walled test, and well-developed rugosities on the early chambers of the final whorl. Through the PLG-GC section, *Pa. rohri* shows a gradual size decrease which closely parallels that of the entire planktic foraminifera assemblage approaching the extinction event. From this perspective, the size changes on *Pa. rohri* can be used as a mirror of the progressive deterioration of PF assemblages. The mean value of the maximum diameter of *Pa. rohri* throughout its biostratigraphic interval (394.99 μm) can therefore be considered a threshold separating larger-sized populations, indicative of optimum ecological conditions, from lower size specimens, that reflect selective environmental pressures (Fig. 6.8).

After an early evolutive phase during which *Pa. rohri* progressively increases both in number of specimens and dimension, from -2.79 m upward this taxon experiences a thriving period, highlighted by the broad dimensional range of populations and by the larger mean maximum diameter of 453.84 μm. However, from -2.40 m to -0.12 m, mean size of *Pa. rohri* decreases to 339.36 μm, and populations are composed of smaller specimens (until 264.33 μm in diameter) with rather uniform size (mean st. dev. of ± 23.81 μm) (Fig. 4.1, Tab. 1 - Supplementary materials). This could be interpreted as a period of high selective pressure that compels the PF to limit the metabolic activity for calcification, reducing the growth and fitness of the organism. Unfortunately, the absence of geochemical data from the GC section makes it impossible to further constrain the role of *Pa. rohri* as ecological indicator through this interval.

Sabatino et al. (2015) reported stable oceanic conditions throughout the sedimentary interval from 0.00 m to 3.00 m of PLG section. Remarkably, *Pa. rohri* seems to record a period of relative ecological optimum as well, reflected on the test diameters 15% larger than the threshold value and on the widest population variability (Fig. 6.8, Tab. 1 - Supplementary materials). A progressive decline in the test-size starts at 3.00 m, concomitant with the reduction of dimensional variability among populations, leading to dimensional threshold crossing at 4.40 m. From this level to the final extinction, *Pa. rohri* is < 400 μm and populations show the occurrence of dwarfed specimens (size <300 μm). The geochemical

investigations conducted in this study have demonstrated a gradual system shifting toward more dysoxic/anoxic conditions starting at 3.00 m and culminating with the deposition of the black shale of the Jacob sub-event. This environmental pressure seems to affect the growth and calcification process of *Pa. rohri*, triggering its long-term decline that persist even during periods of apparently stable oceanographic conditions (i.e. the "mute zone"). Moreover, from 6.00 m upward, massive detrital inputs destabilize the water column structure and provide large nutrients supply in a short time. The resulting regime shift toward mesotrophic to eutrophic conditions, confirmed by temporary blooms of Radiolaria and concomitant enrichments on productivity proxies as barium, may have further hindered the attempts at survival of *Pa. rohri* and all other Aptian k-strategist, leading to their final extinction at 6.50 m. The increasing trophic levels, on the other hand, favoured the thriving of very small-sized opportunistic/disaster Albian taxa and siliceous plankton, in analogy with the general trend observed in actual frontal mixing zones and high-fertility upwelling areas (Schmidt et al., 2004).

Abrupt increases of radiolarian abundances concomitant to the decline of large k-strategist PF have been reported from different sites and geological times (e.g. Leckie, 1984, 1987; Erbacher et al., 1996; Erbacher and Thurow, 1997; Stoll and Schrag, 2000; Leckie et al., 2002; Luciani et al., 2010). The common factor is the sudden shift from an oligotrophic ecosystem to eutrophication, due to enhanced upwelling or changes in nutrient fluxes. Brasier (1995) suggests that oligotrophic environments tend to support communities with higher species diversity than eutrophic ones, and contain more specialized species. If the nutrient levels of an oligotrophic-adapted system rise too high, blooms of plankton reduce water clarity (i.e. 'green water') and limited water transparency will shift primary production further towards the phytoplankton, favouring the suspension feeders. Studies of sediment traps on the deep ocean floor confirm that fluxes of siliceous diatom and radiolarian skeletons are indeed good indicators of high ocean productivity (Takahashi 1986; Schrader and Sorknes 1991), and consequently rests of diatoms, radiolarians and biogenic opal can therefore be used to provide estimates of past ocean fertility.

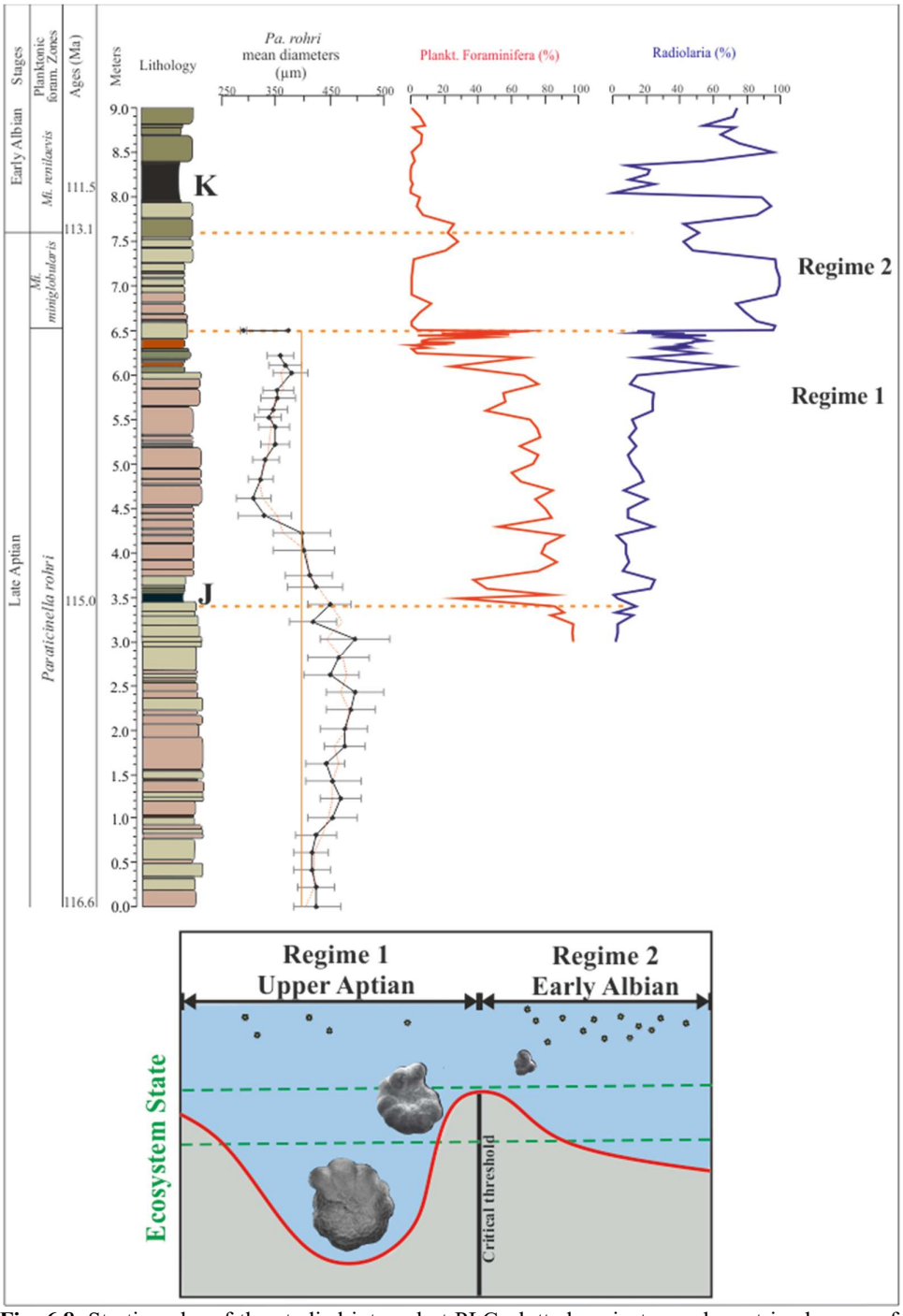

Fig. 6.8. Stratigraphy of the studied interval at PLG plotted against morphometric changes of *Pa. rohri* through the 0.00 m – 6.50 m interval of PLG section, and relative abundance of planktonic foraminifera and Radiolaria from 3.00 m to 9.00 m. The cartoon at the bottom simplify the effects of regime shift on two upper Aptian *Pa. rohri* (decreasing size) and a specimens of *Mi. miniglobularis*. Green dots symbolize primary productivity. Key to simbols: J = Jacob event; K = Kilian event.

6.5.2 The size-record of Pa. rohri at the South Atlantic Ocean

The dimensional variation of *Pa. rohri* through the DSDP Site 511 succession provide interesting information and very useful points of comparison to the PLG record. Above all, the mean maximum diameter through its biostratigraphic range is of 448.40 μm, larger than those recorded at PLG. This probably means that, in the South Atlantic, the oceanic environment was more advantageous for the ecological requirement of *Pa. rohri*, allowing it to spend large part of the metabolic activity for the biocalcification of larger tests. Using the mean diameter as ecological threshold indicator as for PLG, *Pa. rohri* shows healthy during most of its range, with test-size close to the mean value except for the early evolutive stages (Fig. 6.9). However, its extinction provides evidence that even the planktonic foraminifera of the South Atlantic Ocean have undergone the dramatic effects of the late Aptian – early Albian ecological shift toward a new eutrophic. The fairly stable dimensional range, and, even more, the size increase of *Pa. rohri* before the extinction, suggest the absence of internal negative feedbacks exacerbating the pressure of external drivers, allowing the system to respond smoothly to global changes.

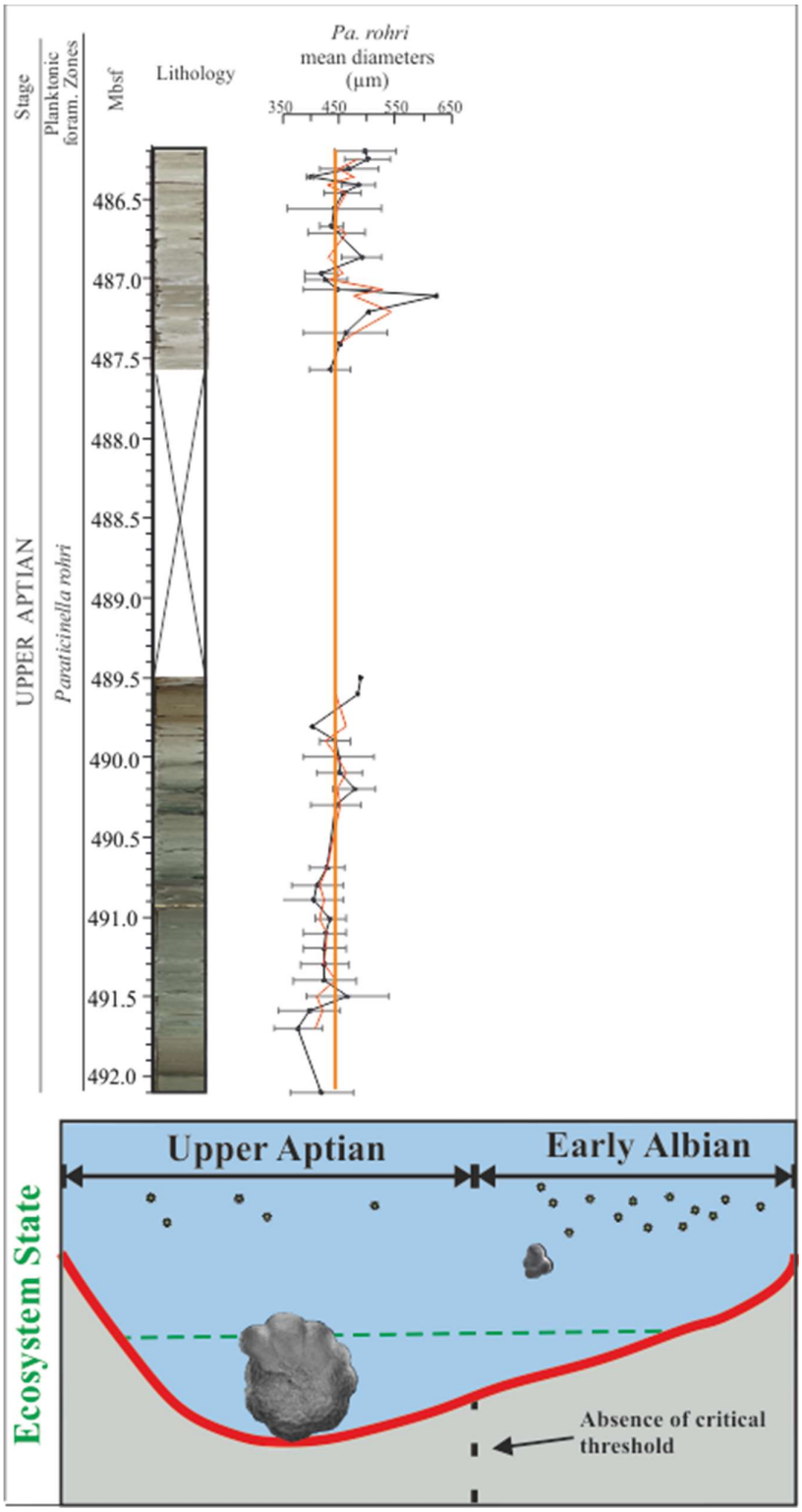

Fig. 6.9. Stratigraphy of the studied interval at DSDP Site 511 plotted against morphometric changes of *Pa. rohri.* The cartoon at the bottom simplify the effects of the global carbon cycle perturbation on the planktonic foraminifera assemblage at the South Atlantic: upper Aptian *Pa. rohri* and early Albian *Mi. miniglobularis*. Green dots symbolize primary productivity.

Chapter 7
Conclusion

The pelagic section of Poggio le Guaine (central Italy) provided a continuous and nearly undisturbed record of late Aptian – early Albian OAE 1b in the western Tethyan Realm. The high-resolution multi–proxy investigations performed in this study and the comparison of the results with the widely separated marine realm of the South Atlantic Ocean, reveals new insights on the potential relationships between ocean events and climate changes, and the feedback responses of ecosystems at basin-scale.

The principal findings of this research can be synthesised as follow:

i) The high-resolution Hg chemostratigraphy along the target interval of Poggio le Guaine section demonstrates relative good match between the timing of large igneous province eruptions and strong perturbations of the global carbon cycle. Major pulses in the large-scale volcanism leading to the emplacement of the Southern Kerguelen Plateau are likely responsible for the climatic fluctuations that punctuated the late Aptian – Early Albian, perturbing the global Atmosphere-Ocean system over longer time scales.
ii) The rapid climatic changes and the complex interaction between global Oceans and Atmosphere synergistically transfer their effects on the pelagic realm. The chain of reactions and subsequent feedbacks are complex and strongly affected by the regional palaeoceanographic settings.
iii) The OAE 1b is the result of the long-term perturbation induced by the SKP emplacement. The peculiar hydrographic and oceanographic features of the PLG sedimentary basin determine brief and intermittent episodes of anoxia/dysoxia, which favoured the enhanced burial and preservation of marine organic carbon. The Jacob, Kilian, Paquier and Leenhardt black-shales levels are therefore the result of repeated mid-term oceanic collapses, characterised by transient disoxic/anoxic of water column. The absence of black shales in the sedimentary record of the South Atlantic Ocean suggests that the local palaeoceanographic conditions hindered the reduction of bottom water ventilation and subsequent anoxia.
iv) Local hydro-climatic variability exacerbated the influence of large scale forcing on ecosystems. The short-term amplification of the hydrologic cycle is a local response to moderate climate variations. This amplification had direct impact on the continental weathering and prevailing wind patterns, resulting in enhanced continental matter and nutrient inputs, thereby destabilizing the ecological niches and trophic equilibrium.

v) The instabilities in global climate and the local destabilizing feedbacks eroded the resilience of the marine ecosystem, pushing it closer to its ecological threshold, that was finally breached by at the AABI. The abrupt and drastic changes in the ecological structure of the pelagic system definitively marks the irreversible regime shift. The new eutrophic ecological state dramatically resulted in profound and sudden changes in the plankton community composition.

vi) The first major planktic foraminifera turnover is the result of the late Aptian – early Albian ecological regime shift. The new mesotrophic – eutrophic conditions were inhospitable for the Aptian k-strategist taxa, which finally lose their resilience capability and go extinct. The early Albian ecosystem promoted the blooming of opportunistic/disaster species and siliceous organism as Radiolaria, which dominate the microfaunal assemblages.

vii) The comparison of the planktonic foraminifera records across the two sections of PLG and DSDP Site 511 provide the evidence that widely separated marine ecosystems have similar response to global drivers. Both South Atlantic and Tethys oceans experience the late Aptian – early Albian regime shift to a new eutrophic ecological state, leading to the dramatic planktonic foraminifera turnover. Consequently, the ecological regime shift and the planktonic foraminifera turnover can be defined as a global response to the global mid-Cretaceous climatic change.

viii) The planktonic foraminifera dwarfism is not an adaptive response to global climatic/environmental changes. It is mostly sustained by the negative internal feedbacks that exacerbate the pressure exerted by the external drivers, eroding the resilience of planktonic foraminifera, which consequently attempt to survive reducing the test size.

References

Abramovich, S., Keller, G., 2003. Planktonic foraminiferal response to the latest Maastrichtian abrupt warm event: A case study from South Atlantic DSDP Site 525A. Marine Micropaleontology 48, 225–249. doi:10.1016/S0377-8398(03)00021-5.

Adams, D.D., Hurtgen, M.T., Sageman, B.B., 2010. Volcanic triggering of a biogeochemical cascade during Oceanic Anoxic Event 2. Nature Geoscience 3(3), 201-204.

Aguado, R., Castro, J.M., Company, M., De Gea, G.A., 1999. Aptian bio-events – an integrated biostratigraphic analysis of the Almadich Formation, Inner Prebetic Domain, SE Spain. Cretaceous Research 20(6), 663 – 683.

Alexander, R., Kagi, R., Woodhouse, G.W., 1981. Geochemical correlation of Windalia oil and extracts of Winning Group (Cretaceous) potential source rocks, Barrow Subbasin, Western Australia. American Association of Petroleum Geologists Bulletin 65, 235–250.

Alroy, J., 2008. Dynamics of origination and extinction in the marine fossil record. Proc. Natl. Acad. Sci. U.S.A. 105, 11536–11542.

Amedro, F., 1992. L'Albien du Bassin Anglo-Parisien: ammonites, zonation phylétique, séquences. The Albian in the Anglo-Paris Basin: ammonites, phyletic zonation, sequences. Bulletin des Centres de Recherches Exploration-Production Elf-Aquitaine 16, 187-233.

Andersen, T., Carstensen, J., Hernandez-Garcia, E., Duarte, C.M., 2009. Ecological thresholds and regime shifts: approaches to identification. Trends in Ecology & Evolution 24(1), 49-57.

Ando, A., Huber, B. T., Premoli Silva, I., 2013. *Paraticinella rohri* (Bolli, 1959) as the valid name for the latest Aptian zonal marker species of planktonic foraminifera traditionally called *bejaouensis* or *eubejaouensis*. Cretaceous Research 45, 275–287.

Angel, R., Claus, P., Conrad, R., 2012. Methanogenic archaea are globally ubiquitous in aerated soils and become active under wet anoxic conditions. ISME Journal 6, 847-862. Doi: 10.1038/ismej.2011.141

Ariya, P.A., Skov, H., Grage, M. M. L., Goodsite, M.E., 2008. Gaseous elemental mercury in the ambient atmosphere: Review of the application of theoretical calculations and experimental studies for determination of reaction coefficients and mechanisms with halogens and other reactants. Adv. Quantum. Chem. 55, 43 – 55. doi:10.1016/S0065-3276(07)00204-3.

Arthur, M.A., Premoli Silva, I., 1982. Development of widespread organic carbon rich strata, in the Mediterranean Tethys. In: Schlanger, S.O., Cita, M.B. (Eds.), Nature and Origin of Cretaceous Carbon-Rich Facies, Academic Press, London, pp. 7–54.

Arthur, M.A., Dean, W.E., Schlanger, S.O., 1985. Variations in the global carbon cycle during the Cretaceous related to climate, volcanism, and changes in atmospheric CO_2. The Carbon Cycle and Atmospheric CO: Natural Variations Archean to Present, 504-529.

Arthur, M.A., Schlanger, S.T., Jenkyns, H.C., 1987. The Cenomanian-Turonian Oceanic Anoxic Event, II. Palaeoceanographic controls on organic-matter production and preservation. Geological Society, London, Special Publications 26(1), 401-420.

Arthur, M.A., Jenkyns, H.C., Brumsack, H.J., Schlanger, S.O., 1990. Stratigraphy, geochemistry and palaeogeography of organic carbon-rich Cretaceous sequences. In: Ginsburg, R.N. & Beaudoin, B. (Eds) Cretaceous Resources, Events and Rhythms. Kluwer, Dordrecht, 75–119.

Arthur, M.A., Miller, K., Charlson, R.J., 1991. Global episodes of moderate to extreme warmth. Advisory Panel Report on Earth System Hystory, G.S. Mountatin, Ed., Joint Oceanographic Institutions Inc., 51-74.

Aubry, M.P., 2009. A sea of Lilliputians. Palaeogeography, Palaeoclimatology, Palaeoecology, 284(1), 88-113.

Bapteste, E., Brochier, C., Boucher, Y., 2005. Higher-level classification of the Archaea: evolution of methanogenesis and methanogens. Archaea 1, 353–363.

Barber, C.J., Grice, K., Bastow, T.P., Alexander, R., Kagi, R.I., 2001. The identification of crocetane in Australian crude oils. Organic Geochemistry 32(7), 943-947.

Barral, A., Gomez, B., Fourel, F., Daviero-Gomez, V., Lécuyer, C., 2017. CO_2 and temperature decoupling at the million-year scale during the Cretaceous Greenhouse. Scientific reports 7, 1-7.

Barron, E.J., 1983, A warm, equable Cretaceous: The nature of the problem: Earth-Science Reviews 19, 305-338

Barron, E.J., Washington, W.M., 1985. Warm Cretaceous climates: High atmospheric CO2 as a plausible mechanism. The Carbon Cycle and Atmospheric CO: Natural Variations Archean to Present, 546-553.

Baudin, F., Fiet, N., Coccioni, R., Galeotti, S., 1998. Organic matter characterisation of the Selli Level (Umbria-Marche Basin, central Italy). Cretaceous Research 19, 701–714.

Bellanca, A., Claps, M., Erba, E., Masseti, D., Neri, R., Premoli-Silva, I., Venezia, F., 1996. Orbitally induced limestone/marlstone rhythms in the Albian-Cenomanian Cismon section (Venetian region, northern Italy): sedimentology, calcareous and siliceous plankton distribution, elemental and isotope geochemistry. Palaeogeography, Palaeoclimatology, Palaeoecology 126, 227-260.

Bellanca, A., Masetti, D., Neri, R., Venezia, F., 1999. Geochemical and sedimentological evidence of productivity cycles recorded in Toarcian black shales from the Belluno Basin, Southern Alps, northern Italy. Journal of Sedimentary Research 69(2).

Bice, K.L., Norris, R.D., 2002, Possible atmospheric CO2 extremes of the middle Cretaceous (late Albian–Turonian). Paleoceanography 17, 22-1 – 22-17.

Blumer, M., Guillard, R.R.L., Chase, T., 1971. Hydrocarbons of marine phytoplankton. Marine Biology 8(3), 183-189.

Bodin, S., Meissner, P., Janssen, N. M., Steuber, T., Mutterlose, J., 2015. Large igneous provinces and organic carbon burial: Controls on global temperature and continental weathering during the Early Cretaceous. Global and Planetary Change 133, 238-253.

Bornemann, A., Pross, J., Reichelt, K., Herrle, J.O., Hemleben, C., Mutterlose, J., 2005. Reconstruction of short-term palaeoceanographic changes during the formation of the Late Albian 'Niveau Breistroffer'black shales (Oceanic Anoxic Event 1d, SE France). Journal of the Geological Societ, 162(4), 623-639.

Bornemann, A., Norris, R.D., Friedrich, O., Beckmann, B., Schouten, S., Damsté, J.S.S., Vogel., J., Hofmann, P., Wagner, T., 2008. Isotopic evidence for glaciation during the Cretaceous supergreenhouse. Science 319(5860), 189-192.

Bourbonniere, R. A., Meyers, P.A., 1996. Sedimentary geolipid records of historical changes in the watersheds and productivities of Lakes Ontario and Erie. Limnology and Oceanography 41(2), 352-359.

Bralower, T.J., Thierstein, H.R., 1984. Low productivity and slow deep-water circulation in mid-Cretaceous oceans. Geology 12(10), 614-618.

Bralower, T.J., Monechi, S., Thierstein, H.R., 1989. Calcareous nannofossil zonation of the Jurassic–Cretaceous boundary interval and correlation with the geomagnetic polarity timescale. Marine Micropaleontology 14, 153–235.

Bralower, T.J., Sliter, W.V., Arthur, M.A., Leckie, R.M., Allard, D., Schlanger, S.O., 1993. Dysoxic/Anoxic Episodes in the Aptian–Albian (Early Cretaceous). In: Pringle, M.S., Sager, W.W., Sliter, W.V., Stein, S. (Eds.), The Mesozoic Pacific: Geology, Tectonics and Volcanism: Am. Geophys. Union Monograph 77, 5–37, doi: 10.1029/GM077p0005.

Bralower, T.J., Arthur, M.A., Feckie, R.M., Sliter, W.V., Allard, D., Schlanger, S.O, 1994. Timing and paleoceanography of oceanic dysoxia/anoxia in the Fate Barremian to Early Aptian (Early Cretaceous). Palaios 9, 335 -369.

Bralower, T.J., CoBabe, E., Clement, B., Sliter, W.V., Osburn, C.L., Longoria, J., 1999. The record of global change in mid–Cretaceous (Barremian–Albian) sections from the Sierra Madre, northeastern Mexico. J. Foramin. Res. 29, 418–437.

Brasier, M.D., 1995. Fossil indicators of nutrient levels. 1: Eutrophication and climate change. Geological Society, London, Special Publications 83(1), 113-132.

Brassell, S.C., Eglinton, G., Maxwell, J.R., Philp, R.P., 1978. Natural background of alkanes in the aquatic environment. Aquatic pollutants: transformation and biological effects, 69-86.

Brassell, S.C., Wardroper, A.M.K., Thompson, I.D., Maxwell, J.R., Eglinton, G., 1981. Specific acyclic isoprenoids as biological markers of methanogenic bacteria in marine sediments. Nature 290, 693–6.

Bray, E.E., Evans, E.D., 1961. Distribution of *n*-paraffins as a clue to recognition of source beds. Geochimica et Cosmochimica Acta 22, 2-15.

Bréhéret, J.G., 1983. Sur des niveaux de black shales dans l'Albien inférieur et moyen du domaine vocontien (sud-est de la France): étude de nannofaciès et signification des paléoenvironnements. Bulletin du Muséum National d'Histoire Naturelle, 113-159.

Bréhéret, J.G., 1988. Episodes de sedimentation riche en matiere organique dans les marnes bleues d'age aptien et albien de la partie pelagique du bassin vocontien. Bulletin de la Société géologique de France 4(2), 349-356.

Bréhéret, J.G.,1994. The mid-Cretaceous organic-rich sediments from the Vocontian zone of the French Southeast Basin. In: Hydrocarbon and petroleum geology of France, Springer Berlin Heidelberg, pp. 295-320.

Bréhéret, J.G., 1997. L'Aptien et l'Albien de la fosse vocontienne (des bordures au bassin): Évolution de la sédimentation et enseignements sur les événements anoxiques. Mémoire Societé Géologique Nord 25, pp164.

Bréhéret, J.G., Delamette, M., 1987. Correlation between basinal organic-rich deposits and shelf phosphate-rich deposits: the example of the vocontian basin and the Helvetic shelf (external Alps) during Aptian and Albian. In: Proceed. 3rd International Cretaceous Symposium, Tübingen.

Bréhéret, J.G., Delamette, M., 1989. Faunal fluctuations related to oceanographical changes in the Vocontian basin (SE France) during Aptian-Albian time. Geobios 22, 267-277.

Bréhéret, J.G., Caron, M., Delamette, M., 1986. Niveaux riches en matière organique dans l'Albien vocontien: quelques caractères du paléoenvironment; essai d'interprétation génétique. Documents du Bureau des Recherches Géologiques et Minières 110, 141-191.

Brock, T.D., 1978. Thermophilic Microorganisms and life at High Temperatures. Springer, New York, pp. 174.

Brocks. J.J., Summons, R.E., 2004. Sedimentary hydrocarbons, biomarkers for early life. In: Treatise on Geochemistry Vol 8, Biogeochemistry. Schlesinger WH (ed) Elsevier - Pergamon, Oxford, pp. 63-115.

Browning, E.L., Watkins, D.K., 2008. Elevated primary productivity of calcareous nannoplankton associated with ocean anoxic event 1b during the Aptian/Albian transition (Early Cretaceous). Paleoceanography 23. PA2213, doi: 10.1029/2007PA001413.

Brumsack, H.J. 1989. Geochemistry of recent TOC-rich sediments from the Gulf of California and the Black Sea. Geologische Rundschau 78(3), 851-882.

Calvert, S.E., Pedersen, T.F., 1993. Geochemistry of Recent oxic and anoxic marine sediments: implications for the geological record. Marine Geology 113, 67–88. http://dx.doi.org/10.1016/0025-3227(93)90150-T.

Carpenter, S.R., Mooney, H.A., Agard, J., Capistrano, D., DeFries, R.S., Diaz, S., Dietz, T., Duraiappah, A.K., Oteng-Yeboah, A., Pereira, H.M., Perrings, C., Reid, W.V., Sarukhan, J., Scholes, R.J., Whhyte, A., 2009. Science for managing ecosystem services: beyond the millennium ecosystem assessment. Proc. Natl Acad. Sci. USA 106, 1305 – 1312. doi:10.1073/pnas.0808772106

Channell, J.E.T., Cecca, F., Erba, E., 1995. Correlation of Hauterivian and Barremian (Early Cretaceous) stage boundaries to polarity chrons. Earth Planetary Scientific Letters 134, 125–140.

Channell, J.E.T., Erba, E., Muttoni, G., Tremolada, F., 2000. Early Cretaceous magnetic stratigraphy in the APTICORE drill core and adjacent outcrop at Cismon (Southern Alps, Italy), and correlation to the proposed Barremian-Aptian boundary stratotype. Geological Society of America Bulletin 112(9), 1430-1443.

Chappe, B., Michaelis, W., Albrecht, P., Ourisson, G., 1979. Fossil evidence for a novel series of archaebacterial lipids. Naturwissenschaften 66(10), 522-523.

Charbonnier, G., Föllmi, K.B., 2017. Mercury enrichments in lower Aptian sediments support the link between Ontong Java large igneous province activity and oceanic anoxic episode 1a. Geology 45(1), 63-66.

Clark, J.P., Philp, R.P., 1989. Geochemical characterization of evaporite and carbonate depositional environments and correlation of associated crude oils in the Black Creek Basin, Alberta. Bulletin of Canadian Petroleum Geology 37(4), 401-416.

Clarke, L.J., Jenkyns, H.C., 1999. New oxygen isotope evidence for long-term Cretaceous climatic change in the Southern Hemisphere. Geology 27(8), 699-702.

Coccioni, R., 1990. Benthonic foraminifera from the Aptian-Albian organic-rich Scisti a Fucoidi of the Poggio le Guaine-Fiume Bosso composite sequence (Umbria-Marche Apennines, Italy). 1st Meeting of the Working Group 2 - Pelagic Facies (IGCP Project 262 "Tethyan Cretaceous Correlation"), Urbino, 14-16 February, 1989, 18-20. Urbino: Centrostampa Università Urbino.

Coccioni, R., 1996. The Cretaceous of the Umbria-Marche Apennines (Central Italy). In: Jost Wiedmann Symposium on Cretaceous Stratigraphy, Paleobiology and Paleobiogeography, Tübingen, 7–10 March 1996. Berichte-Reports, Geologische–Paläontologisches Institut, Universität Kiel, 76, 129 – 136.

Coccioni, R., Battistini, F., 1989. Stratigraphy of the Early Aptian-Late Albian Scisti a Fucoidi in the Umbria-Marche area. In: Coccioni R., Monechi S. and Parisi G., Eds., Volume of Abstracts, 1st Meeting of the Working Group 2 - Pelagic Facies (IGCP Project 262 "Tethyan Cretaceous Correlation"), Urbino, 14-16 February 1989, 11-17. Urbino: Centrostampa Università Urbino.

Coccioni, R., Cocon, F., 1987. Hedbergella rhinoceros sp. n., a potential new biostratigraphic marker from Late Aptian-Early Albian Marne a Fucoidi (Central Italy). Rivista Italiana di Paleontologia e Stratigrafia 93, 469–478.

Coccioni, R., Galeotti, S., 1993. Orbitally induced cycles in benthonic foraminiferal morphogroups and trophic structures distribution patterns from the Late Albian "Amadeus Segment" (Central Italy). Journal of Micropaleontology 12, 227–239.

Coccioni, R., Luciani, V.. 2004. Planktonic foraminifera and environmental changes across the Bonarelli event (OAE2, latest Cenomanian) in its type area: A high-resolution study from the Tethyan reference Bottaccione section (Gubbio, Central Italy). Journal of Foraminiferal Research 34, 109–129. doi:10.2113/0340109.

Coccioni, R., Luciani, V., 2005. Planktonic foraminifers across the Bonarelli Event (OAE2, latest Cenomanian): The Italian record: Palaeogeography, Palaeoclimatology, Palaeoecology 224, 167–185. doi:10.1016/j.palaeo.2005.03.039.

Coccioni, R., Luciani, V., 2006. Guembelitria irregularis bloom at the K-T boundary: Morphological abnormalities induced by impact related extreme environmental stress?, In Cockell, C., Koeberl, C., and Gilmour, I., eds., Biological Processes Associated with Impact Events: Impact Studies Volume 8: Heidelberg, Springer, p. 179–196, doi:10.1007/3-540-25736-5_8.

Coccioni, R., Nesci, O., Tramontana, M., Wezel, F.C., Moretti, E., 1987a. Descrizione di un livello-guida 'radiolaritico-bituminoso-ittiolitico' alla base delle Marne a Fucoidi nell'Appennino umbromarchigiano. Bollettino della Società Geologica Italiana 106(I), 183- 192.

Coccioni, R., Nesci, O., Tramontana, M., Wezel, F.C., Moretti, E., 1987b. Descrizione di un livello-guida "radiolaritico-bituminoso-ittiolitico" alla base delle Marne a Fucoidi nell'Appennino umbro-marchigiano. Bollettino della Società Geologica Italiana 106, 183–192.

Coccioni, R., Battistini, F., Perugini, M., 1989a. Planktonic foraminiferal biostratigraphy of the Scisti a Fucoidi in the Poggio le Guaine and Fiume Bosso sections (Umbria-Marche basin). In: Coccioni R., Monechi S. and Parisi G., Eds., Volume of Abstracts 1st Meeting of the Working Group 2 - Pelagic Facies (IGCP Project 262 "Tethyan Cretaceous Correlation"), Urbino, 14-16 February, 1989, 18-20. Urbino: Centrostampa Università Urbino.

Coccioni, R., Franchi, R., Nesci, O., Wezel, F. C., Battistini. F., Pallecchi, P. 1989b. Stratigraphy and mineralogy of the Selli Level (Early Aptian) at the base of the Marne a Fucoidi in the UmbroMarchean Apennines, Italy. In Wiedmann, J. (Ed.), Creiuceous of the Western Tethys. Proceedings 3rd International Cretaceous Symposium, TubinRen lY87, 563 -584.

Coccioni, R., De Poli, A., Erba, E., Lottaroli, F., Premoli Silva, I., 1990a. Lithostratigraphy and biostratigraphy of the Aptian-Albian Scisti a Fucoidi Formation (central Italy): evidence for hiatuses and their paleotectonic and paleoenviromental implications. In: Comitato Centenario Raffaele Piccinini, Eds., 3° Convegno Internazionale "Fossili, Evoluzione, Ambiente", Pergola, 21-28 ottobre 1990, 41. Ostra Vetere (AN), Italy: Tecnostampa.

Coccioni, R., Franchi, R., Nesci, O., Perilli, N., Wezel, F.C. Battistini, F., 1990b. Stratigrafia, micropaleontologia e mineralogia delle Marne a Fucoidi delle sezioni di Poggio le Guaine e del Fiume Bosso (Appennino umbro–marchigiano). In: Comitato Centinario Raffaele Piccinini Ed., Atti 3° Convegno Internazionale "Fossili, Evoluzione, Ambiente", Pergola, 21–28 Ottobre 1990, 1. Ostra Vetere (AN) Italy, Tecnostampa.E. Schweizerbart Verlagsbuchhandlung, Stuttgart.

Coccioni, R., Erba, E., Premoli Silva, I., 1991. Biostratigrafia a plancton calcareo dell'intervallo Barremiano-Aptiano nella sezione di Gorgo a Cerbara (Marche) ed implicazioni nell'evoluzione. Paleopelagos 1, 125–127.

Coccioni, R., Erba, E., Premoli-Silva, I., 1992. Barremian–Aptian calcareous plankton biostratigraphy from the Gorgo a Cerbara section (Marche, central Italy) and implication for plankton evolution. Cretaceous Research 13, 457 – 467.

Coccioni, R, Luciani, V., Marsili, A., 2006. Cretaceous oceanic anoxic events and radially elongated chambered planktonic foraminifera: Paleoecological and paleoceanographic implications. Palaeogeogr. Palaeoclimatol. Palaeoecol. 235, 66–92. doi: 10.1016/j.palaeo.2005.09.024.

Coccioni, R., Jovane, L., Bancalà, G., Bucci, C., Fauth, G., Frontalini, F., Janikian, L., Savian, J., Paes de Almeida, R., Mathias, G.L., Trindade, R.I.F., 2012. Umbria–Marche Basin, Central Italy: A Reference Section for the Aptian–Albian Interval at Low Latitudes. Scientific Drilling 13, 42 – 46.

Coccioni, R., Sabatino, N., Frontalini, F., Gardin, S., Sideri, M., Sprovieri, M., 2014. The neglected history of Oceanic Anoxic Event 1b: insights and new data from the Poggio le Guaine section (Umbria–Marche Basin). Stratigraphy 11, 245 – 282.

Coffin, M.F., Eldholm, O., 1994. Large igneous provinces: Crustal structure, dimensions, and external consequences. Rev. Geophys. 32, 1-36.

Coffin, M.F., Pringle, M.S., Duncan, R.A., Gladczenko, T.P., Storey, M., Müller, R.D., Gahagan, L.A., 2002. Kerguelen hotspot magma output since 130 Ma. Journal of Petrology 43(7), 1121-1137.

Commendatore, M.G., Nievas, M.L., Amin, O., Esteves, J.L., 2012. Sources and distribution of aliphatic and polyaromatic hydrocarbons in coastal sediments from the Ushuaia Bay (Tierra del Fuego, Patagonia, Argentina). Marine environmental research 74, 20-31.

Cordey, W.G., Berggren, W.A., Olsson, R.K., 1970. Phylogenetic trends in the planktonic foraminiferal genus Pseudohastigerina Banner and Blow, 1959: Micropaleontology, v. 16, p. 235–242, doi:10.2307/1485120.

Cynar, F.J., Yayanos, A.A., 1991. Enrichment and characterization of a methanogenic bacterium from the upper layer of the ocean. Curr. Microbiol. 23, 89-96.

Davis, C, Pratt, L., Sliter, W., Mompart, L., Murat, B., 1999. Factors influencing organic carbon and trace metal accumulation in the Upper Cretaceous La Luna Formation of the western Maracaibo Basin, Venezuela. In Barrera, E., and Johnson, C.C., (Eds.), Evolution of the Cretaceous Ocean-Climate System: Boulder, Colorado, Geological Society of America Special Paper 332.

DeLong, E.F., 1992. Archaea in coastal marine environments. Proc. Natl. Acad. Sci. USA 89(12), 5685-9.

DeLong, E.F., Wu, K.Y., Prézelin, B.B., Jovine, R.V., 1994. High abundance of Archaea in Antarctic marine picoplankton. Nature 371(6499), 695-697.

De Wit, R., Caumette, P.,1995. An overview of the brown-coloured isorenieratene-containing green sulphur bacteria (Chlorobiaceae). Organic Geochemistry: Developments and applications to energy, climate, environment and human history, 908-909.

de Young, B., Barange, M., Beaugrand, G., Harris, R., Perry, R.I., Scheffer, M., 2008. Regime shifts in marine ecosystems: detection, prediction and management. Trends Ecol. Evol. 23, 402 – 409. doi:10.1016/j.tree.2008.03.008

DeBoer, P.L. (1982). Cyclicity and the storage of organic matter in Middle Cretaceous pelagic sediments, In: Cyclic and event stratification. Springer Berlin Heidelberg, pp. 456-475.

Dickens, G.R., Owen, R.M., 1994. Late Miocene-early Pliocene manganese redirection in the central Indian Ocean: Expansion of the intermediate water oxygen minimum zone. Paleoceanography 9(1), 169-181.

Dickens, G.R., Fewless, T., Thomas, E., Bralower, T.J., 2003. Excess barite accumulation during the Paleocene–Eocene thermal maximum: massive input of dissolved barium from sea-floor gas-hydrate reservoirs. In: Wing, S.L., Gingerich, P.D., Schmitz, B., Thomas, E. (Eds.), Causes and consequences of globally warm climates in the Early Paleogene. Geol. Soc. Am. Spec. Pap 369, pp. 11–23.

Didyk, B.M., Simoneit, B.R.T., Brassell, S.T., Eglinton, G., 1978. Organic geochemical indicators of palaeoenvironmental conditions of sedimentation. Nature 272(5650), 216-222.

Dumitrescu, M., Brassell, S.C., 2005. Biogeochemical assessment of sources of organic matter and paleoproductivity during the early Aptian Oceanic Anoxic Event at Shatsky Rise, ODP Leg 198. Organic Geochemistry 36(7), 1002-1022.

Duncan, R.A., 2002. A time frame for construction of the Kerguelen Plateau and Broken Ridge. Journal of Petrology 43(7), 1109-1119.

Dymond, J., Collier, R., 1996. Particulate barium fluxes and their relationships to biological productivity. Deep-Sea Research II 43, 1283–1308. http://dx.doi.org/10.1016/0967-0645(96)00011-2.

Dymond, J., Suess, E., Lyle, M., 1992. Barium in deep-sea sediment: a proxy for paleoproductivity. Paleoceanography 7, 163–181. http://dx.doi.org/10.1029/92PA00181

Eglinton, G., Hamilton, R.J., 1967. Leaf epicuticular waxes. Science 156(3780), 1322-1335.

Eldhom, O., Coffin, M.F., 2000. Large igneous provinces and plate tectonics. The history and dynamics of global plate motions, 309-326.

Elvert, M., Suess, E., Whiticar, M.J.,1999. Anaerobic methane oxidation associated with marine gas hydrates: superlight C-isotopes from saturated and unsaturated C20 and C25 irregular isoprenoids. Naturwissenschaften 86(6), 295-300.

Erba, E., 1988. Aptian-Albian calcareous nannofossil biostratigraphy of the Scisti a Fucoid cored at Piobbico (Central Italy).. Rivista italiana di Paleontologia e Stratigrafia 94, 249-284.

Erba, E. 1992. Calcareous nannofossil distribution in pelagic rhythmic sediments (Aptian-Albian Piobbico core, central Italy). Rivista Italiana di Paleontologia e Stratigrafia (Research In Paleontology and Stratigraphy), 97(3-4).

Erba, E., 1994. Nannofossils and superplumes: the Early Aptian “nannoconid crisis”. Palaeoceanography 9, 483–501.

Erba, E., 1996. The Aptian stage. In: Rawson, P.F., (Eds.), Proceedings of the 2nd International Symposium on Cretaceous Stage Boundaries. Bullettin de l'Institut Royal des Sciences Naturelles de Belgique 66, pp. 31–43 (supplement).

Erba, E., 2004. Calcareous nannofossils and Mesozoic oceanic anoxic events. Marine Micropaleontology 52, 85–106.

Erba, E., Larson, R.L., 1991. Nannofossils and superplumes. EOS 72, 301

Erba, E., Coccioni, R., Premoli Silva, I., 1989. The Scisti a Fucoidi in the Umbria–Marche area: the Apecchiese road sections. In: Cresta, S., Monechi, S., Parisi, G. (Eds.), Mesozoic–Cenozoic Stratigraphy in the Umbria–Marche area–Geological Field Trips in the Umbria–Marche Apennines (Italy): Memorie Descrittive della Carta Geologica d'Italia 39, 146–164.

Erba, E., Premoli Silva, I. Watkins, D. K., 1996. Cretaceous calcareous plankton stratigraphy of Sites 872 through 879, Proceeding in Ocean Drilling Program Scientific Results 144, 157– 169.

Erba, E., Bottini, C., Weissert, H.J., Keller, C.E., 2010. Calcareous nannoplankton response to surface-water acidifcation around Oceanic Anoxic Event 1a. Science 329, 428–432.

Erba, E., Duncan, R.A., Bottini, C., Tiraboschi, D., Weissert, H., Jenkyns, H.C., 2015. Environmental consequences of Ontong Java Plateau and Kerguelen Plateau volcanism. The Geological Society of America, Special Pubblications 511: 271 – 303.

Erbacher, J., Thurow, J., 1997. Influence of oceanic anoxic events on the evolution of mid-Cretaceous radiolaria in the North Atlantic and western Tethys. Marine Micropaleontology 30(1-3), 139-158.

Erbacher, J., Thurow, J., Littke, R., 1996. Evolution patterns of radiolaria and organic matter variations: a new approach to identify sea–level changes in mid–Cretaceous pelagic environments. Geology 24, 499−502, doi: 10.1130/0091 7613(1996)024<0499:EPORAO>2.3.CO;2

Erbacher, J., Gerth, W., Schmiedl, G., Hemleben, C., 1998. Benthic foraminiferal assemblages of late Aptian-early Albian black shale intervals in the Vocontian Basin, SE France, Cretaceous Research 19, 805–826.

Erbacher J., Hemleben, C., Huber, B.T., Markey, M., 1999. Correlating environmental changes during early Albian oceanic anoxic event 1B using benthic foraminiferal paleoecology. Mar. Micropaleontol. 38, 7 – 28. doi: 10.1016/S0377-8398(99)00036-5.

Erbacher, J., Huber, B.T., Norris, R.D., 2001. Increased thermohaline stratification as a possible cause for an oceanic anoxic event in the Cretaceous Period. Nature 409, 325 – 327.

Ernst, R.E., 2014. Large Igneous Provinces. Cambridge University Press.

Fassell, M.L., Bralower, T.J., 1999. Warm, equable mid-Cretaceous: Stable isotope evidence, In Barrera, E., Johnson, C., (Eds.). Evolution of the Cretaceous ocean-climate system: Geological Society of America Special Paper 332, 121-142.

Fiet, N., Masure, E., 2001. Les dinoflagellés albiens du bassin de Marches–Ombrie (Italie): proposition d'une biozonation pour le domaine téthysien. Cretaceous Res. 22, 63–77, doi: 10.1006/cres.2000.0237

Florin, T. H., Zhu, G., Kirk, K.M., Martin, N.G., 2000. Shared and unique environmental factors determine the ecology of methanogens in humans and rats. The American journal of gastroenterology, 95(10), 2872-2879.

Föllmi, K.B., 2012. Early Cretaceous life, climate and anoxia. Cretaceous Research 35, 230-257.

Föllmi, K.B., Gainon, F., 2008. Demise of the northern Tethyan Urgonian carbonate platform and subsequent transition towards pelagic conditions: the sedimentary record of the Col de la Plaine Morte area, central Switzerland. Sedimentary Geology 205(3), 142-159.

Föllmi, K.B., Godet, A., Bodin, S., Linder, P., 2006. Interactions between environmental change and shallow water carbonate buildup along the northern Tethyan margin and their impact on the Early Cretaceous carbon isotope record. Paleoceanography 21(4).

Font, E., Adatte, T., Sial, A.N., Drude de Lacerda, L., Keller, G., Punekar, J., 2016, Mercury anomaly, Deccan volcanism, and the end-Cretaceous mass extinction. Geology 44, 171 – 174. doi:10.1130/G37451.1

Forster, A., Schouten, S., Baas, M., Damsté, J.S.S., 2007. Mid-Cretaceous (Albian–Santonian) sea surface temperature record of the tropical Atlantic Ocean. Geology 35(10), 919-922

Fowler, M.G., 1992. The influence of Gloeocapsomorpha prisca on the organic geochemistry of oils and organic-rich rocks of late Ordovician age from Canada. In Early Organic Evolution: Implications for Mineral and Energy Resources (ed. M. Schidlowski et al.), pp. 336-356. Springer-Verlag.

Francois, R., Honjo, S., Manganini, S.J., Ravizza, G.E., 1995. Biogenic barium fluxes to the deep sea: implications for paleoproductivity reconstructions. Glob. Biogeochem. Cycles 9, 289–303. http://dx.doi.org/10.1029/95GB00021.

Frey, F.A., Coffin, M.F., Wallace, P.J., Weis, D., Zhao, X., Wise, S.W., Antretter, M., 2000. Origin and evolution of a submarine large igneous province: the Kerguelen Plateau and Broken Ridge, southern Indian Ocean. Earth and Planetary Science Letters 176(1), 73-89.

Frey, F.A., Weis, D., Borisova, A.Y., Xu, G., 2002. Involvement of continental crust in the formation of the Cretaceous Kerguelen Plateau: new perspectives from ODP Leg 120 sites. Journal of Petrology 43(7), 1207-1239.

Frey, F.A., Coffin, M.F., Wallace, P., Weis, D., 2003. Leg 183 synthesis: Kerguelen Plateau-Broken Ridge: A large igneous province. Proc. ODP Sci. Results 183.

Friedrich, O., Reichelt, K., Herrle, J.O., Lehmann, J., Pross, J., Hemleben, C., 2003. Formation of the Late Aptian Niveau Fallot black shales in the Vocontian Basin (SE France): evidence from foraminifera, palynomorphs, and stable isotopes. Marine Micropaleontology 49(1), 65-85.

Friedrich, O., Nishi, H., Pross, J., Schmiedl, G., Hemleben, C., 2005. Millennial- to centennial-scale interruptions of the Oceanic Anoxic Event 1b (Early Albian, mid–Cretaceous) inferred from benthic foraminiferal repopulation events. Palaios 20, 64 – 77.

Frijia, G., Parente, M., 2008. *Reticulinella kaeveri* Cherchi, Radoičić and Schroeder: a marker for the middle-upper Turonian in the shallow water carbonate facies of the peri-adriatic area. Bollettino della Società Geologica Italiana 127, 275–284

Fürsich, F.T., Berndt, R., Scheuer, T., Gahr, M., 2001. Comparative ecological analysis of Toarcian (Lower Jurassic) benthic faunas from southern France and east-central Spain: Lethaia, v. 34, p. 169–199, doi:10.1111/j.1502-3931.2001.tb00048.x.

Galand, P.E., Fritze H., Conrad R., Yrjälä K., 2005. Pathways for methanogenesis and diversity of methanogenic archaea in three boreal peatland ecosystems. Appl. Environ. Microbiol. 71, 2195–2198. Doi: 10.1128/AEM.71.4.2195-2198.2005 [

Galeotti, S., Sprovieri, M., Coccioni, R., Bellanca, A., Neri, R., 2003. Orbitally modulated black shale deposition in the upper Albian Amadeus Segment (central Italy): a multi-proxy reconstruction. Palaeogeography, Palaeoclimatology, Palaeoecology 190, 441 – 458.

Gelpi, E., Schneider, H., Mann, J., Oro, J., 1970. Hydrocarbons of geochemical significance in microscopic algae. Phytochemistry 9(3), 603-612.

Goossens, H.D., De Leeuw, J.W., Schenck, P.A., Brassell, S.C., 1984. Tocopherols as likely precursors of pristane in ancient sediments and crude oils. Nature 312(5993), 440-442.

Gradstein, F.M., Ogg, J.G., Schmitz, M., Ogg, G., (Eds.). 2012. The geologic time scale 2012. Elsevier.

Grantaman, P.J., Wakelfield, L.L., 1988. Variations in the sterane carbon number distributions of marine source rock-derived crude oils through geological time. Organic Geochemistry 12, 61-73.

Grasby, S.E., Sanei, H., Beauchamp, B., Chen, Z., 2013. Mercury deposition through the Permo-Triassic Biotic Crisis. Chem. Geol. 351, 209 – 216. http://dx.doi.org/10.1016/j.chemgeo.2013.05.022.

Grasby, S.E., Beauchamp, B., Bond, D.P.G., Wignall, P., Talavera, C., Galloway, J.M., Piepjohn, K., Reinhardt, L., Blomeier, D., 2015. Progressive environmental deterioration in northwestern Pangea leading to the latest Permian extinction. Bull. of the Geol. Soc. Am. 127, 1331 – 1347.

Greenwood, P.F., Summons, R.E.. 2003. GC–MS detection and significance of crocetane and pentamethylicosane in sediments and crude oils. Organic Geochemistry 34(8), 1211-1222.

Grippo, A., Fischer, A.G., Hinnov L.A., Herbert, T.M., Premoli Silva I., 2004. Cyclostratigraphy and chronology of the Albian stage (Piobbico core, Italy). SEPM (Society for Sedimentary Geology) Special Publications 81, 57–81.

Han, J., Calvin, M., 1969. Hydrocarbon distribution of algae and bacteria, and microbiological activity in sediments. Proceedings of the National Academy of Sciences, 64(2), 436-443.

Hantschel, T., Kauerauf, A.I., 2009. Fundamentals of basin and petroleum systems modeling. Springer Science & Business Media. DOI 10.1007/978-3-540-72318-9

Harris, A.H., Mundel, P., 1974. Size reduction in bighorn sheep (Ovis canadensis) at the close of the Pleistocene: Journal of Mammalogy, 55, 678–680, doi:10.2307/1379563

Hart, M.B., Ball, K.C., 1986. Late Cretaceous anoxic events, sea-level changes and the evolution of the planktonic foraminifera. In: Summerhayes, C.P., and Shackleton, N.I., (Eds.), North Atlantic Palaeoceanography, Geological Society Special Publication 21, 67-78.

Hart, M.B., Leary, P.N., 1991. Stepwise mass extinctions: the case for the Late Cenomanian event. Terra Nova 3, 142–147.

Hartgers W.A., Sinninghe Damsté, J.S., de Leeuw, J.W., 1994a. Geochemical significance of alkylbenzene distributions in flash pyrolysates of kerogens, coals and asphaltenes. Geochim. Cosmochim. Acta 58, 1759-1775.

Hartgers W.A., Sinninghe Damsté J.S., Requejo A.G., Allan J., Hayes J.M., de Leeuw J.W., 1994b. Evidence for only minor contributions from bacteria to sedimentary organic carbon. Nature 369, 224-227.

Hatch, J. R., Leventhal, J.S., 1992. Relationship between inferred redox potential of the depositional environment and geochemistry of the Upper Pennsylvanian (Missourian) Stark Shale Member of the Dennis Limestone, Wabaunsee County, Kansas, USA. Chemical Geology, 99(1-3), 65-82.

Hay, W.W., 2008. Evolving ideas about the Cretaceous climate and ocean circulation. Cretaceous Research. 29 (5–6), 725– 753.

Hay, W.W., Deconto, R., Wold, C. N., Wilson, K. M., Voigt, S., Schulz, M., Wold-Rossby, A., Dullo, W.C., Ronov, A. B., Balukhovsky, A.N., SöDing, E., 1999, Alternative global Cretaceous paleogeography, in Barrera, E., Johnson, C. (eds.), Evolution of the Cretaceous Ocean-Climate System. Geological Society of America Special Paper 332, p. 1–47.

Hays, J.D., Pitman, W.C., 1973. Lithospheric plate motion, sea level changes and climatic and ecological consequences. Nature 246, 18–22.

Heldt, M., Lehmann, J., Bachmann, M., Negra, H., Kuss, J., 2010. Increased terrigenous influx but no drowning: palaeoenvironmental evolution of the Tunisian carbonate platform margin during the Late Aptian. Sedimentology 57(2), 695-719.

Herbert, T.D., Fischer, A.G., 1986. Milankovitch climatic origin of mid-Cretaceous black shale rhythms in central Italy. Nature 321(6072), 739-743.

Herbert, T.D., Premoli Silva, I., Erba, E., Fischer, A.G., 1995. Orbital chronology of Cretaceous–Paleocene marine sediments. In: Berggren, W.A., Kent, D.V., Aubry, M-P., Hardenbol, J. (Eds.), Geochronology, Time Scale and Global Stratigraphic Correlation Society for Sedimentary Geology. Special Publication 54, pp. 81–93

Herrle, J.O., 2002. Mid–Cretaceous paleoceanographic and paleoclimatologic implications on black shale formation of the Vocontian Basin and Atlantic: Evidence from calcareous nannofossils and stable isotopes. Tübinger Mikropaläontologische Mitteilungen 27, 114.

Herrle, J.O., Mutterlose, J., 2003. Calcareous nannofossils from the Aptian–Lower Albian of southeast France: palaeoecological and biostratigraphic implications. Cretaceous Res. 24, 1 – 22. doi: 10.1016/S0195-6671(03)00023-5.

Herrle, J.O., Pross, J., Friedrich, O., Kößler, P., Hemleben, C., 2003a. Forcing mechanisms for mid–Cretaceous black shale formation: evidence from the Upper Aptian and Lower Albian of the Vocontian Basin (SE France). Palaeogeogr. Palaeoclimatol. Palaeoecol. 190, 399–426, doi: 10.1016/S0031-0182(02)00616-8.

Herrle, J.O., Pross, J., Friedrich, O., Hemleben, C., 2003b. Short-term environmental changes in the Cretaceous Tethyan Ocean: micropalaeontological evidence from the Early Albian Oceanic Anoxic Event 1b. Terra Nova 15(1), 14-19.

Herrle, J.O., Kössler, P., Friedrich, O., Erlenkeuser, H., Hemleben, C., 2004. High resolution carbon isotope records of the Aptian to lower Albian from SE France and the Mazagan Plateau (DSDP Site 545): a stratigraphic tool for paleoceanographic and paleobiologic reconstruction. Earth and Planet. Sci. Lett. 218, 149–161, doi: 10.1016/S0012-821X(03)00646-0.

Herrle, J.O., Kössler, P., Bollmann, J., 2010. Palaeoceanographic differences of early Late Aptian black shale events in the Vocontian Basin (SE France). Palaeogeography, Palaeoclimatology, Palaeoecology 297(2), 367-376.

Hinrichs, K.U., Boetius, A., 2002. The anaerobic oxidation of methane: new insights in microbial ecology and biogeochemistry. In: Ocean margin systems Springer Berlin Heidelberg, pp. 457-477.

Hochuli, P.A., Menegatti, A.P., Weissert, H., Riva, A., Erba, E., Silva, I.P., 1999. Episodes of high productivity and cooling in the early Aptian Alpine Tethys. Geology 27(7), 657-660.

Hoefs, M.J.L., Sinnighe Damsté, J.S., De Lange, G.J., De Leeuw, J.W., 1997. Changes in kerogen composition across an oxidation front in Madeira Abyssal Plain turbidites as revealed by pyrolysis GC-MS. Proceedings in Ocean Drilling Program, Scientific Result, 157.

Hofmann, P., Stüsser, I., Wagner, T., Schouten, S., Sinnighe Damsté J.S., 2008. Climate–Ocean coupling off North–West Africa during the Lower Albian: The Oceanic Anoxic Event 1b. Palaeogeogr. Palaeoclimatol. Palaeoecol. *262,* 157–165, doi: 10.1016/j.palaeo.2008.02.014.

Holbourn, A., Kuhnt, W., Soeding, E., 2001. Atlantic paleobathymetry, paleoproductivity and paleocirculation in the late Albian: the benthic foraminiferal record. Palaeogeography, Palaeoclimatology, Palaeoecology 170(3), 171-196.

Holzer, G., Oró, J., Tornabene, T.G., 1979. Gas chromatographic±mass spectrometric analysis of neutral lipids from methanogenic and thermoacidophilic bacteria. Journal of Chromatography 186, 795-809

Houtz, R.E., Hayes, D.E., Markl, R.G., 1977. Kerguelen Plateau bathymetry, sediment distribution and crustal structure. Marine Geology 25(1-3), 95101-98130.

Hu, G., Hu, W., Cao, J., Yao, S., Liu, W., Zhou, Z., 2014. Fluctuation of organic carbon isotopes of the Lower Cretaceous in coastal southeastern China: Terrestrial response to the Oceanic Anoxic Events (OAE1b). Palaeogeography, Palaeoclimatology, Palaeoecology 399, 352 – 362.

Huang, W.Y., Meinschein, W.G., 1979. Sterols as ecological indicators. Geochimica et cosmochimica acta 43(5), 739 – 745.

Huang, C., Hinnov, L., Fischer, A. G., Grippo A., Herbert, T., 2010. Astronomical tuning of the Aptian Stage from Italian reference sections. Geology 30, 899–902, doi: 10.1130/G31177.1.

Huber, B.T., Leckie, M., 2011. Planktic foraminiferal species turnover across deep–sea Aptian/Albian boundary sections. J. Foramin. Res. 41, 53–95. doi: 10.2113/gsjfr.41.1.53.

Huber, B.T, Hodell, D.A., Hamilton, C.P, 1995, Mid- to Late Cretaceous climate of the southern high latitudes: Stable isotopic evidence for minimal equator-to-pole thermal gradients: Geological Society of America Bulletin, v. 107, p. 1164-1191.

Huber, B.T., Norris, R.D., MacLeod, K.G., 2002. Deep-sea paleotemperature record of extreme warmth during the Cretaceous. Geology 30, 123–126.

Huber, B.T., Macleod, K.G., Gröcke, D.R., Michal Kucera, M., 2011. Paleotemperature and paleosalinity inferences and chemostratigraphy across the Aptian/Albian boundary in thesubtropical North Atlantic. Paleoceanography 26, PA4221. doi: 10.1029/2011PA002178.

Hughes, W.B., Holba, A.G., Dzou, L.I., 1995. The ratios of dibenzothiophene to phenanthrene and pristane to phytane as indicators of depositional environment and lithology of petroleum source rocks. Geochimica et Cosmochimica Acta, 59(17), 3581-3598.

Hughes, T.P., Linares, C., Dakos, V., van de Leemput, I.A., van Nes, E.H., 2013. Living dangerously on borrowed time during slow, unrecognized regime shifts. Trends in ecology & evolution, 28(3), 149-155.

Hunt, J.M., 1996. Petroleum Geochemistry and Geology. 2nd Edition, W.H. Freeman And Co., New York, pp. 743.

Iba, Y., Sano, S.I., 2007. Mid-Cretaceous step-wise demise of the carbonate platform biota in the Northwest Pacific and establishment of the North Pacific biotic province. Palaeogeography, Palaeoclimatology, Palaeoecology 245(3), 462 – 482.

Illich, H.A., 1983. Pristane, phytane, and lower molecular weight isoprenoid distributions in oils. AAPG bulletin 67(3), 385-393.

Ingram, B., Coccioni, R., Montanari, A., Richter, F.M., 1994. Strontium isotopic composition of mid-Cretaceous seawater. Science, 264 546–550.

Isozaki, Y., Aljinovic, D., 2009. End-Guadalupian extinction of the Permian gigantic bivalve Alatoconchidae: End of gigantism in tropical seas by cooling: Palaeogeography, Palaeoclimatology, Palaeoecology, v. 284, p. 11–21, doi:10.1016/j.palaeo.2009.08.022.

Jenkyns, H.C., 2010. Geochemistry of oceanic anoxic events. Geochem. Geophys. Geosystems 11.

Jones, B., Manning, D.A., 1994. Comparison of geochemical indices used for the interpretation of palaeoredox conditions in ancient mudstones. Chemical Geology, 111(1-4), 111-129.

Jones, D.S., Martini, A.M., and Kunio, K., 2016, Did volcanism trigger the Late Ordovician mass extinction? Mercury data from South China: Geological Society of America Abstracts with Programs, v. 40, No. 7, doi:10.1130/abs /2016AM-280651

Kanzari, F., Syakti, A.D., Asia, L., Malleret, L., Piram, A., Mille, G., Doumenq, P., 2014. Distributions and sources of persistent organic pollutants (aliphatic hydrocarbons, PAHs, PCBs and pesticides) in surface sediments of an industrialized urban river (Huveaune), France. Science of the Total Environment 478, 141-151.

Karl, D.M., Tilbrook, B.D. 1994. Production and transport of methane in oceanic particulate organic matter. Nature 368,732–734.

Kasten, S., Haese, R.R., Zabel, M., Rühlemann, C., Schulz, H.D., 2001. Barium peaks at glacial terminations in sediments of the equatorial Atlantic Ocean—relicts of deglacial productivity pulses? Chemical Geology 175, 635–651. http://dx.doi.org/10.1016/S0009-2541(00)00377-6.

Kauffman, E.G., 1973. Cretaceous Bivalvia, In: Hallam, A., (Ed.), Atlas of Palaeobiogeography: Elsevier, Amsterdam, p. 353–383.

Keller, G., 1989. Extended K-T boundary extinctions and delayed populational change in planktic foraminiferal faunas from Brazos River Texas: Paleoceanography, v. 4, p. 287–332, doi:10.1029/PA004i003p00287.

Keller, G., 1993. The Cretaceous-Tertiary boundary transition in the Antarctic Ocean and its global implications: Marine Micropaleontology, v. 21, p. 1–45, doi:10.1016/0377-8398(93)90010-U.

Keller, G., 2003a. Guembelitria–dominated planktic foraminiferal assemblages mimic early Danian in central Egypt: Marine Micropaleontology, v. 47, p. 71–99, doi:10.1016/S0377-8398(02)00116-0.

Keller, G., 2003b. Biotic effects of volcanism and impacts: Earth and Planetary Science Letters, v. 215, p. 249–264, doi:10.1016/S0012-821X(03)00390-X.

Keller, G., 2004. Paleoecology of late Maastrichtian–early Danian planktic foraminifera in the eastern Tethys (Israel and Egypt): Journal of Foraminiferal Research, v. 34, p. 49–73, doi:10.2113/0340049.

Keller, G., 2005. Biotic effects of late Maastrichtian mantle plume volcanism: Implications for impacts and mass extinctions: Lithos, v. 79, p. 317–341, doi:10.1016/j.lithos.2004.09.005.

Keller, G., Abramovich, S., 2009. Lilliput effect in late Maastrichtian planktic foraminifera: Response to environmental stress: Palaeogeography, Palaeoclimatology, Palaeoecology, v. 284, p. 47–62, doi:10.1016/j.palaeo.2009.08.029

Keller, G., Pardo, A., 2004. Disaster opportunists Guembelitrinidae: index for environmental catastrophes. Marine Micropaleontology 53(1), 83-116.

Keller, G., Lopez-Oliva, J.G., Stinnesbeck, W., Adatte, T. 1997. Age, stratigraphy and deposition of near K/T siliciclastic deposits in Mexico: Relation to bolide impact? Geological Society of America Bulletin, 109, 410–428.

Keller, G., Adatte, T., Stinnesbeck, W., Rebolledo-Vieyra, M., Urrutia Fuccugauchi, J., Kramar, G., Stueben, D., 2004. Chicxulub predates the K/T boundary mass extinction. Proceedings of the National Academy of Sciences of the USA, 101, 3753–3758

Keller, G., Adatte, T., Berner, Z., Harting, M., Baum, G., Prauss, M., Stueben, D., 2007. Chicxulub impact predates K–T boundary: new evidence from Brazos, Texas. Earth and Planetary Science Letters, 255(3), 339-356.

Kemper, E., Schmitz, H.H., 1981. Glendonite - Indikatoren des polarmarinen Ablagerungsmilieus. Geologische Rundshau 70 (2), 759-773

Kennedy, W.J., Gale, A.S., Huber, B.T., Petrizzo, M.R., Bown, P., Barchetta, A., Jenkyns, H.C., 2014. Integrated stratigraphy across the Aptian/Albian boundary at Col de Pré-Guittard (southeast France): A candidate Global Boundary Stratotype Section. Cretaceous Res. 51, 248–259, doi:10.1016/j.cretres.2014.06.005.

Kerr, A.C., 1998. Oceanic plateau formation: a cause of mass extinction and black shale deposition around the Cenomanian–Turonian boundary. Journal of Geological Society, London 155, 619–626.

Knittel, K., Lösekann, T., Boetius, A., Kort, R., Amann, R., 2005. Diversity and distribution of methanotrophic archaea at cold seeps. Applied and environmental microbiology 71(1), 467-479.

Koga, Y., Nishihara, M., Morii, H., Akagawa-Matsushita, M., 1993. Ether lipids of methanogenic bacteria: structures, comparative aspects, and biosyntheses. Microbiol. Rev. 57, 164-182.

Koopmans, M.P., de Leeuw, J.W., Sinninghe Damsté, J.S., 1996a Novel cyclised and aromatised diagenetic products of β-carotene in the Green River Shale. Organic Geochemistry, 26(7-8), 451-466.

Koopmans, M.P., Schouten, S., Kohnen, M.E., Damsté, J.S.S., 1996b. Restricted utility of aryl isoprenoids as indicators for photic zone anoxia. Geochimica et Cosmochimica Acta 60(23), 4873-4876.

Koopmans, M.P., Rijpstra, W.I.C., Klapwijk, M.M., de Leeuw, J.W., Lewan, M.D., Damsté, J.S.S., 1999. A thermal and chemical degradation approach to decipher pristane and phytane precursors in sedimentary organic matter. Organic Geochemistry 30(9), 1089-1104.

Kuroda, J., Ogawa, N.O., Tanimizu, M., Coffin, M.F., Tokuyama, H., Kitazato, H., Ohkouchi, N., 2007. Contemporaneous massive subaerial volcanism and late cretaceous Oceanic Anoxic Event 2. Earth and Planetary Science Letters 256(1), 211-223.

Kuypers, M.M.M., Blokker, P., Erbacher, J., Kinkel, H., Pancost, R.D., Schouten, S., Sinninghe Damsté, J.S., 2001. Massive expansion of marine Archaea during a mid–Cretaceous oceanic anoxic event. Science 293, 92–95, doi: 10.1126/science.1058424.

Kuypers, M.M.M., Blokker, P., Hopmans, E.C., Kinkel, H., Pancost, R.D., Schouten, S., Sinninghe Damsté, J.S., 2002. Archaeal remains dominate marine organic matter from the early Albian oceanic anoxic event 1b. Palaeogeogr. Palaeoclimatol. Palaeoecol. 185, 211–234, doi: 10.1016/S0031-0182(02)00301-2.

Kump, L.R., Pavlov, A., Arthur, M.A., 2005. Massive release of hydrogen sulfide to the surface ocean and atmosphere during intervals of oceanic anoxia. Geology 33(5), 397-400.

Kuntz, L.B., Laakso, T.A., Schrag, D.P., Crowe, S.A., 2015. Modeling the carbon cycle in Lake Matano. Geobiology 13(5), 454-461.

Larson, R.L., 1991. Latest pulse of Earth: Evidence for a mid-Cretaceous superplume. Geology 19(6), 547-550.

Leckie, M., 1984. Mid–Cretaceous planktonic foraminiferal biostratigraphy off central Morocco, Deep Sea Drilling Project Leg 79, Sites 545 and 547. Initial Rep. of the Deep Sea Drilling Project 79, 579–620, doi: 10.2973/dsdp.proc.79.122.1984.

Leckie, R.M., 1987, Paleoecology of mid-Cretaceous planktonic foraminifera: A comparison of open ocean and epicontinental sea assemblages: Micropaleontology, v. 33, p. 164–176, doi:10.2307/1485491

Leckie, RM., 1989. A paleoceanographic model for the early evolutionary history of planktonic foraminifera. Palaeogeography, Palaeoclimatology, Palaeoecology 73:107–38.

Leckie, R.M., Bralower, T.J., Cashman R., 2002. Oceanic anoxic events and plankton evolution: biotic response to tectonic forcing during the mid–Cretaceous. Paleoceanography 17, 13 – 29. doi: 10.1029/2001PA000623

Lees, K., Pitois, S., Scott, C., Frid, C., Mackinson, S., 2006. Characterizing regime shifts in the marine environment. Fish and fisheries 7(2), 104-127.

Li, J., Hu, X., Zhao, K., Cai, Y., Sun, T., 2016. Paleoceanographic evolution and chronostratigraphy of the Aptian Oceanic Anoxic Event 1a (OAE1a) to oceanic red bed 1 (ORB1) in the Gorgo a Cerbara section (central Italy). Cretaceous Research 66, 115-128.

Liaaen-Jensen, S., 1978. Chemistry of carotenoid pigments. Photosynthetic bacteria, 233-247.

Lijmbach, G.W.M., 1975. On the origin of petroleum. Proceedings of the 9th World Petroleum Congress 2, 357–69.

Lindberg, S., Bullock, R., Ebinghaus, R., Engstrom, D., Feng, X., Fitzgerald, W., Pirrone, N., Prestbo, E., Seigneur, C., 2007. A synthesis of progress and uncertainties in attributing the sources of mercury in deposition. AMBIO: a Journal of the Human Environment 36(1), 19-33.

Lirer, F., 2000. A new technique for retrieving calcareous microfossils from lithified lime deposits. Micropaleontology 46, 365–369.

Lockwood, R., 2005. Body size, extinction events, and the early Cenozoic record of veneroid bivalves: A new role for recoveries: Paleobiology, v. 31, p. 578–590, doi:10.1666/04070.1.

Luciani, V., Giusberti, L., Agnini, C., Fornaciari, E., Rio, D., Spofforth, D. J., & Pälike, H., 2010.. Ecological and evolutionary response of Tethyan planktonic foraminifera to the middle Eocene climatic optimum (MECO) from the Alano section (NE Italy). Palaeogeography, Palaeoclimatology, Palaeoecology, 292(1), 82-95.

Ludvigson, G.A., Joeckel, R.M., González, L.A., Gulbranson, E.L., Rasbury, E.T., Hunt, G.J., Kirkland, J.I., Madsen, S., 2010. Correlation of Aptian-Albian carbon isotope excursions in continental strata of the Cretaceous foreland basin, eastern Utah, USA. Journal of Sedimentary Research 80(11), 955-974.

Ludwig, W.G., Krasheninnikov, V.A., and the shipboard scientific party, 1981. Initial Reports DSDP, 71: Washington (U.S. Govt. Printing Office)

Ludwig, W.G., Krasheninnikov, V.A., and the shipboard scientific party, 1983. Site 511. Deep Sea Drilling Project Initial Report 71, 21–109.

Mackenzie, A.S., McKenzie, D., 1983. Isomerization and aromatization of hydrocarbons in sedimentary basins formed by extension. Geological Magazine, 120(5), 417-470.

Mackenzie, A.S., Patience, R.L., Maxwell, J.R., Vandenbroucke, M., Durand, B., 1980. Molecular parameters of maturation in the Toarcian shales, Paris Basin, France—I. Changes in the configurations of acyclic isoprenoid alkanes, steranes and triterpanes. Geochimica et Cosmochimica Acta, 44(11), 1709-1721

Mackenzie, A.S., Patience, R.L., Maxwell, J.R., 1981. Molecular changes and the maturation of sedimentary organic matter. In: Origin and Chemistry of Petroleum (Edited by Atkinson G. and Zuckerman J. J.), Chap. 1, pp. 1-31. Pergamon Press, Oxford.

Mackenzie, A.S., Brassell, S.C., Eglinton, G., Maxwell, J.R., 1982. Steroid hydrocarbons and the thermal history of sediments. Nature (London) 295, 223~26.

Mackenzie, A.S., Li, R.W., Maxwell, J.R., Moldowan, J.M., Seifert, W.K., 1983. Molecular measurements of thermal maturation of Cretaceous Shales from the Overthrust Belt, Wyoming, USA. In Advances in Organic Geochemistry 1981 (Edited by Bjor~y M. et al.), pp. 496-503. Wiley, Chichester.

Mackenzie, A.S., Maxwell, J.R., Coleman, M.L., Deegan, C.E., 1984. Biological marker and isotope studies of North Sea crude oils and sediments. In Proc. llth Worm Pet. Congr., Vol. 2, pp. 45--56. Wiley, Chichester.

MacLeod, N., 1990. Effects of late Eocene impacts on planktic foraminifera, in Sharpton, V.L., and Ward, P.D., eds., Global Catastrophes in Earth History; An Interdisciplinary Conference on Impacts, Volcanism, and Mass Mortality: Geological Society of America Special Paper 247, p. 595–606, doi:10.1130/SPE247-p595.

MacLeod, N., Ortiz, N., Fefferman, N., Clyde, W., Schulter, C., and MacLean, J., 2000. Phenotypic response of foraminifera to episodes of global environmental change, in Culver, S.J., and Rawson, P., eds., Biotic Response to Global Environmental Change: The Last 145 Million Years: Cambridge, Cambridge University Press, p. 51–78.

Madhavaraju, J., Lee, Y.I., González-León, C.M., 2013. Carbon, oxygen and strontium isotopic signatures in Aptian-Albian limestones of the Mural Formation, Cerro Pimas area, northern Sonora, Mexico. Journal of Iberian Geology, Madrid, 39, 73-88.

Mancini, E.A., 1978. Origin of the Grayson micromorph fauna (Upper Cretaceous) of north-central Texas: Journal of Paleontology, 52, 1294–1314.

Marchegiani, L., Bertotti, G., Cello, G., Deiana, G., Mazzoli, S., and Tondi, E., 1999. Pre-orogenictectonics in the Umbria – Marche sector of the Afro-Adriatic continental margin: Tectonophysics 315, 123 – 143.

Maurer, F., van Buchem, F.S., Eberli, G.P., Pierson, B.J., Raven, M.J., Larsen, P.H., Al-Husseini, M.I., Vincent, B., 2013. Late Aptian long-lived glacio-eustatic lowstand recorded on the Arabian Plate. Terra Nova 25, 87-94.

May, R.M., 1977. Thresholds and breakpoints in ecosystems with a multiplicity of stable states. Nature 269:471–7

McAnena, A., Flögel, S., Hofmann, P., Herrle, J.O., Griesand, A., Pross, J., Talbot, H.M., Rethemeyer, J., Wallmann, K., Wagner, T., 2013. Atlantic cooling associated with a marine biotic crisis during the mid–Cretaceous period. Natural Geosciences 6, 558–561, doi: 10.1038/ngeo1850

McDonald, J.H., Grasso, A.M., Rejto, L.K., 1999. Patterns of temperature adaptation in proteins from *Methanococcus* and *Bacillus*. Mol. Biol. Evol. 16, 1785-1790.

McKenzie D., Mackenzie, A.S., Maxwell, J.R. Sajgo, C., 1983. Isomerisation and aromatization of hydrocarbons in stretched sedimentary basins. Nature (London) 301, 504-506.

McKinney, M. L., 1990. Trends in body-size evolution. Evolutionary trends, 75-118.

Metcalfe, B., Twitchett, R.J., and Price-Looyd, N., 2011. Changes in size and growth rate of 'Lilliput' animals in the earliest Triassic: Palaeogeography, Palaeoclimatology, Palaeoecology, v. 308, p. 171–180, doi:10.1016/j.palaeo.2010.09.011.

Millán, M.I., Weissert, H.J., Lópex-Horgue, M.A., 2014. Expression of the late Aptian cold snaps and the OAE1b in a highly subsiding carbonate platform (Aralar, northern Spain). Palaeogeography, Palaeoclimatology, Palaeoecology 411, 167–179

Millennium Ecosystem Assessment. 2005 Ecosystems and human well-being: synthesis, p. 137. Washington, DC: Island Press.

Mohr, B.A.R.,Wähnert, V., Lazarus, D., 2002. Mid-Cretaceous palaeobotany and palynology of the central Kerguelen Plateau, southern Indian Ocean (ODP Leg 183, Site 1138). Proceedings of the Ocean Drilling Program, scientific results, Vol. 183 (ed. by F.A. Frey, M.F. Coffin, P.J. Wallace and P.G. Quilty), pp. 1–39. Ocean Drilling Program, College Station, TX.

Morford, J.L., Emerson, S., 1999. The geochemistry of redox sensitive trace metals in sediments. Geochimica et Cosmochimica Acta 63(11), 1735-1750.

Morten, S.D., Twitchett, R.J., 2009. Fluctuations in the body size of marine invertebrates through the Pliensbachian–Toarcian extinction event: Palaeogeography, Palaeoclimatology, Palaeoecology, v. 284, p. 29–38, doi:10.1016/j.palaeo.2009.08.023.

Moullade, M., Granier, B., Tronchetti, G., 2011. The Aptian Stage: back to fundamentals. Episodes 34(3), 148 – 156.

Munsell, A.H., 1907. A Color Notation: A Measured Color System, Based on the Three Qualities, Hue, Value, and Chroma, with Illustrative Models, Charts, and a Course of Study Arranged for Teachers. GH Ellis.

Mutter, R.J., and Neuman, A.G., 2009, Recovery from the end-Permian extinction event: Evidence from "Lilliput Listracanthus": Palaeogeography, Palaeoclimatology, Palaeoecology, v. 284, p. 22–28, doi:10.1016/j.palaeo.2009.08.024.

Mütterlose, J., Bornemann, A., Herrle, J.O., 2005. Mesozoic calcareous nannofossils — state of the art. Paläontologische Zeitschrift 79, 113–133.

Mutterlose, J., Bornemann, A., Herrle, J., 2009. The Aptian–Albian cold snap: Evidence for. Neues Jahrbuch für Geologie und Paläontologie-Abhandlungen 252(2), 217-225.

Nascimento-Silva, M.V., Sial, A.N., Ferreira, V.P., Neumann, V.H., Barbosa, J.A., Pimentel, M.M., de Lacerda, L.D., 2011. Cretaceous-Paleogene transition at the Paraíba Basin, Northeastern, Brazil: Carbon-isotope and mercury subsurface stratigraphies. Journal of South American Earth Sciences 32(4), 379-392.

Nelson, G.C., Bennett, E.M., Berhe, A.A., Cassman, K.G., DeFries, R., Dietz, T., Dobermann, A., Dobson, A., Janetos, A., Levy, M., Marco, D., Nakicenovic, N., O'Neill, B., Norgaard, R., Petschel-Held, G., Ojima, D.S., Pingali, P.L., Watson, R., Zurek, M., 2006. Anthropogenic drivers of ecosystem change: an overview. Ecology and Society 11:29

Noble, R.A., Henk, F.H., 1998. Hydrocarbon charge of a bacterial gas field by prolonged methanogenesis: an example from the East Java Sea, Indonesia. Organic Geochemistry 29(1), 301-314.

Norris, R.D., Bice, K.L., Magno, E.A., Wilson, P.A., 2002, Jiggling the tropical thermostat in the Cretaceous hothouse: Geology, v. 30, p. 299–302.

Obermajer, M., Fowler, M.G., Snowdon, L.R., 1999. Depositional environment and oil generation in Ordovician source rocks from southwestern Ontario, Canada: organic geochemical and petrological approach. American Association of Petroleum Geologists Bulletin 83, 1426-53.

Ogg, J.C., Hinnov, L.A., 2012. Cretaceous. In: Gradstein, F.M., et al. (Eds.), The Geologic Time Scale 2012, pp. 793–853 http://dx.doi.org/10.1016/B978-0-444-59425-9.00027-5

Oglesby, R., Park, J., 1989. Effect of precessional insolation changes on Cretaceous climate and cyclic sedimentation. Journal of Geophysical Research: Atmospheres, 94(D12), 14793-14816.

Okano, K., Sawada, K., Takashima, R., Nishi, H., Okada, H., 2008. Further examples of archaeal-derived hydrocarbons in mid-Cretaceous oceanic anoxic event (OAE) 1b sediments. Organic Geochemistry 39 (8), 1088–1091, doi: 10.1016/j.orggeochem.2008.04.022.

Operto, S., Charvis, P., 1995. Kerguelen Plateau: A volcanic passive margin fragment?. Geology 23(2), 137-140.

Ourisson, G., Rohmer, M., Poralla, K., 1987. Prokaryotic hopanoids and other polyterpenoid sterol surrogates. Annual Reviews in Microbiology, 41(1), 301-333.

Ourisson, G., Rohmer, M., 1992. Hopanoids. 2. Biohopanoids: a novel class of bacterial lipids. Accounts of Chemical Research 25(9), 403-408.

Pacton, M., Fiet, N., Gorin, G., Spangenberg, J.E., 2007. Lower Cretaceous oceanic anoxic event OAE1b: organic matter accumulation mediated by bacterial activity. Geophysical Research Abstract 9, 09956.

Pancost, R.D., Damsté, J.S.S., de Lint, S., van der Maarel, M.J., Gottschal, J.C., 2000. Biomarker evidence for widespread anaerobic methane oxidation in Mediterranean sediments by a consortium of methanogenic archaea and bacteria. Applied and Environmental Microbiology 66(3), 1126-1132.

Pancost, R.D., Hopmans, E.C., Damsté, J.S., Party, T.M.S.S., 2001. Archaeal lipids in Mediterranean cold seeps: molecular proxies for anaerobic methane oxidation. Geochimica et Cosmochimica Acta 65(10), 1611-1627.

Pancost, R.D., Boot, C.S., 2004. The palaeoclimatic utility of terrestrial biomarkers in marine sediments. Marine Chemistry 92(1), 239-261

Pardo, A., Keller, G., 2008. Biotic effects of environmental catastrophes at the end of the Cretaceous and early Tertiary: Guembelitria and Heterohelix blooms. Cretaceous Research, 29(5), 1058-1073

Patruno, S., Triantaphyllou, M.V., Erba, E., Dimiza, M.D., Bottini, C., Kaminski, M.A., 2015. The Barremian and Aptian stepwise development of the 'Oceanic Anoxic Event 1a' (OAE 1a) crisis: Integrated benthic and planktic high-resolution palaeoecology along the Gorgo a Cerbara stratotype section (Umbria–Marche Basin, Italy). Palaeogeography, Palaeoclimatology, Palaeoecology 424, 147–182

Payne, J.L., 2005. Evolutionary dynamics of gastropod size across the end-Permian extinction and through the Triassic recovery interval: Paleobiology, v. 31, p. 269–290, doi:10.1666/0094-8373(2005)031[0269:EDOGSA]2.0.CO;2.

Paytan, A., Griffith, E.M., 2007. Marine barite: recorder of variations in ocean export productivity. Deep-Sea Research II 54, 687–705. http://dx.doi.org/10.1016/j.dsr2.2007.01.007

Pedersen, T.F., Calvert, S.E., 1990. Anoxia vs. productivity: what controls the formation of organic-carbon-rich sediments and sedimentary Rocks?(1). AAPG Bulletin, 74(4), 454-466.

Percival, L.M.E., Witt, M.L.I., Mather, T.A., Hermoso, M., Jenkyns, H.C., Hesselbo, S.P., Al-Suwaidi, A.H., Storm, M.S., Xu, W., and Ruhl, M., 2015. Globally enhanced mercury deposition during the end-Pliensbachian extinction and Toarcian OAE: A link to the Karoo–Ferrar large igneous province. Earth Planet. Sci. Lett. 428, 267 – 280. doi:10.1016/j.epsl.2015.06.064.

Peters K.E., Moldowan M.J., 1993. The Biomarker Guide. Prentice Hall International, New York.

Peters, K.E., Walters, C.C., Moldowan, J.M., 2005. The biomarker guide (Vol. 1&2). Cambridge University Press.

Petrizzo, M.R., Huber, B.T., Gale, A., Barchetta, A., Jenkyns, H.C., 2012. Abrupt planktic foraminiferal turnover across the Niveau Kilian at Col de Pré-Guittard (Vocontian Basin, southeast France): new criteria for defining the Aptian/Albian boundary. Newsletters on Stratigraphy 45, 55-74, doi:10.1127/0078-0421/2012/0013

Petrizzo, M.R., Huber, B.T., Gale, A.S., Barchetta, A., Jenkyns, H.C., 2013. Erratum:Abrupt planktic foraminiferal turnover across the Niveau Kilian at Col de Pre-Guittard (Vocontian Basin, southeast France): new criteria for defining the Aptian/Albian boundary. Newsletters on Stratigraphy 46, 93.

Piper, D.Z., Perkins, R.B.,2004. A modern vs. Permian black shale—the hydrography, primary productivity, and water-column chemistry of deposition. Chemical geology 206(3), 177-197.

Pirrie, D., Doyle, P., Marshall, J.D., Ellis, G., 1995. Cool Cretaceous climates: new data from the Albian of Western Australia, Journal of Geological Society of London 152, 739-742.

Plancq, J., Mattioli, E., Pittet, B., Simon, L., Grossi, V., 2014. Productivity and sea-surface temperature changes recorded during the late Eocene–early Oligocene at DSDP Site 511 (South Atlantic). Palaeogeography, Palaeoclimatology, Palaeoecology 407, 34-44.

Pouliot, J., Galand, P.E., Lovejoy, C., Vincent, W.F., 2009. Vertical structure of archaeal communities and the distribution of ammonia monooxygenase A gene variants in two meromictic High Artic lakes. Environmental Microbiology 11(3), 687-699.

Premoli Silva, I., Sliter, W.V., 1999. Cretaceous paleoceanography: Evidence from planktonic foraminiferal evolution, in: Barrera, E., Johnson, C.C. (Eds.), Evolution of the Cretaceous Ocean-Climate System. Special Papers Geological Society of America 332, 301 – 328.

Premoli Silva, I., Erba, E., Salvini, G., Locatelli, C., Verga, D., 1999. Biotic changes in Cretaceous oceanic anoxic events of the Tethys. Journal of Foraminiferal Research 29(4), 352-370.

Price, G.D., 2003. New constraints upon isotope variation during the early Cretaceous (Barremian–Cenomanian) from the Pacific Ocean. Geological Magazine 140(5), 513-522.

Price, G.D., Nunn, E.V., 2010. Valanginian isotope variation in glendonites and belemnites from Arctic Svalbard: Transient glacial temperatures during the Cretaceous greenhouse. Geology 38, 251-254.

Price, G.D., Sellwood, B.W., Corfield, R.M., Clarke, L., Cartlidge, J.E., 1998a. Isotopic evidence for palaeotemperatures and depth stratification of middle Cretaceous planktonic foraminifera from the Pacific Ocean. Geological Magazine 135, 183–191.

Price, G.D., Valdes, P.J., Sellwood, B.W., 1998b. A comparison of GCM simulated Cretaceous “greenhouse” and “icehouse” climates: implications for the sedimentary record. Palaeogeography, Palaeoclimatology, Palaeoecology 142, 123–138.

Price, G.D., Williamson, T., Henderson, R.A., Gagan, M.K., 2012. Barremian–Cenomanian palaeotemperatures for Australian seas based on new oxygen-isotope data from belemnite rostra. Palaeogeography, Palaeoclimatology, Palaeoecology 358, 27-39.

Pyle, D.M., Mather, T.A., 2003. The importance of volcanic emissions for the global atmospheric mercury cycle. Atmospheric Environment. 37, 5115–5124 (2003)

Quinby-Hunt, M.S., Wilde, P., 1994. Thermodynamic zonation in the black shale facies based on iron-manganese-vanadium content. Chemical Geology 113(3-4), 297-317.

Raia, P., Barbera, C., Conte, M., 2003. The fast life of a dwarfed giant: Evolutionary Ecology, v. 17, p. 293–312, doi:10.1023/A:1025577414005

Requejo A.G., Allan J., Creany S., Gray N.R., Cole K.S., 1992. Aryl isoprenoids and diaromatic carotenoids in Paieozoic source rocks and oils from the Western Canada and Williston basins. Organic Geochemestry 19, 245-264.

Retallack, G.J., 2001. A 300-million-year record of atmospheric carbon dioxide from fossil plant cuticles. Nature, 411(6835), 287-290.

Rielley, G., Collier, R.J., Jones, D.M., Eglinton, G., 1991. The biogeochemistry of Ellesmere Lake, UK—I: source correlation of leaf wax inputs to the sedimentary lipid record. Organic Geochemistry 17(6), 901-912.

Risatti, J.B., Rowland, S.J., Yon, D.A., Maxwell, J.R., 1984. Stereochemical studies of acyclic isoprenoids—XII. Lipids of methanogenic bacteria and possible contributions to sediments. Organic Geochemistry 6, 93-104.

Riveros, A.J., 2007. On Lilliputians and Brobdingnagians. Trends in Ecology and Evolution 22, 115–116

Robaszynski, F., Caron, M., 1995. Foraminifères planctoniques du Crétacé: commentaire de la zonation Europe−Méditerranée. Bulletin de la Societé Géologique de France 166, 681−692.

Rocha, J., Yletyinen, J., Biggs, R., Blenckner, T., Peterson, G., 2015. Marine regime shifts: drivers and impacts on ecosystems services. Phil. Trans. R. Soc. B, 370(1659), 20130273.

Ryan, W.B., Cita, M.B., 1977. Ignorance concerning episodes of ocean-wide stagnation. Marine Geology 23(1-2), 197-215.

Sabatino, N., Coccioni, R., Salvaggio Manta, D., Baudin, F., Vallefuoco, M., Traina, A., Sprovieri, M., 2015. High-resolution chemostratigraphy of the late Aptian–early Albian oceanic anoxic event (OAE 1b) from the Poggio le Guaine section (Umbria–Marche Basin, central Italy). Palaeogeography, Palaeoclimatology, Palaeoecology 426, 319 – 333.

Sanei, H., Grasby, S.E., Beauchamp, B., 2012. Latest Permian mercury anomalies. Geology 40, 63 – 66. http://dx.doi.org/10.1130/G32596.1

Satolli, S., Besse, J. And Calamita, F., 2008. Paleomagnetism of Aptian−Albian sections from the Northern Apennines (Italy): Implications for the 150–100 Ma apparent polar wander of Adria and Africa. Earth and Planetary Science Letters 276, 115–128.

Scheffer, M., Carpenter, S., Foley, J., Folke, C., Walker B., 2001 Catastrophic shifts in ecosystems. Nature 413, 591 – 596. (doi:10.1038/35098000).

Scheffer, M., Carpenter, S, 2003 Catastrophic regime shifts in ecosystems: linking theory to observation. Trends Ecol. Evol. 18, 648 – 656. (doi:10.1016/j.tree.2003.09.002).

Schlanger, S.O., Jenkyns, H.C., 1976. Cretaceous anoxic events: causes and consequences. Geologie en Mijnbouw 55, 179–184.

Schlanger, S.O., Jenkyns, H.C., Premoli-Silva, I., 1981. Volcanism and vertical tectonics in the Pacific Basin related to the global Cretaceous transgressions. Earth and Planetary Science Lettetters 52, 435- 449.

Schouten, S., van der Marel, M.J.E.C., Huber, R., Sinninghe Damsté, J.S., 1997. 2,6,10,15,19-Pentamethylicosenes in Methanolobus bombayensis, a marine methanogenic archaeon, and methanosarcina mazei. Organic Geochemistry 26, 409-414

Schouten, S., Wakeham, S.G., Damsté, J.S.S., 2001a. Evidence for anaerobic methane oxidation by archaea in euxinic waters of the Black Sea. Organic Geochemistry 32(10), 1277-1281.

Schouten, S., Rijpstra, W.I.C., Kok, M., Hopmans, E.C., Summons, R.E., Volkman, J.K., Damsté, J.S., 2001b. Molecular organic tracers of biogeochemical processes in a saline meromictic lake (Ace Lake). Geochimica et Cosmochimica Acta 65(10), 1629-1640.

Schouten, S., Hartgers, W.A., Lòpez, J.F., Grimalt, J.O., & Damsté, J.S.S., 2001c. A molecular isotopic study of 13 C-enriched organic matter in evaporitic deposits: recognition of CO 2-limited ecosystems. Organic Geochemistry 32(2), 277-286.

Schouten, S., Hopmans, E. C., Schefuß, E., Sinnighe Damste, J. S., 2002. Distributional variations in marine crenarchaeotal membrane lipids: a new tool for reconstructing ancient sea water temperatures?. Earth and Planetary Science Letters 204(1), 265-274.

Schrader, H., Sorknes, R., 1991. Peruvian coastal upwelling: Late Quaternary productivity changes revealed by diatoms. Marine Geology, 97(3-4), 233-249.

Seifert, W.K., Moldowan, J.M., 1978. Applications of steranes, terpanes and monoaromatics to the maturation, migration and source of crude oils. Geochimica et Cosmochimica Acta 42(1), 77-95.

Seifert, W.K., Moldowan, J.M., 1979. The effect of biodegradation on steranes and terpanes in crude oils. Geochimica et Cosmochimica Acta 43(1), 111-126.

Seifert, W.K., Moldowan, J.M., 1980. Paleoreconstruction by biological markers.

Sellwood, B.W., Price, G.D., Valdes, P.L., 1994. Cooler estimates of Cretaceous temperatures: Nature 370, 453-55.

Stefanova, M., 2000. Head-to-head linked isoprenoids in Miocene coal lithotypes. Fuel 79, 755–758.

Sial, A.N., Lacerda, L.D., Ferreira, V.P., Frei, R., Marquillas, R.A., Barbosa, J.A., Gaucher, C., Windmöller C.C., Pereira N.S., 2013. Mercury as a proxy for volcanic activity duringextreme environmental turnover: The Cretaceous–Paleogene transition. Palaeogeogr. Palaeoclimatol. Palaeoecol 387, 153 – 164.

Sial, A.N., Chen, J., Lacerda, L.D., Frei, R., Tewari, V.C., Pandit, M.K., Gaucher., C., Ferreira, V.P., Cirilli, S., Peralta, S., Korte, C., Barbosa, J.A., Pereira, N.S., 2016. Mercury enrichment and Hg isotopes in Cretaceous–Paleogene boundary successions: Links to volcanism and palaeoenvironmental impacts. Cretaceous Research 66, 60 – 81.

Siesser, W. G., Rogers, J. (1976). Authigenic pyrite and gypsum in South West African continental slope sediments. Sedimentology 23(4), 567-577.

Sininghe Damsté, J.S., Schouten, S., 2006. Biological markers for anoxia in the photic zone of the water column. In: Volkman J.K. (eds) Marine Organic Matter: Biomarkers, Isotopes and DNA. The Handbook of Environmental Chemistry, vol 2N. Springer, Berlin, Heidelberg. https://doi.org/10.1007/698_2_005

Sinnighe Damsté, J.S., Schouten, S., van Duin, A.C., 2001. Isorenieratene derivatives in sediments: possible controls on their distribution. Geochimica et Cosmochimica Acta 65(10), 1557-1571.;

Sinnighe Damsté, J.S., Rijpstra, W.I.C., Hopmans, E.C., Prahl, F.G., Wakeham, S.G., Schouten, S., 2002. Distribution of membrane lipids of planktonic Crenarchaeota in the Arabian Sea. Applied and Environmental Microbiology, 68(6), 2997-3002.

Sinton, C.W., Duncan, R.A., 1997. Potential links between ocean plateau volcanism and global ocean anoxia at the Cenomanian-Turonian boundary. Economic Geology 92(7-8), 836-842.

Słowakiewicz, M., Tucker, M.E., Perri, E., Pancost, R.D., 2015. Nearshore euxinia in the photic zone of an ancient sea. Palaeogeography, Palaeoclimatology, Palaeoecology, 426, 242-259.

Schmidt, M.W., Spero, H.J., Lea, D.W., 2004. Links between salinity variation in the Caribbean and North Atlantic thermohaline circulation. Nature, 428(6979), 160-163.

Speranza, F., Satolli, S., Mattioli, E., Calamita, F., 2005. Magnetic stratigraphy of Kimmeridgian–Aptian sections from Umbria–Marche (Italy): new details on the M polarity sequence. Journal of Geophysics Research B: Solid Earth 110 (12), 1–26 (art. no. B12109)

Spötl, C., Vennemann, T.W., 2003. Continuous-flow isotope ratio mass spectrometric analysis of carbonate minerals. Rapid communications in mass spectrometry, 17(9), 1004-1006.

Stein, M., Föllmi, K.B., Westermann, S., Godet, A., Adatte, T., Matera, V., Fleitmann, D., Berner, Z., 2011. Progressive palaeoenvironmental change during the Late Barremiane EarlyAptian as prelude to Oceanic Anoxic Event 1a: evidence from the Gorgo a Cerbara section (Umbria–Marche basin, central Italy). Palaeogeography, Palaeoclimatology, Palaeoecology, 302, 396–406.

Stoll, H.M., Schrag, D. P., 2000. High-resolution stable isotope records from the Upper Cretaceous rocks of Italy and Spain: Glacial episodes in a greenhouse planet? Geol. Soc. Am. Bull., 112, 308–319.

Summons, R.E., Powell, T.G., 1986. Chlorobiaceae in Palaeozoic seas revealed by biological markers, isotopes and geology. Nature 319, (6056), 763-765.

Summons, R.E., Powell, T.G., 1987. Identification of aryl isoprenoids in source rocks and crude oils: biological markers for the green sulphur bacteria. *Geochimica et Cosmochimica Acta*, *51*(3), 557-566.

Takahashi, K., 1986. Seasonal fluxes of pelagic diatoms in the subarctic Pacific, 1982–1983. Deep Sea Research Part A. Oceanographic Research Papers, 33(9), 1225-1251.

Takai, K., Horikoshi, K., 1999. Genetic diversity of archaea in deep-sea hydrothermal vent environments. Genetics 152(4), 1285-1297.

Takashima, R., Sano, S.I., Iba, Y., Nishi, H., 2007. The first Pacific record of the Late Aptian warming event. Journal of the Geological Society 164(2), 333-339.

Tantawy, A.A.A., Keller, G., Pardo, A., 2009. Late Maastrichtian volcanism in the Indian Ocean: effects on calcareous nannofossils and planktic foraminifera. Palaeogeography, Palaeoclimatology, Palaeoecology, 284(1), 63-87.

Tarduno, J.A., Brinkman, D.B., Renne, P.R., Cottrell, R.D., Scher, H., Castillo, P., 1998. Evidence for extreme climatic warmth from Late Cretaceous Artic vertebrates. Science 282, 2241–2244.

Tarduno, J.A., Sliter, W.V., Mayer, H., 1991. Mantle plume volcanism and the formation of the Ontong Java plateau. Extended Abstract, Clatech Plume Symposium. Pasadena.

Tejada, M.L.G., Suzuki, K., Kuroda, J., Coccioni, R., Mahoney, J.J., Ohkouchi, N., Sakamoto, T.,Tatsumi, Y., 2009. Ontong Java Plateau eruption as a trigger for the early Aptian oceanic anoxic event. Geology 37, 855–858.

Ten Haven, H.L., de Leeuw, J.W., Rullkötter, J., Sinninghe Damsté, J.S., 1987. Restricted utility of the pristane/phytane ratio as a palaeoenvironmental indicator. Nature 330, 641–3

Thibodeau, A.M., Ritterbush, K., Yager, J.A., West, A.J., Ibarra, Y., Bottjer, D.J., Berelson, W.M., Bergquist, B.A., and Corsetti, F.A., 2016, Mercury anomalies and the timing of biotic recovery following the end-Triassic mass extinction: Nature Communications, v. 7, p. 1–8, doi:10.1038/ncomms11147

Thibodeau, A.M., Bergquist, B.A., 2017. Do mercury isotopes record the signature of massive volcanism in marine sedimentary records?. Geology, 45(1), 95-96.

Thiel, V., Peckmann, J., Seifert, R., Wehrung, P., Reitner, J., Michaelis, W., 1999. Highly isotopically depleted isoprenoids: molecular markers for ancient methane venting. Geochim. Cosmochim. Acta 63, 3959–3966.

Thomas, E., 2003, Extinction and food at the seafloor: A high-resolution benthic foraminiferal record across the Initial Eocene Thermal Maximum, Southern Ocean Site 690, in Wing, S.L., Gingerich, P.D., Schmitz, B., and Thomas, E., eds., Causes and Consequences of Globally Warm Climates in the Early Paleogene: Geological Society of America Special Paper 369, p. 319–332, doi:10.1130/0-8137-2369-8.319.

Tiraboschi, D., Erba, E., Jenkyns, H.C., 2009. Origin of rhythmic Albian black shales (Piobbico core, central Italy): Calcareous nannofossil quantitative and statistical analyses and paleoceanographic reconstructions. Paleoceanography, 24(2).

Tissot, B.P., Welte, D.H., 1978. Petroleum formation and occurrence: a new approach to oil and gas exploration. New York, Springer Verlag, 50-70.

Tornaghi, M.E., Premoli Silva, I., Ripepe, M., 1989. Lithostratigraphy and planktonic foraminiferal biostratigraphy of the Aptian-Albian "Scisti a Fucoidi", In the Piobbico core, Marche, Italy: background for cyclostratigraphy. Rivista Italiana di Paleontologia e Stratigrafia 95, 223-264.

Torres, M.E., Brumsack, H.J., Bohrmann, G., Emeis, K.C., 1996. Barite fronts in continental margin sediments: a new look at barium remobilization in the zone of sulfate reduction and formation of heavy barites in diagenetic fronts. Chemical Geology 127, 125–139. http://dx.doi.org/10.1016/0009-2541(95)00090-9.

Trabucho Alexandre, J., Tuenter, E., Henstra, G.A., van der Zwan, K.J., van de Wal, R.S., Dijkstra, H.A., de Boer, P.L., 2010. The mid-Cretaceous North Atlantic nutrient trap: Black shales and OAEs. Paleoceanography, 25(4).

Trabucho Alexandre, J., Van Gilst, R.I., Rodríguez-López, J.P., De Boer, P.L., 2011. The sedimentary expression of oceanic anoxic event 1b in the North Atlantic. Sedimentology 58, 1217-1246. http://dx.doi.org/10.1111/j.1365-3091.2010.01202.x.

Tribovillard, N.P., Gorin, G.E., 1991. Organic facies of the early Albian Niveau Paquier, a key black shales horizon of the Marnes Bleues Formation in the Vocontian Trough (Subalpine Ranges, SE France). Palaeogeography, Palaeoclimatology, Palaeoecology 85(3-4), 227 – 237.

Tribovillard, N., Algeo, T.J., Lyons, T., Riboulleau, A., 2006. Trace metals as paleoredox and paleoproductivity proxies: an update. Chemical geology 232(1), 12-32.

Tsikos, H., Jenkyns, H.C., Walsworth-Bell, B., Petrizzo, M.R., Foster, A., Kolonic, S., Erba, E., Premoli Siva, I., Baas, M., Wagner, T., Sinninghe Damsté, J.S., 2004. Organic carbon deposition in the Cretaceous of the Ionian Basin, NW Greece: the Paquier Event (OAE 1b) revisited. Geological Magazine 141, 401–416, doi: 10.1017/S0016756804009409.

Turchyn, A. V., Schrag, D. P., Coccioni, R., Montanari, A., 2009. Stable isotope analysis of the Cretaceous sulfur cycle. Earth and Planetary Science Letters 285, 115–123.

Turgeon, S.C., Creaser, R.A., 2008. Cretaceous oceanic anoxic event 2 triggered by a massive magmatic episode. Nature 454(7202), 323-326.

Twitchett, R.J., 1999. Palaeoenvironment and faunal recovery after the end-Permian mass extinction: Palaeogeography, Palaeoclimatology, Palaeoecology, v. 154, p. 27–37, doi:10.1016/S0031-0182(99)00085-1.

Twitchett, R.J., 2006. The palaeoclimatology, palaeoecology and palaeoenvironmental analysis of mass extinction events: Palaeogeography, Palaeoclimatology, Palaeoecology, v. 232, p. 190–213, doi:10.1016/j.palaeo.2005.05.019.

Twitchett, R.J., 2007, The Lilliput effect in the aftermath of the end-Permian extinction event: Palaeogeography, Palaeoclimatology, Palaeoecology, v. 252, p. 132–144, doi:10.1016/j.palaeo.2006.11.038.

Twitchett, R.J., Looy, C.V., Morante, R., Visscher, H., and Wignall, P.B., 2001, Rapid and synchronous collapse of marine and terrestrial ecosystems during the end-Permian crisis: Geology, v. 29, p. 351–354, doi:10.1130/0091-7613(2001)029<0351:RASCOM>2.0.

Tyson, R.V., 1995. Palynological kerogen classification. In Sedimentary Organic Matter. Springer Netherlands, pp. 341-365.

Unida, S., Patruno, S., 2016. The palynostratigraphy of the Upper Maiolica, Selli Level and the Lower Marne a Fucoidi units in the proposed Barremian/Aptian (Lower Cretaceous) GSSP stratotype at Gorgo a Cerbara, Umbria–Marche Basin, Italy. *Palynology*, *40*(2), 230-246.

Urbanek, A., 1993. Biotic crises in the history of Upper Silurian graptoloids: a palaeobiological model. Historical Biology, 7(1), 29-50.

Vakhrameev, V.A., 1991, Jurassic and Cretaceous Floras and Climates of the Earth: Cambridge University Press, Cambridge, 318p.

Vink, A., Schouten, S., Sephton, S., Sinninghe Damste¤, J.S., 1998. A newly discovered norisoprenoid, 2, 6, 15, 19-tetramethylicosane, in Cretaceous black shales. Geochim. Cosmochim. Acta 62, 965^970.Volkman and Maxwell, 1986

von Breymann, M.T., Emeis, K.C., Suess, E., 1992. Water depth and diagenetic constraints on the use of barium as apalaeoproductivity indicator. In: Summerhayes, C.P., Prell, W.L., Emeis, K.C. (Eds.), Upwelling Systems: Evolution since the Early Miocene. Geological Society Special Publication 64, pp. 273–284.

Volkman, J.K., Maxwell, J.R., 1986. Acyclic isoprenoids as biological markers. Methods in geochemistry and geophysics 24, 1-42.

Volkman, J., 2003. Sterols in microorganisms. Applied microbiology and Biotechnology 60(5), 495-506.

Volkman, J.K., 2014. Acyclic isoprenoid biomarkers and evolution of biosynthetic pathways in green microalgae of the genus Botryococcus. Organic Geochemistry 75, 36-47.

Von Breymann, M.T., Emeis, K.C., Suess, E., 1992. Water depth and diagenetic constraints on the use of barium as a palaeoproductivity indicator. Geological Society, London, Special Publications, 64(1), 273-284.

Wade, B. S., Olsson, R.K., 2009. Investigation of pre-extinction dwarfing in Cenozoic planktonic foraminifera. Palaeogeography, Palaeoclimatology, Palaeoecology, 284(1), 39-46.

Wade, B.S., Twitchett, R.J., 2009. Extinction, dwarfing and the Lilliput effect: Palaeogeography, Palaeoclimatology, Palaeoecology, v. 284, p. 1–3, doi:10.1016/j.palaeo.2009.08.019.

Wagner, T., Wallmann, K., Herrle, J.O., Hofmann, P., Stuesser, I., 2007. Consequences of moderate ~25,000 yr lasting emission of light CO2 into the mid-Cretaceous ocean. Earth and Planetary Science Letters 259, 200–211.

Wagner, T., Herrle, J.O., Sinninghe Damsté, J., Schouten, S., Stuesser, I., Hofmann, P., 2008. Rapid warming and salinity changes of Cretaceous surface waters in the subtropical North Atlantic. Geology 36, 203–206, doi: 10.1130/G24523A.1.

Walker, B., Holling, C.S., Carpenter, S., Kinzig, A., 2004. Resilience, adaptability and transformability in social–ecological systems. Ecology and society, 9(2).

Waples, D.W., 1985. Geochemistry in petroleum exploration. Inter.Human Res. Develop. Corporation, Boston, pp. 232.

Ward, D.M., Brassell, S.C., Eglinton, G., 1985. Archaebacterial lipids in hot spring microbial mats. Nature 318, 656–659. doi: 10.1038/318656a0.

Wedepohl, K.H., 1971. Environmental influences on the chemical composition of shales and clays. In: Ahrens, L.H., Press, F., Runcorn, S.K., Urey H.C. (Eds.), Physics and Chemistry of the Earth, pp. 307–331, Pergamon, Oxford, UK.

Wedepohl, K.H., 1991. The composition of the upper Earth's crust and the natural cycles of selected elements. Metals in natural raw materials. Natural resources. In: Merian, E. (Ed.), Metals and their Compounds in the Natural Environment, pp. 3–17, VCH, Weinheim, Germany

Weissert, H., 1990. Siliciclastics in the Early Cretaceous Tethys and North Atlantic Oceans: Documents of periodic greenhouse climate conditions. Mem. Soc. Geol. Ital, 44, 59-69.

Weissert, H., Erba, E., 2004. Volcanism, CO_2 and palaeoclimate: a Late Jurassic–Early Cretaceous carbon and oxygen isotope record. J. Geol. Soc. Lond. 161, 695–702, doi: 10.1144/0016-764903-087.

Weissert, H., Lini, A., 1991. Ice age interludes during the time of Cretaceous greenhouse climate, In: Müller, D.W., McKenzie, J.A., Weissert, H., (Eds.), Controversies in Modern Geology. Academic Press, London, 173 – 191.

Weissert, H., Lini, A., Föllmi, K.B., Kuhn, O., 1998. Correlation of Early Cretaceous carbon isotope stratigraphy and platform drowning events: a possible link Palaeogeogr. Palaeoclimatol. Palaeoecol 137, 189 – 203.

Wheeley, J.R., Twitchett, R.J., 2005. Palaeoecological significance of a new Griesbachian (Early Triassic) gastropod assemblage from Oman: Lethaia, v. 38, p. 37–45, doi:10.1080/0024116051003150.

Wilson, P.A., Jenkyns, H.C., Elderfield, H., and Larson, R.L., 1998, The paradox of drowned carbonate platforms and the origin of Cretaceous Pacific guyots: Nature, v. 392, p. 889–894

Wilson, P.A., Norris, R.D., Cooper, M.J., 2002, Testing the Cretaceous greenhouse hypothesis using glassy foraminiferal calcite from the core of the Turonian tropics on Demerara Rise: Geology 30, 607–610.

Wingert, W.S., Pomerantz, M., 1986. Structure and significance of some twenty-one and twenty-two carbon petroleum steranes. Geochimica et Cosmochimica Acta 50(12), 2763-2769.

Whitman, W.B., Bowen, T.L., Boone, D.R., 1992. The methanogenic bacteria. In: Balows, A., Trüper, H.G., Dworkin, M., Harder, W., Schleifer, K.H., (Eds), The prokaryotes, Second Edition. Springer-Verlag, New York, Berlin, pp. 3352-3378.

Wortmann, U.G., Hesse, R., Zacher, W., 1999. Major-element analysis of cyclic black shales: Paleoceanographic implications for the Early Cretaceous deep western tethys. Paleoceanography 14(4), 525-541.

Wortmann, U.G., Herrle, J.O., and Weissert, H., 2004, Altered carbon cycling and coupled changes in Early Cretaceous weathering patterns: Evidence from integrated carbon isotope and sandstone records of the western Tethys: Earth and Planetary Science Letters, v. 220, p. 69–82

Yamaguchi, T., Norris, R.D., Bornemann, A., 2012. Dwarfing of ostracodes during the Paleocene–Eocene Thermal Maximum at DSDP Site 401 (Bay of Biscay, North Atlantic) and its implication for changes in organic carbon cycle in deep-sea benthic ecosystem: Palaeogeography, Palaeoclimatology, Palaeoecology, v. 346–347, p. 130–144, doi:10.1016/j.palaeo.2012.06.004.

Yu Xinke, F.P, Philp, R.P., 1990. Novel biomarkers found in South Florida Basin. Organic Geochemistry 15, 433 – 438.